ACKNOWLEDGEMENTS

It is a great pleasure for me to express my deepest gratitude to Prof. Dr. M. Lütfi Öveçoğlu for his supervision and invaluable guidance at every stage of the preparation of this study.

I would like to expres my sincere thanks to Prof. Dr. İsmail Duman and Assist. Prof. Dr. Burak Özkal.

I am also thankful to Res. Assist. Duygu AĞAOĞULLARI, Hasan GÖKÇE, Özge BALCI for his supports and helps.

Many thanks to my friends Şeyma Duman, Kübra Yumakgil and Ceren İmer for their friendship. I feel so lucky for educating with them.

I want to thank to Res. Assist. A. Umut Söyler, Aziz Genç and Ö. Utku Demirkan for their guidance and helpful ideas.

I would like to express thanks to all members of the Particulate Materials Laboratories.

I would also like to express my thanks to the Scientific and Research Council of Turkey (TÜBİTAK) for providing financial support for the Project 110M130 during my graduate education.

Last but not least, I would like to express my deep sense ofgratiutude to my beloved parents and my family members for their immense patience, moral support, courage and inspiration.

January 2013 Didem OVALI

TABLE OF CONTENTS

Page

ABBREVERATIONS

BPR **:** Ball-to-powder ratio
CTE **:** Coefficient of thermal expansion
MA **:** Mechanical Alloying
MMC **:** Metal Matrix Composite
ODS : Oxide Dispersoid-Strengthened
PCA **:** Process Control Agent
PM **:** Powder Metallurgy
PRMMC **:** Particulate Reinforced Metal Matrix Composite
PSA **:** Particle Size Analyzer
SEM **:** Scanning Electron Microscope

LIST OF TABLES

Page

LIST OF FIGURES

Page

Microstructural and Physical Characterization of Mechanically Alloyed W-1 wt % Ni–x WB (x=0.5, 1.0, 2.0, 4.0) and W-1 wt % Ni- 2 WB–y La_2O_3 (y=0.5, 1) Powders and Sintered Composites

SUMMARY

Tungsten and its alloys are candidate materials for various elevated temperature structural applications due to their excellent properties such as high melting point, high modulus, high resistance of thermal shock, low coefficient of thermal expansion (CTE) and good high temperature strength and stiffness. In general, it is very difficult to fabricate tungsten because of its high melting point, low ductility, and low workability. Even using powder metallurgy (P/M) techniques, processing requires very high sintering temperatures up to 2400 - 2800 °C to get near fully dense tungsten. The addition of small quantities of some transition metals, such as Pd, Pt, Ni, Co, and Fe makes it possible to reduce greatly the sintering temperature of W(~1400 ^{o}C).

As dispersion strengtheners, refractory carbide and nitride phases, such as TiC, VC, ZrC, HfC, TiN etc. have been mainly used to improve the mechanical properties of tungsten and its alloys. In addition to these refractory carbide and nitride materials, transition metal diborides are very promising candidates as reinforcements in W due to their high melting point, high hardness, good electrical and thermal conductivities.

Tungsten has high ductile to brittle transition temperature and the strength of tungsten decreases with increasing temperature. The rare-earth oxides improve the low-temperature brittleness and decreases ductile to brittle transition temperature in Mo and W materials.

In this study, W-1 wt % Ni composites reinforced with varios amount of WB powders mechanically alloyed for different durations and fabricated. Additionally, W-1 wt % Ni-2 wt % WB composite reinforced with two different amount of La_2O_3 particles (0.5, 1) and manufactured. Microstructural and phase characterizations of the composite powders and sintered samples were carried out via X-Ray diffraction (XRD), scanning electron microscopy (SEM). Particle size measurements and surface area analysis of the powders were carried out using laser particle size analyzer (PSA) and Brunauer-Emmett-Teller (BET), respectively. Sintered densities were measured by the Archimedes density method. Addition to this, electron probe microanalysis (EPMA) and energy dispersive x-rayspectroscopy (EDS) analysis are conducted for some sintering samples. Furthermore, Vickers microhardness and wear resistance measurements experiments of the sintered samples were also conducted.

Mekanik Alaşımlanmış W - ağ. % 1 Ni – ağ. % x WB (x=0.5, 1.0, 2.0, 4.0) ve W - ağ. 1 %Ni - ağ. % 2 WB – ağ. % y La2O3 (y=0.5, 1) Toz ve Sinter Kompozitlerin Mikroyapısal ve Fiziksel Karakterizasyonu

ÖZET

Dünyadaki en ağır metallerden biri oldan Volfram 19.25 g/cm^3 yoğunlupğuna sahiptir. Ergime noktası 3387°C ve 3422°C arasındadır. Volfram, periyodik tabloda VI grubunda yer alan bir geçiş elementidir. Volfram ve volfram alaşımları yüksek ergime sıcaklıkları, yüksek elastik modülleri, termal şoka karşı dayanımları, düşük termal genleşme katsayıları ve yüksek sıcaklıklarda gösterdiği mukavemet ve direngenliklerinden dolayı yüksek sıcaklıklarda kullanılacak malzemelerin geliştirilmesinde matriks malzemesi olarak öne çıkmaktadırlar.

Volfram, sünek-gevrek geçiş sıcaklığı yüksek olan bir geçiş metalidir ve sıcaklık arttıkça mukavemeti düşmektedir. Nadir toprak oksitleri ise volfram ve molibden gibi malzemelerin yapılarına katılarak bu geçiş sıcaklığını düşürmekte ve bu malzemelerin düşük sıcaklıktaki gevrekliğinden doğan sorunları engellemektedir.

Volfram ve alaşımları yüksek ergime sıcaklıkları, yüksek elastik modülleri, termal şoka karşı dayanımları, düşük termal genleşme katsayıları ve yüksek sıcaklıklarda gösterdiği mukavemet ve direngenliklerinden dolayı yüksek sıcaklıklarda kullanılacak malzemelerin geliştirilmesinde matriks malzemesi olarak öne çıkmaktadırlar. Genel olarak, yüksek ergime noktası ve düşük sünekliğinden dolayı volfram ürünlerinin üretimi zordur. Toz metallurjisi yöntemleri kullanılsa bile yoğunluğu yüksek volfram üretimi için, 2400 - 2800 °C gibi çok yüksek sıcaklıklara ihtiyaç vardır. Pd, Pt, Ni, Co, ve Fe gibi bazı geçiş metallerinin çok küçük miktarlardaki katkısı ile volframın sinterlenme sıcaklığı büyük oranda indirilebilir (~1400 ^{o}C).

Kompozit malzemeler teknolojik problemlerin üstesinden gelebilmek için uzun süredir kullanılmaktadır. Metal matriks kompozit malzemeler ileri teknoloji malzemeler grubunda yer alan, genellikle var olan malzemelerin kullanımının uygun olmadığı yüksek sıcaklık uygulamalarında kullanılan malzeme grubudur. Malzemelerin tek başlarına yeterli olmadıkları durumlarda kullanım koşulları sağlanamadığından yeni malzemelere olan ihtiyaç da giderek artar.

Metal matriksli kompozit malzemeler sınıfında yer alan partikül esaslı metal matriks kompozitler, üretimlerinde kullanılan malzemelerin kolay temini, ayrıca toz metalurjisi yönteminin avantajları, düşük maliyetleri ve üretimlerinin kolaylığı göz önüne alındığında kuvvetli bir malzeme grubunu oluştururlar. Partikül takviyeli kompozitler seramik ve metallerde tek başına bulunmayan eşsiz bir mikroyapı ve özellik kombinasyonuna sahiptirler. Uzay ve otomotiv sektörlerinin yanı sıra birçok farklı uygulamada kullanılan bu malzemeler karakteristik olarak izotropik kimyasal ve mekanik özellikler içerirler. Bunun yanı sıra, göreceli olarak daha ucuz olmaları, kolay şekil alabilme ve işlenebilme gibi özelliklere de sahiptirler.

Partikül takviyeli kompozitler yüksek elastik modül, yüksek sıcaklıklarda çalışabilme, düşük yoğunluk, termal şok direnci, yüksek elektik ve termal iletkenlik gibi bazı avantajlara sahiptirler. Partikül takviyeli metal matriks kompozitler, metallerde ve aynı zamanda seramiklerde tek başlarına bulunmayan özelliklerin eşsiz bir bileşimini oluştururlar. Bu kompozitler, matriks dayanımını arttıran partiküllerin homojen dağılımları ile oluşurlar. Genel olarak, yüksek tokluk, sertlik ve takviyelendirilmemiş matriks malzeme ile kıyaslandığında daha düşük yoğunluklarda daha fazla dayanım göstermelerinin yanı sıra iyi aşınma dayanımı gösterirler.

Metal matris kompozitler genel olarak, ana matris yapısı içine farklı özelliklere sahip ikincil fazların ve/veya pekiştiricilerin ilave edilmesi ile üretilmektedirler. Kullanılan malzemelerin birbiriyle uyumlu olması ve nihai ürünün uygulama alanı için yeterli mekaniksel, ısıl ve fiziksel özellikre sahip olması yani kısaca ürün performansının istenilen seviyede olarak ihtiyaçlara cevap vermesi kompozit üretiminde önemli bir parametredir. Partikül pekiştiricili kompozitler genel olarak iki grupta toplanabilirler. Bunlardan ilki daha büyük boyutlu ve miktarca yapıya daha fazla ilave edilen büyük partikül pekiştiricili kompozitlerdir. Diğer grup ise yapıya daha az ancak çok küçük oyutlarda partiküllerin ilavesi ile oluşturulan partikül pekiştiricili kompozitlerdir. Bu iki grup arasındaki temel ayrım pekiştirme mekanizmaları arasındaki farklılık ile yapılmaktadır.

Partikül takviyeli metal veya seramik matrisli kompozitler tozlarının elde edilmesinde en çok kullanılan yöntemlerden birisi olarak mekanik alaşımlama tekniği söylenebilir. Bu yöntem ile oldukça küçük boyutlarda, hatta gevrek yapılı tozlarda nano boyutlu ve yapıya homojen olarak dağıtılmış tozlar üretilebilinmektedir. Mekanik alaşımlama, faz diyagramlarındaki sınırlamaları kaldırarak, termodinamik denge bakımından teorikte mümkün olmayan ya da diğer üretim yöntemleri kullanılarak oluşturulamayacak kompozisyondaki alaşımların üretilmesinin önünü açmaktadır.

Toz metalurjisi metal matris kompozit üretiminde en genel olarak kullanılan üretim yöntemlerinden birisidir. Geçmişi milattan önce 1200 yıllarına kadar gitmektedir. Temel olarak bu yöntemde yapılan karıştırılan ya da ön alaşımlanan tozlar bir kalıp yardımıyla istenilen biçimde şekillendirilir ve daha sonra kontrollü atmosfere sahip bir fırında sinterlenerek partiküllerin birbiri ile bağlanması sağlanır. Toz metalurjisi diğer üretim yöntemlerine göre çok daha ekonomik bir yöntemdir. Ergitme ya da döküm içermediğinden dolayı üretim maliyetleri oldukça düşüktür. Ayrıca tozların karıştırılarak, metal bazlı kompozit üretilmesi de daha kolay bir tekniktir. Toz metalujisi üretim tekniklerinden biri olan mekanik alaşımlama bu çalışmada kullanılmıştır. Mekanik alaşımlama ile oldukça ince boyutlu ve yapıda düzgün dağılmış tozlar üretilebilinmektedir. Ayrıca bu teknik ile normalde oda sıcaklığında üretilemeyecek kimyasal kompozisyonlar ya da diğer üretim yöntemleri kullanılarak oluşturulamayacak alaşımlar üretilebilmektedir. Mekanik alaşımlama bilya toz çarpışmaları sonucu istenilen homojen yapının öğütme işlemi ile elde edilmesi prensibine dayanır. Bunun yanında uygulanan kuvvet ile tozlarda oluşan plastik deformasyon sonucunda malzemede iş sertleşmesi meydana gelir. Mekanik alaşımlama ile üretilen bu tozlar daha sonra uygun şekillendirme yöntemi seçilerek preslenir. Bu aşama toz metalurjisinde önemli bir kademedir ve sinterleme sonrası elde edilecek olan parçadan beklenen özelliklere başarılı bir presleme işlemi ile ulaşılabilinir.Numuneler düzgün bir şekilde preslendikten sonra üretimin genel olarak son kademesi olan sinterlemeye geçilir. Sinterleme yüksek sıcaklık etkisi ile partiküllerin birbirine bağlanması işlemidir. Ergime

noktasının altındaki sıcaklıklarda atomik boyutta taşınım ile gerşekleşebileceği gibi bazı durumlarda sıvı faz oluşumu ile de gerçekleştirilebilir.

Volfram ve alaşımlarının mekanik özelliklerinin geliştirilmesi amacıyla TiC, ZrC, HfC, TiN, Y_2O_3, La_2O_3, Sm_2O_3, ThO_2, ZrO_2 gibi çeşitli refrakter karbürler, nitrürler ve oksit fazları takviye elemanı olarak kullanılmaktadır. Bu takviye elemanları, volfram tane sınırlarına ve içlerine yerleşerek, tane büyümesi ve dislokasyon hareketini engellemekte ve malzemenin yüksek sıcaklık dayanımını artırmaktadır. Ayrıca, refrakter karakterli karbür ve nitrürlere ek olarak yüksek ergime sıcaklığı, yüksek sertlik değerleri ve iyi termal iletkenlikleri göz önünde bulundurularak geçiş metali borürleri de volfram alaşımlarında katkı malzeme olarak kullanılmaya adaydır.

Volfram ve volfram alaşımlarının, türbin, otomobil uygulamalarından elektronik endüstrisine kadar birçok uygulaması mevcuttur. Ayrıca ağır alaşımlar (heavy alloys) olarak da bilinen bu alaşımlar yüksek yoğunluğa sahip malzemelerin gereksinim duyulduğu kinetik enerji penetratörleri, balans ağırlıkları ve motor aksamında kullanım alanı bulmaktadır. Genellikle oksijene kapalı sistemlerdeki yüksek sıcaklık uygulamalarında radyasyon kalkanı ve ısıtıcı elemanların geliştirilmesinde önem taşımaktadır. Bazı uygulamalarda da, kazıyıcı elektrot veya döner ark fırını elektrodu olarak kullanılmaktadır. Volfram ve çeşitli malzemelerin farklı oranlardaki katkısıyla geliştirilen volfram esaslı kompozitler, farklı malzeme özelliklerinin mükemmel bir kombinasyonunu sağladığından, uygulama alanları daha da genişlemektedir.

Bu çalışmada, çeşitli oranlarda WB tozları ile takve edilmiş W-1 wt % Ni kompozitleri farklı sürelerde mekanik alaşımlanmıştır. Buna ilave olarak, W-1 wt % Ni-2 wt % WB kompozitine de iki farklı oranda (0.5, 1) La_2O_3 dispersoid katkısı mekanik alaşımlama yapılmıştır.Mekanik alaşımlama yapıla bütün tozlar 1400°C' de 1 saat süre ile sinterlenmiştir.

Üretilen toz ve sinter kompozit numunelerin mikroyapısal karakekterizayonları ve faz analizleri, X ışınları difraksiyonu (XRD), taramalı elektron mikroskobu (SEM) kullanılarak yapılmıştır. Mekanik alaşımlama yapılmış tozlara partikül boyut ölçümü (PSA) ve partikül yüzey alanı ölçümü (BET) yapılmıştır. Ayrıca seçilen bazı sinter numunelerine EPMA ve EDS analizleri yapılmıştır. Sinterlenmiş numunelerin yoğunlukları Arşimet tekniğiyle hesaplanmış ve mikrosertlik deneyleri Vickers mikrosertlik cihazı kullanılarak gerçekleştirilmiştir. Bunların dışında sinterlenen bazı numunerlere aşınma testi uygulanmıştır.

1. INTRODUCTION

Not only tungsten has high density value of 19.25 g/cm^3, but it is also one of the heaviest metals in the world. Its melting point varies between 3387°C and 3422°C which is extremely high among all elements except carbon. Tungsten (W) is a transition element which belongs to group VI in the periodic table. In addition to high modulus of compression and elasticity, tungsten has also very high thermal creep resistance, high thermal and electrical conductivity and a very high coefficient of electron emission. Furthermore, tungsten has superior mechanical properties like good high temperature strength, good corrosion resistance and low coefficient of thermal expansion. Due to these properties, tungsten is an attractive material for many important structural applications at high temperatures (Lassner, 1999)

High temperature strength of tungsten is enhanced with fine dispersed particles. As dispersion strengtheners, refractory carbide, nitride and oxide phases have been used primarily to develop the mechanical properties of tungsten and its alloys. The carbides and nitrides can be dispersed along the grain boundaries, and cause strengthening of the grain boundary and hinder the migration of the grain boundary at high temperature (Song et al.,2002).

Tungsten and tungsten alloys dominate the market in applications for which a high-density material is required, such as kinetic energy penetrators, counterweights and flywheels (Lassner, 1999). The high melting point of tungsten makes it an attractive choice for structural applications exposed to very high temperatures. In addition, tungsten is used at lower temperatures for applications that can use its high elastic modulus, density, or shielding characteristics to advantage (Lassner, 1999)

Metal matrix composites (MMCs), like all composites, consist of at least two chemically and physically distinct phases, suitably distributed to provide properties not obtainable with either of the individual phases. Generally, there are two phases, e.g., a fibrous or particulate phase, distributed in a metallic matrix (Chawla and Chawla, 2006). The reinforcing constituent is in most cases a ceramic, although there

are exceptions to this and MMCs can be taken to encompass materials "reinforced" with relatively soft and/or compliant phases, such as graphitic flakes, lead particles, or even gases (Clyne, 2000). It is also possible to use refractory metals, intermetallics, or semiconductors, rather than true ceramics (Clyne, 2000). The mechanical properties of the MMC's highly depend on the volume fraction and the type of the reinforcement as well as the type of the matrix (Stjernstoft, 2004). On the other hand, while continuous fiber-reinforcement provides the most effective strengthening in a given direction, particle-reinforcement provides cost-effectiveness and especially isotropic properties to the composite (Chawla and Shen, 2001).

As interesting and appropriate matrix materials with their high melting point, high modulus, high resistance of thermal shock, low coefficient of thermal expansion (CTE) and good high temperature strength and stiffness, in this last decade, tungsten and its alloys have received attention with a view of improving the high temperature mechanical properties (Song et. al., 2002). Generally, it is very difficult to fabricate tungsten because of its high melting point, low ductility, and even using powder metallurgy techniques, processing requires very high sintering temperatures up to 2400 – 2800 ^{o}C to get near fully dense tungsten (Li and German, 1983). The addition of small quantities of some transition metals such as Pd, Pt, Ni, Co, and Fe makes it possible to greatly reduce the sintering temperature of W (Li and German, 1983; German and Munir, 1976; Vajek, 1959; Hayden and Brophy, 1963).

Beside all the attention that the composites received for the last 20 years, there is another group of materials which have found applications in various industries, such as defense and aerospace in recent years, namely nanostructured materials or nanomaterials (Cahn, 2001). These materials exhibit unique microstructures and superior mechanical properties (Han et al., 2005). Nanotechnology is regarded world wide as one of the key technologies of the 21st century, and nanotechnological products and processes hold an enormous economic potential for the markets of the future (Zweck and Luther, 2003). Thus, the combination of composite materials and nanostructured materials, namely "nanocomposites" with the appropriate matrix and reinforcing phase constituents would be candidate materials for industrial applications, such as defense, aerospace and as cutting tools materials (Coskun, 2006).

As dispersion strengtheners, refractory carbide, nitride and oxide phases, such as TiC, VC, ZrC, HfC, TiN, Y_2O_3, La_2O_3, Sm_2O_3, ThO_2, ZrO_2, etc. have been mainly used to improve the mechanical properties of tungsten and its alloys (Song et. al., 2002; Song et. al., 2003b; Lee et. al., 2004). Keeping the above concepts in mind, the aim of this study has been to develop and characterize nanostructured WB and La_2O_3 particle-reinforced tungsten composite powders and their consolidated and sintered counterparts. Ni used as activation agent to investigate activated sintering of mechanically alloyed W-WB.

2. LITERATURE REVIEW

2.1 Metal Matrix Composites

2.1.1 Historical background

Examples of metal matrix composites data back to ancient civilisations. Copper awls from Cayonu (Turkey) date back to about 7000 BC and were made by a repeated lamination and hammering process, which gave rise to high levels of elongated non-metallic inclusions (Baci, 1997). Among the first composite materials to attract scientific as well as practical attention were the dispersion hardened metal systems (Clyne, 1993). These developed from a work in 1924 by Schmidt on consolidated mixtures of aluminium/alumina powders and led to extensive research in the 1950s and 1960s (Hanson, 1971). Precipitation hardening in metals was developed in the 1940s. In both dispersion hardening, and precipitation hardening the strengthening mechanism uses small particles (fine oxide particles or non-shearable precipitates) to impede dislocation motion (Orowan, 1948; Mott and Nabarro, 1948).

In the 1970s 'dual phase' steels were discovered, which are similar to what is now known as a particulate MMC. These steels are produced by annealing fairly low carbon steels in the $\alpha+\gamma$ phase field and then quenching, which converts the γ phase to martensite (Khomskaya, 2010). The resulting steel has approximately 20% of quite hard, rather coarse martensite particles distributed in a soft ferrite matrix. This strong, tough, and formable material is now used in car bodywork. Research in fibrous metal matrix composites flourished in the 1960s, with concentration on aluminum and copper matrix systems reinforced with tungsten and boron fibers. In these systems, the principal role of the matrix is to transmit and distribute the applied load to the fibers. Investigation of continuously reinforced composites withered during the 1970s, primarily due to high cost and production limitations (Baci, 1997). However, due to the continuing need for high temperature, high strengthlstiffness materials in turbine engines and other applications, these composites are now being reevaluated with attention towards titanium matrices (Palazotto, et al., 1988). In

discontinuously reinforced composites both the matrix and the reinforcement bear substantial proportions of the load. During the 1980s their development was primarily based on Al-based composites reinforced with Sic and Al,O, particles and short fibers. Low cost, high workability, good transverse properties, and significant increases in performance have made them the most commercially attractive system for many applications (Baci, 1997).

2.1.2 General introductions

Metal composite materials (MMC) open up unlimited possibilities for modern material science and development. From this potential, metal matrix composites fulfill most of the desired conceptions of the designer. This material group becomes interesting for use as constructional and functional materials, if the property profile of conventional materials either does not reach the increased standards of specific demands, or is the solution of the problem (Park and Seo, 2011). However, the technology of MMCs is in competition with other modern material technologies, for example powder metallurgy. The advantages of the composite materials are only realized when there is a reasonable cost – performance relationship in the component production. The use of a composite material is obligatory if a special property profile can only be achieved by application of these materials (Park and Seo, 2011). A classification of the composite materials are given in Figure 2.1(Kainer, 2006)..

The possibility of combining various material systems (metal – ceramic – nonmetal) gives the opportunity for unlimited variation. The properties of these newmaterials are basically determined by the properties of their single components. Figure 2.2 shows the allocation of the composite materials into groups of various types of materials (Kainer, 2006).

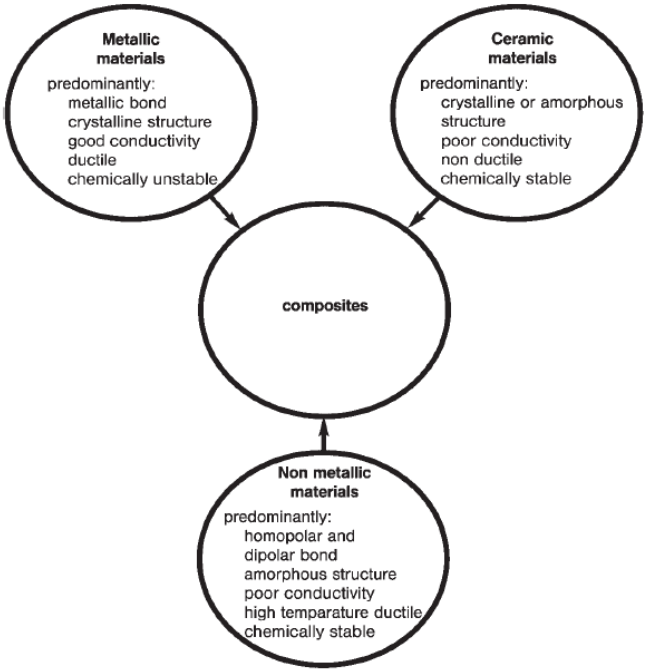

Figure 2.1: Classification of the composite materials within the group of materials (Kainer, 2006).

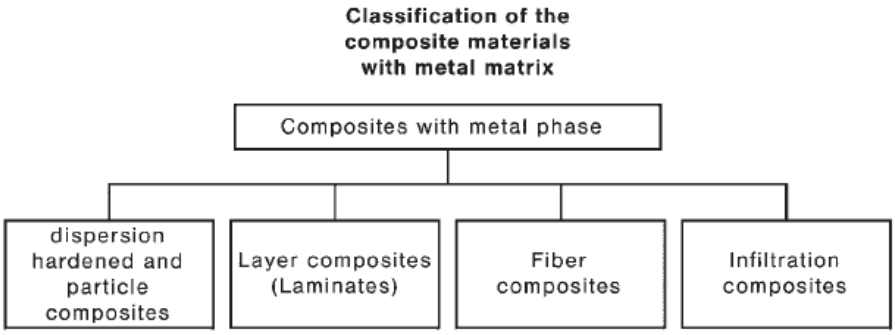

Figure 2.2: Classification of composite materials with metal matrixes (Kainer,2006).

In most cases, the reinforcing material is a ceramic, although there are exceptions to this and MMC's can be taken to encompass materials "reinforced" with relatively soft and/or compliant phases, such as graphitic flakes, lead particles, or even gases. It is also possible to use refractory metals, intermetallics, or semiconductors, rather than true ceramics (Clyne, 2000). Generally, there are three types of MMC's: i) particle reinforced MMC's, ii) short fiber or whisker reinforced MMC's, iii) continuous fiber or sheet reinforced MMC's (Chawla and Chawla, 2006). Figure 2.3 shows the schematic representations of these three major types of metal matrix composites.

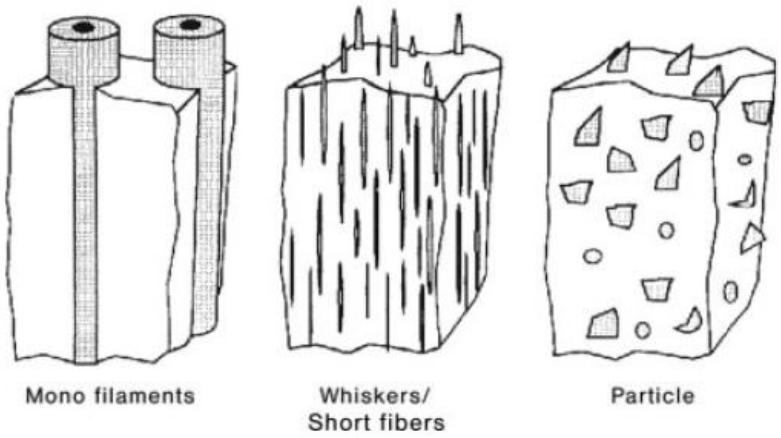

Figure 2.3: Schematic presentation of three shapes of metal matrix composite materials (Clyne and Withers, 1993).

Metal matrix composites (MMC's), as well as all composites, consist of at least two chemically and physically distinct phases, suitably distributed to provide properties not obtainable with either of the individual phases. Generally, there are two phases for MMC's, e.g., a fibrous or particulate phase, distributed in a metallic matrix (Chawla and Chawla, 2006). Metals are chosen as the matrix material in MMC structures. Because in general, the metals have;

a) higher application temperature ranges,

b) higher transverse stiffnesses and strengths,

c) generally high toughness values,

d) high radiation resistances,

e) high electric and thermal conductivities,

f) higher strength-to-density, stiffness-to-density ratios, as well as better fatigue resistances, lower coefficients of thermal expansion (CTE) and better wear resistances than with monolithic metals,

g) can be fabricated with conventional metal working equipment (Akovali and Uyanik, 2001).

2.1.3 Particulate reinforced metal matrix composites

In last decades, MMC's have become attractive candidate materials for aerospace, automotive and a lot of other applications due to their physical and mechanical

properties. More recently, especially particulate reinforced metal matrix composites (PRMMC's) have received an increasing attention because of their relatively low costs, good formability and machinability as well as characteristic isotropic properties (Ibrahim et al., 1991; Tjong and Ma, 2000; Sun et al., 2003).

Early studies on MMC's were about the development and investigation of the behavior of continuous fiber reinforced high performance hybrid materials (Park and Seo, 2011). However, extensive industrial application of these composites has been hindered because of the high production costs of the reinforcement fiber. So, availability of relatively inexpensive reinforcements and the development of various processing methods which result in reproducible microstructures and properties really enhanced the interest on PRMMC's (Ibrahim et al., 1991). These materials exhibit a unique combination of microstructure and properties which is not found in either ceramics or metals alone. These properties of PRMMC's mainly depend on the microstructure and properties of the matrix materials, the nature, distribution, size and shape of particles as well as the interfacial behavior between matrix and the reinforcement phase constituents (Liu et al., 1994). An optimum combination of mechanical properties can be achieved when fine and thermally stable ceramic particulates are dispersed uniformly in the metal matrix (Tjong and Ma, 2000). PRMMC's are most commonly produced either by melt incorporation and casting technique or powder blending and consolidation (Clyne, 2001).

There are two sub-classifications of PRMMC's (Schwartz, 1984). These are large particle and dispersion strengthened composites. The distinction between these two groups is based on reinforcement or strengthening mechanism. The aim of using the term "large" is to point out that particle–matrix interactions cannot be related to the atomic or molecular level; so, preferably, continuum mechanics is used. Generally, the particulate phase is harder and stiffer than the matrix. These reinforcing particles tend to restrain movement of the matrix phase in the neighborhood of each particle. Basically, the matrix transfers some of the applied stress to the particles, which carry a fraction of the load. The degree of reinforcement or improvement of mechanical behavior depends on strong bonding at the matrix–particle interface. For dispersion-strengthened composites, particles are normally much smaller than the former one, having diameters between 0.01 and 0.1 μm (10 and 100 nm). This time, particle–matrix interactions cause strengthening to occur on the atomic or molecular level.

The mechanism of strengthening is similar to that for precipitation hardening. Since the matrix carry the major portion of an applied load, the small dispersed particles hinder or impede the motion of dislocations. So, plastic deformation is restricted such that yield and tensile strengths, as well as hardness, improve. (Schwartz, 1984).

2.1.3.1 Large particle composites

The term ‘large’ is used to denote that particle-matrix interactions can not be treated on atomic or molecular level and ‘continuum mechanics’ should be used. For large particle reinforced composites, the reinforcing material is usually harder and stiffer than the matrix and they tend to restrain movement of the matrix (Chawla and Shen, 2001). The matrix transfers some of the applied stress to the particles. The efficiency of reinforcement mostly depends on interaction at the particle-matrix interface (Akovali and Uyanik, 2001). These composites are generally used as cutting tools for hardened steels. The hard carbide particles provide the cutting surface but, are not themselves capable of withstanding the cutting stresses because of their brittleness. Toughness is increased by their inclusion in the ductile metal matrix, which insulate the carbide particles from one another and prevents particle-to-particle crack propagation. Both matrix and particulate phases are quite refractory, to withstand the high temperatures generated by the cutting action on materials that are extremely hard (Askeland, 1984; Schwartz, 1984).

2.1.3.2 Dispersion strengthened composites

In dispersion-strengthened composites, the fine dispersions of oxide, carbide, or boride particles cancel the motion of dislocations so that the matrix is strengthened relatively to the effectiveness of the dispersions as a barrier to the motion of dislocations (Ohring, 1995; Asthana et al., 2006). The applied stress must be sufficiently enough to bend the dislocation line into a semicircular loop to make the dislocation pass through a dispersoid. Calculations show that interparticle separation for effective dispersion hardening should be between 0.01 and 0.3 μm (10 – 300 nm). To achieve this range of spacing between the dispersoid, the particle diameters sh ould be less than 100 nm at volume fractions below 15% (Asthana et al., 2006). Of many dispersion-hardened alloy systems, only a few have reached commercial significance.

Precipitation hardened systems normally exhibit higher strengths at room temperature, because it is generally possible to achieve finer distributions in precipitation hardened systems. However, dispersion strengthened systems show advantages at elevated temperature, because of the high thermal stability of the oxide particles. While extremely low volume fractions are desirable in terms of ductility, dispersoid contents as high as 15 vol% have been used in applications requiring good high temperature strength and creep resistance. Creep is effectively suppressed because the dislocations must climb over the dispersoids by diffusive processes and this results in creep rates decreasing with increasing dispersoid size (Clyne, 2001).

Aluminum, nickel, and tungsten, copper and titanium, have showed successful results in laboratory and developmental stages (Schwartz, 1984). The development of oxide dispersion-strengthened (ODS) composites has led to considerable improvements in the elevated-temperature strength and creep-resistance of the matrix alloys (Krajnikov et al.,1997; Sakasegawa et al., 2008; Redsten et al., 1995). The ODS composites contain small (< 15%) amounts of fine second-phase particles, which prevent recrystallization and grain coarsening, and act as barriers to the motion of dislocations. Small quantities of fine oxide ceramics improve the strength without degrading the valuable matrix properties (Asthana et al., 2006).

2.1.4 Fabrication of PRMMC's

There are various processing techniques used to fabricate PRMMC's. These fabrication methods can be grouped according to the temperature of the metal matrix during the process. So, there are liquid phase processes, solid state processes and two phase processes. Main liquid phase processes are molten metal mixing process, melt infiltration process and melt oxidation process. On the other hand, major solid state processes are powder metallurgy and high-energy-high-rate process. Finally, two phase processes are sprey deposition, rheocasting and variable co-deposition of multi-phase materials (VCM) process (Chawla, 2006; Ibrahim et al., 1991; Lloyd, 1994; Yang and Chung, 1989).

The selection of one particular process over the others depends on various factors which are types of materials and their properties, final desired properties, size, shape and complexity of the part, subsequent processing and overall cost of the process (Lindroos et al., 2004).

The interfacial behavior between the particles and matrix is one of the most important variables which affect the properties of the PRMMC's. Unfortunately, most of the particles used in PRMMC's possess poor wettability with the matrix, which results in a poor distribution of the reinforcement phase as well as a weak particle-matrix interface (Liu et al., 1994). Various processing techniques have been developed over the last two decades which try to optimize the structure and properties of PRMMC's (Ibrahim et al., 1991; Schwartz, 1997). Among these techniques, there were some luxurious ones to enhance the wettability by, for instance, introducing some kind of surface coating to the particles before fabrication. However, this preprocessing of particles increased the cost of PRMMC's further, so their commercial use was limited. In addition, some recently developed PRMMC's, using state-of-the-art high performance materials, such as tungsten, molybdenum, niobium and tantalum as the matrix material, are difficult to fabricate by using conventional liquid metallurgy process because these materials have incredibly high melting temperatures (Liu et al., 1994). In these cases, powder metallurgy seems more attractive and has become the most important fabrication technique for this group of PRMMC's.

2.2 Powder Metallurgy

The powder metallurgy (PM) route is the most commonly used method for the preparation of PRMMC's (Liu et al., 1994; Huda et al., 1995). Blending of metallic powders with ceramic particles is a versatile technique for the PRMMC production (Clyne, 2001). In the basic process, mixed or prealloyed powders are fed into a die, compacted a desired shape and then this pressed powder is sintered in a controlled atmosphere furnace to convert the mechanical bonds to the metallurgical bonds that link the powder particles (Newkirk and Kohser, 2004).When higher strength discontinuous MMC's are required, PM processes are often used because segregation, brittle reaction products, and high residual stresses from solidification shrinkage can be minimized (Campbell, 2006). In addition, with the advent of rapid solidification and mechanical alloying technology, the matrix alloy can be produced as a prealloyed powder, rather than starting with elemental blends (Campbell, 2006).

Powder metallurgy method is widely used to produce PRMMC's based on its advantages which of some are listed below:

1. PM method is more economical than many other techniques in production of PRMMC's, since no melting and casting is involved (Huda et al., 1995).
2. The process offers the possibility of using a wide range of reinforcement volume fraction and size (Huda et al., 1995).
3. Production by PM results in a homogeneous distribution of reinforcements in the matrix material (Huda et al., 1995).
4. PM offers superior mechanical properties as a result of high dislocation density, small subgrain sizes and limited recrystallization during the process (Das et. al., 2002).

Powder Metallurgy (PM) may be defined as the art of producing metal powders and using them to make serviceable objects. This method has gained popularity because of the high strength, ductility and toughness values which can be achieved by using this production route. One of the outstanding uses of powder metallurgy is the combination of hard materials in a metallic matrix, which serves as the basis of cemented-carbide products (Miracle, 2005). Moreover, powder metallurgy is more economical than most other manufacturing processes.

Powder Metallurgy processing involves the following steps:

1. Blending of matrix alloy and reinforcement in powder form,
2. Compacting (cold pressing) the homogeneous blend to roughly 80% density,
3. Degassing the preform (which has an open interconnected pore structure) to remove volatile contaminants (lubricants and mixing and blending additives), water vapor, and gases, and
4. Consolidation by vacuum hot pressing or hot isostatic pressing.

Powder metallurgy methods involve cold pressing and sintering, or hot pressing, to produce MMCs. The matrix and the reinforcement powders are blended to produce a homogeneous distribution. The blending stage is followed by cold pressing to produce what is called a green body, which is about 80% dense and can be easily handled. The cold pressed green body is canned in a sealed container and degassed to remove any absorbed moisture from the particle surfaces. The final step is hot pressing, uniaxial or isostatic, to produce a fully dense composite. The hot pressing

temperature can be either below or above that of the matrix alloy solidus (Åström, 2001).

2.2.1 Mechanical alloying

2.2.1.1 History and definition of mechanical alloying

In order to improve the properties and performance of materials, significant developments in mechanical, chemical, and physical properties have been achieved through chemistry modifications and conventional thermal, mechanical, and thermo-mechanical processing methods. (Suryanarayana, 2001). As a result, non-equilibrium processing of materials has attracted the attention of a number of scientists and engineers due to the possibility of producing better and improved materials than it is possible by conventional methods (Suryanarayana et al., 2001; El-Eskandarany, 2001)

The structure and constitution of advanced materials can be better controlled by processing them under non-equilibrium conditions and mechanical alloying (MA) is such a processing method that materials can be produced under non-equilibrium conditions (Suryanarayana, 2001). MA can be defined as a powder metallurgy process for producing composite metal powders with a controlled fine microstructure by repeated cold welding, fracturing and rewelding of powder particles in a high–energy ball mill (Öveçoğlu, 1987; Benjamin, 1992; Suryanarayana et al., 2001). It utilizes various types of milling machines in which a blend of different powders is subjected to a highly energetic compressive force (Tang et. al., 2004).

The mechanical alloying (MA) process was first employed during the pioneering work of Benjamin at the International Nickel Company's Paul D. Merica Research Laboratory in the late 1960's (Benjamin, 1970). It started as an industrial necessity to produce oxide-dispersion-strengthened nickel-based superalloys for gas turbine engine components (Öveçoğlu, 1987; Suryanarayana et al., 2001; Delogu et al., 2003). However, the subsequent discovery of metastable phase formation by MA opened the door to important applications in Materials Science (Delogu et al., 2003). In addition to the metastable phases, equilibrium phases of commercially useful and scientifically interesting materials can be also synthesized by MA (Suryanarayana et al., 2001).

MA is a simple and versatile technique, as well as an economically feasible process with important technical advantages. One of the greatest advantages of MA is in the synthesis of novel alloys, e.g., alloying of normally immiscible elements, which is not possible by any other technique (La Caer et al., 2002). The reason for that is that MA is a completely solid-state processing technique and therefore limitations imposed by phase diagrams do not apply for this process (Suryanarayana et al., 2001). Furthermore, MA holds an advantage over traditional ball milling processes which is to produce a material whose internal homogeneity is independent of the initial starting particle size. It is not uncommon to obtain mechanically-alloyed dispersions with less than 1 μm interparticle spacing from initial powder sizes of 50-100 μm average diameters (Goff, 2003).

2.2.1.2 Types of mills

Different types of high-energy milling equipment are used to produce mechanically alloyed powders. These equipment include Spex Mixer/mills, planetary ball mills, attritor mills and commercial mills. They have different capacity, efficiency of milling and additional arrangements for cooling, heating, etc (Suryanarayana, 2001; Goff, 2003).

Spex Mixer/mills are most commonly used for laboratory investigations and they mill about 10-20 g powder at a time depending on the density of starting constituents (Goff, 2003). The common variety of these mills has one vial, containing the sample and grinding balls, secured in the clamp and shakes the milling container in three-mutually perpendicular directions at about 1200 rpm resulting in powder microstructural refinement with time (Suryanarayana, 2001; Goff, 2003). Ball-ball and ball-container collisions continually trap and refine the powder constituents with time ultimately leading to an overall homogeneously dispersed microstructure (Goff, 2003). There are different vial materials available for the Spex mixer/mills, which are hardened steel, alumina, tungsten carbide, zirconia, stainless steel, silicon nitride, agate, plastic, and methacrylate (Suryanarayana, 2001). Typical Spex mill and tungsten carbide vial set can be seen in Figure 2.4.

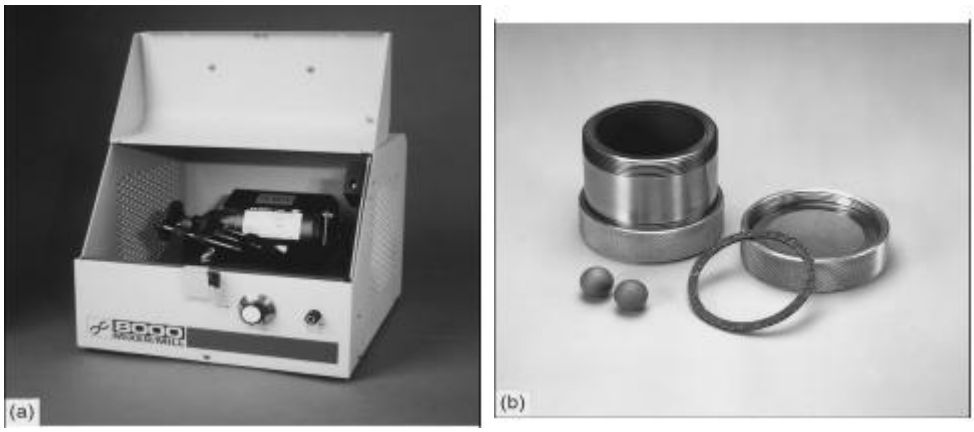

Figure 2.4: a) A typical Spex shaker mill **b)** Tungsten carbide vial set consisting of the vial, lid, gasket, and balls (Suryanarayana, 2001).

Another popular mill for conducting MA experiments is the planetary ball mill in which a few hundred grams of the powder can be milled at a time. It is called the planetary ball because of its vial's planet-like movement. The centrifugal force produced by the vials rotating around their own axes act on the vial contents, consisting of material to be ground and the grinding balls. As a result, powders are trapped between the rotating balls and the walls of the vial and refined. Even though the linear velocity of the balls in this type of mill is higher than that in the Spex mills, the frequency of impacts is much more in the Spex mills (Suryanarayana, 2001).

Therefore, compared to Spex mills, planetary ball mills can be considered lower energy mills (Suryanarayana, 2001). In Figure 2.5, a schematic view of ball motion in a planetary ball mill can be seen.

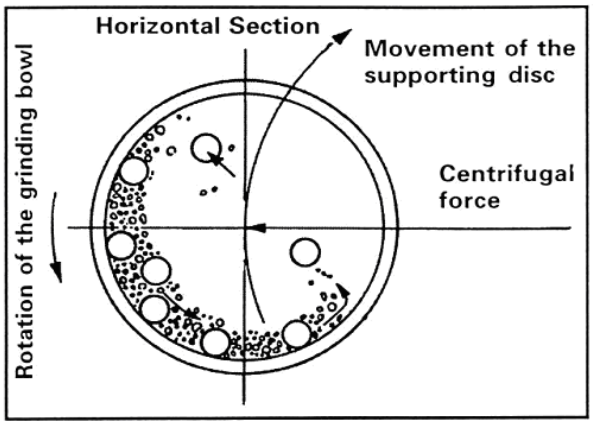

Figure 2.5: A schematic view of ball motion in a planetary ball mill (El-Eskandarany, 2001).

Another type of mills is the attritor mills. In attritor mills, large quantities of powder (from about 0.5 to 40kg) can be milled at a time (Suryanarayana, 2001). It contains a vertical shaft with a series of impellers that rotates in the tank of about 250 rpm (Goff, 2003). As the shaft rotates, the balls drop on the metal powder that is being ground. The impellers energize the ball charge, causing powder size reduction because of impact between balls, between balls and container wall, and between balls, agitator shaft, and impellers. The rate of grinding increases with the speed of rotation. However, at high speeds the centrifugal force acting on the balls exceeds the force of gravity, and the balls are pinned to the wall of the container. At this point the grinding action stops (Suryanarayana, 2001). Schematic view of an attritor mill is given in Figure 2.6.

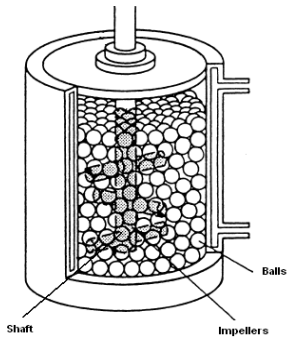

Figure 2.6: A schematic view of an attritor mill (Goff, 2003).

The milling time decreases with an increase in the energy of the mill. Roughly, it can be estimated that a process that takes only a few minutes in the Spex mill may take hours in an attritor and a few days in a commercial mill (Suryanarayana, 2001).

2.2.1.3 Proccess variables during milling

MA is a complex process involving optimization of a number of process variables to achieve the desired product phase, microstructure, and/or properties. These will decide the nature of the phase formed (solid solution, intermetallic, or amorphous phase, etc.) in the milled powder. For a given composition of the powder, the type (material) of the milling container and the milling medium, ball-to-powder ratio, milling atmosphere, milling time, use of a process control agent (PCA), etc. can be listed as the important variables that have an important effect on the final constitution of the milled powder (Suryanarayana, 2001).

The material used for the milling container (grinding vessel, vial) is important since the impact of the grinding medium on the inner walls of the container will result in tiny fractions of milling material that fracture off and disperse into the composite powder (Monov et al., 2012). These can contaminate the powder or alter the chemistry of the powder. If the material of the grinding vessel is different from that of the powder, then the powder may be contaminated with the grinding vessel material (Suryanarayana, 2001; Goff, 2003). Regardless of the type of MA process, the most appropriate type of container and milling media for the given system should be chosen. Generally, milling media that is made of a similar material as that of the material to be processed is used to reduce contamination during processing (Goff, 2003). Additionally, the density of the grinding medium should be high enough so that the balls create enough impact force on the powder (Suryanarayana, 2001).

Another important issue is the ball-to-powder ratio (BPR). This has been varied by different investigators from a value as low as 1:1 to as high as 220:1. Generally, a ratio of 10:1 is most commonly used while milling the powder in a small capacity mill such as a SPEX mill. The BPR has an important effect on the time required to achieve a particular phase in the powder being milled. The higher the BPR, the shorter is the time required (Suryanarayana, 2001).

Milling atmosphere is also an important variable for the MA process. The major effect of the milling atmosphere is on the contamination of the powder (El-Eskandarany, 2001). The powders are milled in containers that have been either vacuumed or filled with an inert gas such as argon or helium. However, high-purity argon is the most common used gas to prevent oxidation and contamination of the powder (Suryanarayana, 2001). The presence of air in the vial cause to produce oxides and nitrides in the powder, especially if the powders are reactive in nature. Thus, the loading and unloading of the powders into the vial has to be carried out inside an atmosphere-controlled glove box (Suryanarayana, 2001; Fecht, 2002).

The time of milling is the most important parameter. In most of the cases, the rate of refinement of the internal structure (particle size, crystallite size, lamellar spacing, etc.) is roughly logarithmic with processing time (Figure 2.7) and therefore the size of the starting particles is relatively unimportant. In a few minutes to an hour, the lamellar spacing usually becomes small and the crystallite (or grain) size is refined to

nanometer dimensions. Normally, the time is so chosen to achieve a steady state between the fracturing and cold welding of the powder particles. Furthermore, milling times required depend on the type of mill used, the intensity of milling, the ball-to-powder ratio, and the temperature of milling. These times have to be decided for each combination of the above parameters and for the particular powder system. However, it should be menioned here that the level of contamination increases and some undesirable phases form if the powder is milled for times longer than required. Therefore, the powder has to be milled just for the required duration and not any longer (Suryanarayana, 2001).

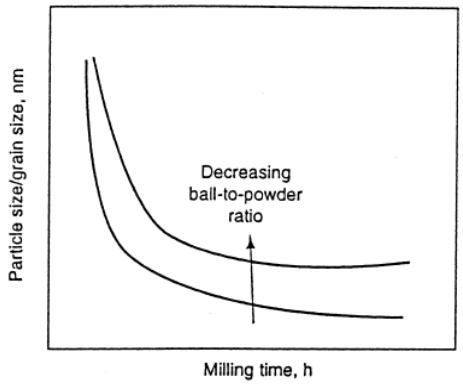

Figure 2.7: Refinement of particle and grain sizes with milling time. Rate of refinement increases with higher milling energy, ball-to powder ratio, lower temperature, etc. (Suryanarayana, 2001).

The use of process control agents (PCA) are another concern in the MA process. Generally, ductile powder particles get cold-welded to each other, due to the heavy plastic deformation during milling. However, true alloying among powder particles can occur only when a balance is maintained between cold welding and fracturing of particles (El-Eskandarany, 2001). In order to provide, a process control agent (PCA) is added to the powder mixture during milling to reduce the cold welding (Öveçoğlu, 1987; Suryanarayana, 2001; Gilman and Benjamin, 1983). The PCA's can be solids, liquids, or gases. They are mostly organic compounds, which act as surface-active agents by adsorbing on the surface of the powder particles and minimizing cold welding between powder particles and thereby inhibiting the agglomeration (Suryanarayana, 2001).

2.2.1.4 Mechanism of mechanical alloying

MA is an advanced fabrication process that can produce ultra-fine and homogenous powders. Even, nanocrystalline materials (with a grain size of few nanometers, usually<100 nm) are also produced by MA of powder mixtures (Ryu et al., 2000). Additionally, it has been recognized that this technique can be used to induce chemical (displacement) reactions in powder mixtures at room temperature or at much lower temperatures than normally required to synthesize pure metals (Suryanarayana et al., 2001).

In any MA process, starting powder constituents are first mixed or blended according to the required stoichiometry for desired composite batches. Then, they are put in the milling container with the appropriate ball charge and milled until a steady state of homogeneous dispersion is achieved (Goff, 2003). The central event of MA is the ball-powder collisions (Fecht, 2002). Microstructural refinement during the MA process occurs due to the repeated cold-welding, fracturing, and cold-welding of the dry powder constituents during their impact between ball-ball and/or ball-container collisions. Figure 2.8 is a schematic representation of the collided balls. The force of the impact plastically deforms the powder particles leading to work hardening and fracture (Suryanarayana, 2001; Fecht, 2002).

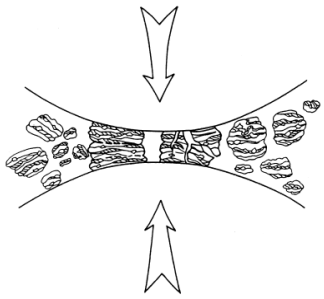

Figure 2.8: Schematic view of a ball-powder-ball collision (Suryanarayana, 2001).

As a result, MA provides several strengthening mechanisms which are oxide dispersion strengthening, carbide dispersion strengthening, fine grain size strengthening, substructural strengthening and solid solution strengthening (Öveçoğlu, 1987, Davis, 1993, Soni, 2001). In order to get better understanding about the physical phenomena that occur during MA processing, it is useful to divide the typical process into three or four stages (Öveçoğlu, 1987; Goff, 2003).

In the early stages of milling, the particles are soft (either ductile-ductile or ductile-brittle material combination), their tendency to weld together and form large particles is high (Suryanarayana, 2001). A broad range of particle sizes develops, with some as large as three times bigger than the starting particles (Suryanarayana, 2001; Goff, 2003). The composite particles at this stage have a characteristic layered structure consisting of various combinations of the starting constituents (Figure 2.9) (Öveçoğlu, 1987; Suryanarayana, 2001).

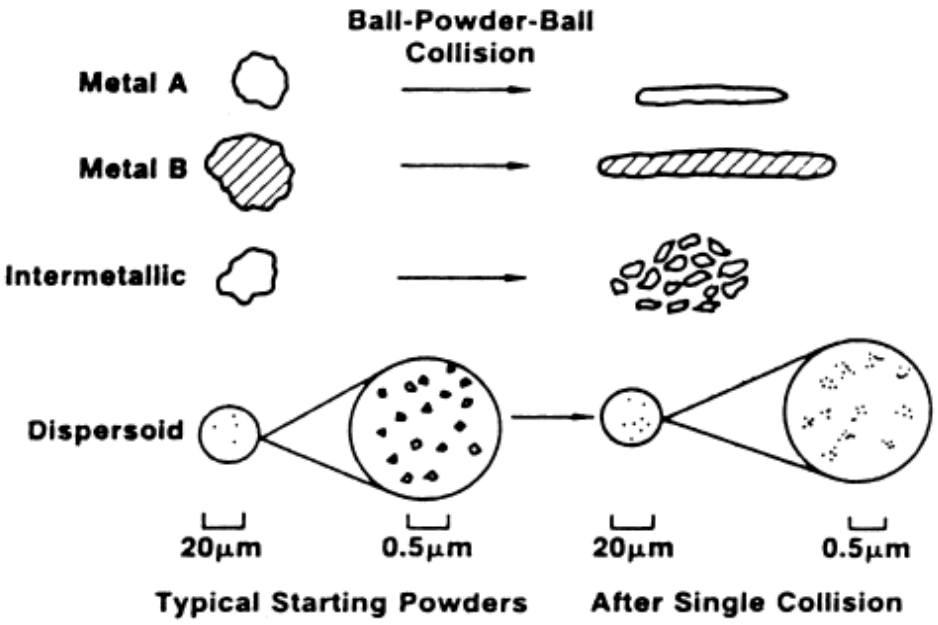

Figure 2.9: Deformation characteristics of starting powders used in a typical MA process (Öveçoğlu, 1987; Suryanarayana, 2001).

As the metallic phases are flattened and overlap during ball collisions, atomically clean surfaces are placed in contact with one another and subsequently cold-weld together, where brittle constituents (intermetallics and dispersoids) are occluded by the ductile constituents thus becoming trapped along cold-weld interfaces (Goff, 2003). Figure 2.10 shows early stage of processing in which particles are layered composites of starting constituents.

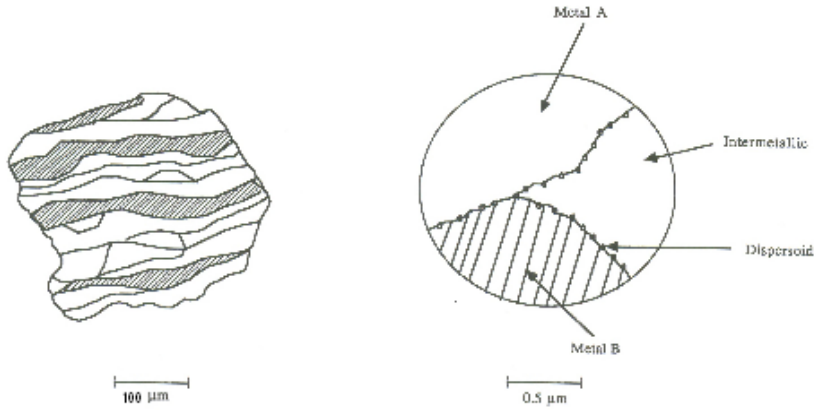

Figure 2.10: Early stage of processing in which particles are layered composites of starting constituents (Öveçoğlu, 1987).

In the intermediate stage, the composite powder particles are further refined due to continual welding and fracturing of excessively work-hardened metallic phases and brittle intermetallics and/or dispersoids (Goff, 2003). At this stage, the tendency to fracture predominates over cold welding (Suryanarayana, 2001). The particles consist of convoluted lamellae. The reduction in particle size, increased microstructural mixing, and elevated temperature of the powder constituents due to the adsorbed kinetic energy of milling balls all help to form areas of solute dissolution throughout the metallic powder matrix (Öveçoğlu, 1987). Thus, this potentially may lead to areas where new phases develop which is mainly due to an overall decrease in atomic diffusion distances between individual phases and decreased activation energies for diffusion due to the increase in temperature (Öveçoğlu, 1987; Goff, 2003). Consequently, the inter-layer spacing decreases and the number of layers in a particle increase (Suryanarayana, 2001). Figure 5.11 is a schematic view of the reduced lamellae thickness, solute dissolution, and formation of new phases in the intermediate stage of processing.

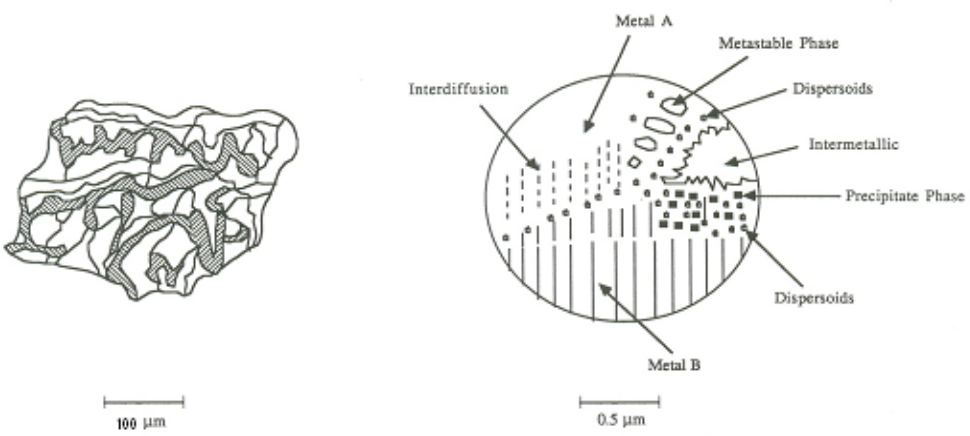

Figure 2.11: Intermediate stage of processing showing reduced lamellae thickness, solute dissolution, and formation of new phases (Öveçoğlu, 1987).

In the final stage (Figure 2.12), steady-state equilibrium is attained when a balance is achieved between the rate of welding and the rate of fracturing. As a result, smaller particles are able to withstand deformation without fracturing and tend to be welded into larger pieces, with an overall tendency to drive both very fine and very large particles towards an intermediate size (Suryanarayana, 2001). Furthermore, individual particle compositions are equal to the starting powder blend composition; the lamellae are no longer optically resolvable; and the dispersoid spacing is equal to the distance between weld interfaces (Öveçoğlu, 1987). At this point, further processing would not improve the dispersoid distribution or serve to enhance the homogeneity of the composite microstructure (Öveçoğlu, 1987; Goff, 2003). The particle size distribution at this stage is narrow, because particles larger than average are reduced in size at the same rate that fragments smaller than average grow through agglomeration of smaller particles (Suryanarayana, 2001).

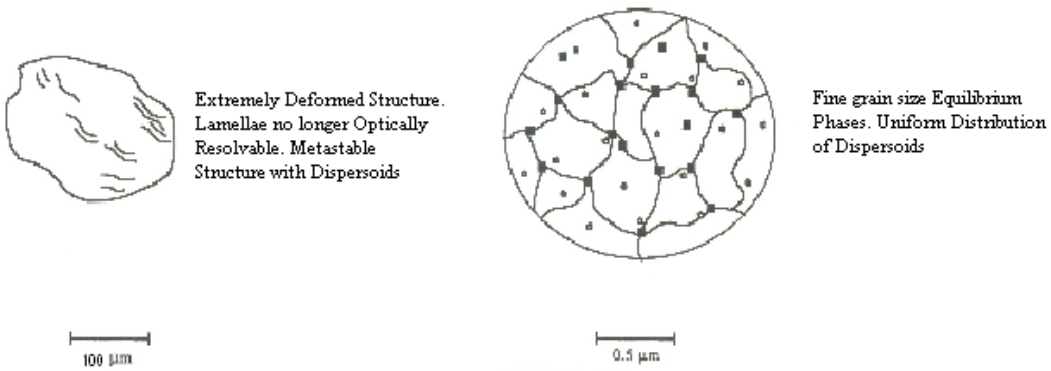

Figure 2.12: The final stage of processing and consolidation (Öveçoğlu, 1987).

In order to complete the MA process and obtain a useable bulk composite form, the powders are heated to a temperature greater than half the melting temperature of the composite powder and consolidated. This serves to further homogenize the microstructure (Goff, 2003). It is possible to conduct MA with three different combinations of metals and alloys, namely ductile-ductile, ductile-brittle and brittle-brittle systems. Therefore, it is convenient to discuss the mechanism of MA also under these categories (Fecht, 2002).

Ductile-ductile combination is thought to be the ideal combination for the MA process. It is suggested that it was necessary to have at least 15% of a ductile component for achieving alloying (Suryanarayana, 2001). This was true because alloying occurs due to the repeated action of cold welding and fracturing of powder particles; cold welding can not occur if the particles are not ductile. In the early stages of MA, the ductile components get flattened into platelet/pancake shapes. A small quantity of the powder, usually one or two particle thickness, also gets welded onto the ball surfaces. This coating of the powder on the grinding medium is advantageous since it prevents excessive wear of the grinding medium and thus preventing the contamination of the powder. However, the thickness of the powder layer on the grinding medium must be kept to a minimum to avoid forming a heterogeneous product (Suryanarayana, 2001). In the next stage, these flattened particles get cold welded together and form a composite lamellar structure of the constituent metals (Öveçoğlu, 1987). An increase in particle size is also observed at this stage (Suryanarayana, 2001). For instance, it has been found that during MA of a Fe-Cu powder mixture, agglomerates of multilayers are formed leading to microstructures very similar to those obtained by cold-rolling (Fecht, 2002). With increasing MA time, the composite powder particles get work hardened, the hardness and consequently the brittleness increases, and the particles get fragmented resulting in particles with more equiaxed dimensions (Suryanarayana, 2001). With further milling, the elemental lamellae of the welded layer and both the coarse and fine powders become convoluted rather than being linear. Alloying begins to occur at this stage due to the combination of decreased diffusion distances (interlamellar spacing), increased lattice defect density, and any heating that may have occurred during the milling operation (Öveçoğlu, 1987). The hardness and particle size tend to reach a saturation value at this stage, called the steady-state processing stage. With further

milling, true alloying occurs at the atomic level resulting in the formation of solid solutions, intermetallics, or even amorphous phases. The layer spacing becomes so fine or disappears at this stage that it is no longer visible under an optical microscope (Öveçoğlu, 1987; Suryanarayana, 2001)

Considering ductile-brittle combinations, in the initial stages of milling, the ductile metal powder particles get again flattened by the ball-powder-ball collisions, while the brittle oxide or intermetallic particles get fragmented. These fragmented brittle particles tend to become occluded by the ductile constituents and trapped in the ductile particles. The brittle constituent is closely spaced along the interlamellar spacings in Figure 2.13 (Öveçoğlu, 1987). With further milling, the ductile powder particles get work hardened, the lamellae get twisted, and refined (Figure 2.13 b). With continued milling, the lamellae get further refined, the interlamellar spacing decreases, and the brittle particles get uniformly dispersed, if they are insoluble, in the ductile matrix (Figure 2.13 c) (Öveçoğlu, 1987; Suryanarayana, 2001). On the other hand, if the brittle phase is soluble, alloying occurs between the ductile and brittle components also and chemical homogeneity is achieved (Suryanarayana, 2001).

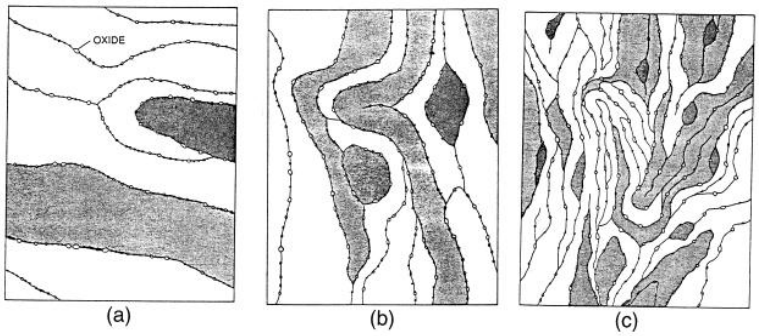

Figure 2.13: Schematics of microstructural evolution during milling of a ductile-brittle combination of powders. This is typical for oxide dispersion strengthened alloys (Suryanarayana, 2001).

If a brittle-brittle combination is the case, it would appear that it is unlikely that alloying occurs in a system consisting of two or more brittle components. The reason for that is that the absence of a ductile component prevents any welding from occurring, and in its absence, alloying is not expected to ocur (Coşkun, 2006). However, alloying has been reported to occur in brittle-brittle component systems such as Si-Ge and Mn-Bi or Fe_2O_3-Cr_2O_3 and ZrO_2-Y_2O_3 (Suryanarayana, 2001;

Fecht, 2002). Milling of mixtures of brittle intermetallics also produced amorphous phases. During milling, the brittle components get fragmented and their particle size gets reduced continuously. However, at very small particle sizes the powder particles behave in a ductile fashion, and further reduction in size is not possible. This is termed the limit of comminution. Furthermore, during milling of brittle-brittle component systems, it has been observed that the harder (more brittle) component gets fragmented and gets embedded in the softer (less brittle) component (Suryanarayana, 2001).

Nanostructured materials that are defined as materials with grain sizes less than 100 nm have received much attention as advanced engineering materials with improved physical and mechanical properties (El-Eskandarany, 2001). Because of the extremely small size of the grains, a large fraction of the atoms in these materials is located in the grain boundaries and as a result the material exhibits enhanced combinations of physical, mechanical, and magnetic properties (compared to material with a more conventional grain size, i.e., >1 μm) (Fecht, 2002) (Suryanarayana, 2001). Nanostructured materials have increased strength, high hardness, extremely high diffusion rates, and consequently reduced sintering times for powder compaction (Suryanarayana, 2001).

Recently, MA process has become a popular method in fabrication of nanocrystalline materials due to its simplicity and relatively inexpensive equipment (El-Eskandarany et al., 2000; El-Eskandarany, 2001). The advantage of using MA for the synthesis of nanocrystalline materials lies in its ability to produce bulk quantities of material in the solid state using simple equipment and at room temperature (Suryanarayana, 2001). In this process, lattice defects are produced by pumping energy into powder particles of typically 50 μm particle diameter. This internal refining process with a reduction of the average grain size by a factor of 10^3-10^4 results from the creation and self organization small-angle and high-angle grain boundaries within the powder particles during the mechanical deformation process (Fecht, 2002). Grain sizes with nanometer dimensions have been observed in almost all MA'd pure metals, intermetallics, and alloys (Suryanarayana, 2001). The elemental processes leading to the formation of nanostructures include three basic stages. Firstly, the deformation is localized in shear bands which contain a high dislocation density (Fecht, 2002). Their typical width is approximately 0.5-1 μm (Suryanarayana, 2001). At a certain

level of strain within the high strained regions, these dislocations annihilate and recombine to small-angle grain boundaries separating the individual grains (Fecht, 2002). This results in a decrease of the lattice strain. With the continuing process, deformation occurs in shear bands located in previously unstrained parts of the material. The grain size decreases steadily and the shear bands unite. The small angle boundaries are replaced by higher angle grain boundaries and, consequently, dislocation-free nanostructured grains are formed (Suryanarayana, 2001).

2.2.2 Sintering

Sintering is a processing technique used to produce density-controlled materials and components from metal or/and ceramic powders by applying thermal energy (Kang, 2005). In sintering, particles bond with one another by atomic diffusion. There are different variables which determine sinterability and the sintered microstructure of a powder compact which given in Table 2.1 (Kang, 2005). All sintering equations contain a number of parameters such as diffusion coefficient, surface tension, particle size, initial pore volume, etc. One can divide these parameters into two classes as: a) intrinsic and b) extrinsic (Upadhyaya, 2001).

1. Intrinsic - these specify the intrinsic properties of the materials being sintered, such as surface tension, diffusion coefficient, vapour pressure, viscosity, etc. These properties change when the chemical composition, ambient atmosphere or temperature changes (Upadhyaya, 2001).

2. Extrinsic - these depend on the geometrical or topological details of a system. These include parameters, as average particle size, particle or pore or grain shape and size distribution, etc (Upadhyaya, 2001).

The driving force for sintering is the minimization of the solid-vapor interface area (i.e., the total area of the powders in contact with the surrounding vapor) and elimination of the regions of sharp curvature at powder contacts. In the initial stages of sintering, small necks form and grow between contacting particles by mass transfer via atomic diffusion. Fine powders increase the driving force for sintering because of a larger surface area per unit volume, which increases the total solid-vapor interfacial energy (Asthana et al., 2006).

Table 2.1: Variables affecting sinterability and microstructure (Kang, 2005).

Variables related to raw materials (material variables)	Powder: Shape, size, size distribution, agglomeration, etc. Chemistry: Composition, impurity, homogeneity, etc.
Variables related to sintering conditions (process variables)	Temperature, time, pressure, atmosphere, heating and cooling rate, etc.

Basically, sintering processes can be divided into two types as: solid state sintering and liquid phase sintering. Solid state sintering occurs when the powder compact is densified wholly in a solid state at the sintering temperature, while liquid phase sintering occurs when a liquid phase is present in the powder compact during sintering (Kang, 2005).

2.2.2.1 Solid state sintering

Solid-state sintering is carried out in protective atmosphere within a furnace at a temperature below the melting point of the base metal. The process leads to a decrease in the surface area, an increase in compact strength and mostly shrinkage in the compact. Sintering for longer durations at high temperature decreases the number of pores and makes the pore shape become smooth. Also, grain growth can be expected (Upadhyaya, 2000).

Various stages and mass transport mechanisms have been proposed to contribute to sintering, as seen in Figure 2.14 **(**Uphadhyaya, 2000; Rahaman, 2005; German, 1996; Ring, 1996). The transport mechanisms detail the paths by which mass moves; for solid-state sintering the candidate processes include surface diffusion, volume diffusion, grain boundary diffusion, viscous flow, plastic flow, and even vapor transport from solid surfaces (German, 1996).

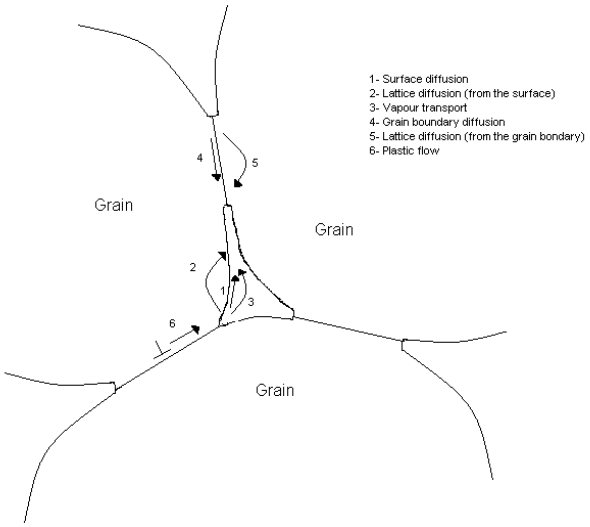

Figure 2.14: Various sintering mechanisms (Uphadhyaya, 2000).

The three stages of sintering and and their schematic densification curve of a powder compact can be seen in Figure2.15 (Kang, 2005). In addition to these three stages, a very first stage occurs when particles come into contact, since there is a weak cohesive cohesive bond at the contacts (German, 1996). The initial sintering stage usually occurs during heating and is characterized by rapid grain growth of the interparticle neck. Although there is a considerable neck growth, the actual volume of the neck is small, so, it takes a small mass to form a neck. In the intermediate stage, the pore structure becomes smooth and develops an interconnected, approximately cylindrical nature. The appearance of isolated pores indicates the final stage of sintering and slow densification (German, 1996).

The three stages of sintering can be described with the highlights listed below:

Initial Stage: Particle surface smoothing and rounding of pores, grain boundaries form, neck formation and growth, homogenization of segregated material by diffusion, open pores and small porosity decreases <12% (Ring, 1996; German, 1996).

Intermediate Stage: Intersection of grain boundaries, shrinkage of open pores, porosity decreases substantially, slow grain growth and differential pore shrinkage and grain growth in heterogeneous material (Ring, 1996, German, 1996).

Final Stage: Closed pores--density >92%, closed pores intersect grain boundaries, pores shrink to a limiting size or disappear and pores larger than the grains shrink very slowly (Ring, 1996, German, 1996).

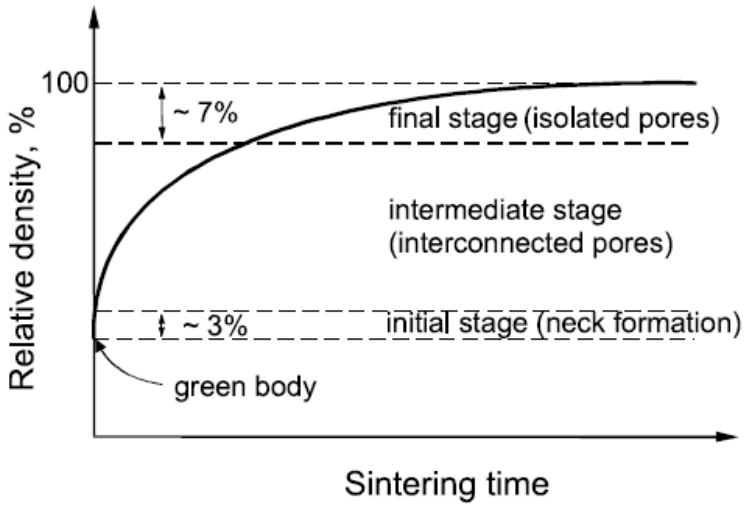

Figure 2.15: Schematic showing the densification curve of a powder compact and the three sintering stages (Kang, 2005).

2.2.2.2 Liquid phase sintering

Liquid phase sintering is a consolidation technique of powder compacts containing more than one component at a temperature above the solidus of the components and hence in the presence of a liquid (German, 1985). Unlike solid state sintering, the microstructure change during liquid phase sintering is fast because of fast material transport through the liquid (Kang, 2005). It is rare that sintering with liquid phase does not imply any chemical reactions, but in the simple case where these reactions do not have a marked influence, surface effects are predominant. The main parameters are therefore: i) quantity of liquid phase, ii) its viscosity, iii) its wettability with respect to the solid, and iv) the respective solubilities of the solid in the liquid and the liquid in the solid (Boch and Leriche, 2001).

There are two kinds of liquid phase sintering namely liquid phase sintering in heterogeneous systems and homogeneous systems. (Uphadhyaya, 2000; German, 1985). In heterogeneous systems, solid material is heated to sintering temperature and a liquid phase is formed which persists throughout sintering and the liquid solidified during cooling. In case of homogeneous systems, as the consalidated powders are heated to sintering temperatures, a liquid phase is formed which gradually disappears as it is soluble in the matrix. Particle rearrangement stage, dissolution-reprecipitation stage, liquid assimilation and solid state grain growth stage are the four main stages of liquid phase sintering process (Ring, 1996).

Modern liquid-phase sintering processes originated with the developement of cemented carbides, bronze bearings and magnetic alloys during 1920s (Uphadhyaya, 2000; German, 1996**)** The developement of Tungsten (W) heavy alloys (W-Ni-Fe or W-Ni-Cu) provided an important theoretical basis fort he process. Today, many products are processed by liquid-phase sintering, including dental porcelains, cemented carbide cutting tools, automotive connection rods and refractory ceramics (German, 1996).

2.2.2.3 Activated sintering

Activated sintering involves a small addition to the powder mix or, more rarely, to the sintering atmosphere in order to promote sintering kinetics. The action of the activator may be to remove the surface oxide from the powder particles or to facilitate more rapid diffusion of the metal's atoms (Upadhyaya, 2000). A high-melting-temperature materials require a high sintering temperature to induce significant diffusion. However, a lower-melting-temperature phase will have inherently faster diffusion rates. Activated sintering occurs when the high-melting-temperature material is soluble in the low-melting-temperature phase, resulting is a short-circuit sintering path. Some of the most dramatic examples of activated sintering occur with the refractory metals like molybdenum, tungsten, chromium, rhenium, and tantalum (German, 1996).

Generally, it is very difficult to fabricate tungsten (W) because of its high melting point and low ductility. Even when the powder metallurgy techniques are used, processing of W requires very high sintering temperatures up to 2400 – 2800 ^{o}C to get nearly full dense structure (Li and German, 1983). The addition of small quantities of some transition metals such as palladium (Pd), platinum (Pt), nickel (Ni), cobalt (Co), and iron (Fe), provides a major reduction in the sintering temperature of W (Li and German, 1983; German and Munir, 1976; Vacek, 1959; Hayden and Brophy, 1963). This reduction of the sintering temperature is due to the decrement of the activation energy between W particles. Activation energy for volume self-diffusion of tungsten, 135 kcal/mol, becomes 68 kcal/mol in the case of Ni activated W (Hayden and Brophy, 1963).

Hayden and Brophy interpreted the mechanism of the activated sintering in terms of three main stages in their study (Hayden and Brophy, 1963). After the appearance on

the tungsten particle surface of a “supporting phase”, formed by activating agent, the dissolution of W at the points of contact between particles takes place and the diffusion of tungsten atoms along the interface between the “supporting phase” and the particle provides densification. On this basis, the distance between the centers of adjacent particles decreases and consequently fuller shrinkage occurs (Hayden and Brophy, 1963; Samsonov and Yakovlev, 1967). Fig. 2.16. is a schematic representation showing the sintering of nickel-coated tungsten powder which Brophy et. al., indicated during their project prepared in U.S. Navy in M.I.T. laboratories (Brophy et. al, 1963).

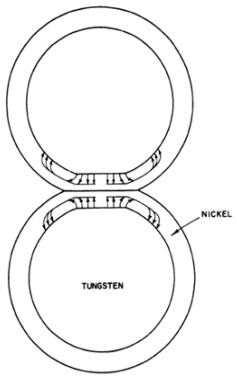

Figure 2.16: Schematic representation of sintering nickel-coated tungsten powder (Brophy et. al., 1963).

Another elucidation of the activated sintering mechanism was accomplished (Toth and Lockington, 1967) where dissolution of tungsten at the activator-tungsten interface is followed by volume diffusion outwards through the activator layer and subsequent surface diffusion. Diffusion through the activator layer to the contact point between adjacent particles results in the formation of sintering “necks” (Toth and Lockington, 1967; Corti, 1986).

Samsonov and Yakovlev stated activated sintering in terms of the electron structure of the activators and tungsten; an increase of the stable d-bonds in the system lowers the free energy, activating the sintering process in which diffusion is accelerated by the activators for which tungsten acts as an electron donor and this ease of electron transfer gives rise to the high solubility in the activating element (Samsonov and Yakovlev, 1969).

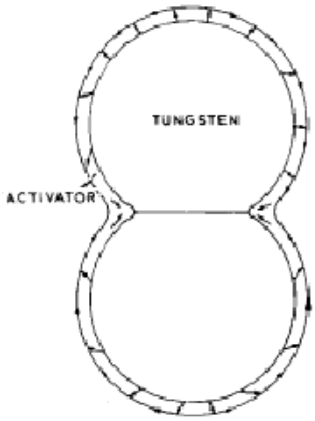

Figure 2.17: Schematic representation of activated sintering of tungsten (Toth and Lockington, 1967).

German and Munir reported that the activator has a role in providing enhanced grain boundary diffusion with the activator layer wetting the interparticle grain boundary. The relative solubility criterion is a prerequisite for enhanced diffusion of the refractory metal. Enhanced mass transport, and hence densification, results from the lowering of the activation energy for the refractory metal in the activator (German and Munir, 1982; Corti, 1986).

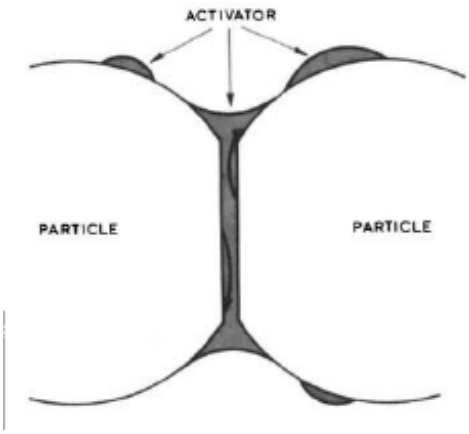

Figure 2.18: Schematic representation of the activated sintering (German and Munir 1982).

3. MATERIALS SELECTION

The matrix of the composites has to be chosen considering two main requirements, matrix has to bind and support the reinforcing phase and, secondly, to satisfy special properties based on the requirements in service. Binding strength between the matrix, whose main function is to transfer and distribute the load to the reinforcement, and the reinforcement depends on the type of matrix and reinforcement (Huda et al., 1995; Lindroos et al., 2004). Matrix-reinforcement interface has significant importance due to its role of determining load transfer and crack resistance of the composite during deformation. It is now widely known that in order to maximize interfacial bond strength, it is necessary to promote wetting (when a liquid phase process is present), control chemical interactions and minimize oxide formation (Ibrahim et al., 1991). On the other hand, the hardness of the matrix is the key factor in supporting the reinforcing phase. Generally, Al, Ti, Mg, Ni, Cu, Pb, Fe, Ag, Zn, Sn and Si are used as the matrix materials (Huda et al., 1995). In addition to these, tungsten (W) has lately received some attention as a matrix material (Song et al., 2002; Song et al., 2003b).

Reinforcement phase in the composites are mainly used to increase the strength, stiffness, temperature resistance capacity and to lower the density. Generally, ceramics are used as the reinforcement phase, which are typically oxides, carbide and nitrides (Huda et al., 1995). Selection criteria for these ceramic reinforcements include elastic modulus, tensile strength, density, melting temperature, thermal stability, coefficient of thermal expansion, size and shape, compatibility with matrix material and cost (Ibrahim et al., 1991). Common reinforcement elements are Common reinforcement elements are TiC, ZrC, SiC, Y_2O_3, Al_2O_3, B_4C and Si_3N_4 (Huda et al., 1995).

3.1 Tungsten

The refractory metals are conveniently described as metals that melt at temperatures above 1850 °C, and for this consideration, twelve metals are in this group namely: tungste (W), rhenium (Re), osmium (Os), tantalum (Ta), molybdenum (Mo), iridium (Ir), niobium (Nb), ruthenium (Ru), hafnium (Hf), rhodium (Rh), vanadium (V), chromium (Cr). Among these, due to their high melting point, high modulus, high resistance of thermal shock, low CTE and good high temperature strength and stiffness properties, tungsten alloys are potential candidates for service conditions which require high strength at elevated temperatures (Song et al., 2002). Properties of tungsten are listed in (Lassner and Schubert, 1999).

A large number of W alloys and composites were investigated in literature before, whereas only some of them achieved technical importance. The aim of alloying W is to improve its chemical, physical and mechanical properties at both ambient conditions and at elevated temperatures. However, alloying of W has been relatively less studied than of some of the other refractory metals. W is mainly used in aerospace applications in the unalloyed form which is much easier and cheaper to produce and fabricate. Also, it has been found that, particularly at temperatures above 2200°C, the strengthening effects of many alloying agents decrease disproportionately (Lassner and Schubert, 1999).

W is mainly consumed in three forms, which are W carbide, alloying additions and pure form. Tungsten carbide (WC) accounts for about 65% of W consumption (Lassner and Schubert, 1999). It is combined with cobalt as a binder to form the so-called cemented carbides, which are used in cutting and wear applications because of their high hardness, good wear resistance, good fracture resistance and high temperature strength (Zhang et al., 2003) Cemented carbides such as WC-Co and WC-Co-TiC are the most widely used material for metalworking. As a consequence, a considerable amount of research effort has been spent to develop alternative cemented carbide systems in order to improve the microstructure and mechanical properties of these materials (Acchar et al., 2004). Characteristically, most of the carbides used in cermets have high hardness, good electrical and thermal conductivity, and high stability. The brittleness of carbides, however, has prevented their use as single-phase materials in highly stressed structural applications and has

led to the development of metal-bonded composites (cemented carbides or cermets) (Coskun, 2006).

Table 3.1: Properties of W (Lassner and Schubert, 1999).

Period	6
Atomic Number	74
Atomic Mass	183.85
Electronegativity	1.7
Space Group	Im3m
Lattice Parameter	3.16524 Ao
Density	19.3 g/cm3
Melting Point	3422 Co
Boiling Point	5663 Co
Specific Heat	0.0317 cal/gK
CTE	4.32-4.68x10-6 K-1 (25 oC)
Tensile Strength	172.4 MPa
Young's Modulus	390-410 GPa
Shear Modulus	156-177 GPa
Bulk Modulus	305-310 GPa
Poisson' Ratio	0.28-0.30
Hardness	350-450 kg/mm2

Metallic W and W alloy mill products account for about 16% of consumption. W and W alloys dominate the market in applications for which a high-density material (19.3 g/cm3) is required, such as kinetic energy penetrators, counterweights, flywheels, and governors. Tungsten and its alloys are also used in radiation shields and x-ray targets. Also in wire form, W is used extensively for lighting, electronic devices, and thermocouples (Lassner and Schubert, 1999; Li and German, 1983).

The high melting point of W makes it an obvious choice for structural applications exposed to very high temperatures. W is also used at lower temperatures for applications that can use its high elastic modulus, density, or shielding characteristics to advantage (Lassner and Schubert, 1999).

3.2 Tungsten Alloys and Composites

Three tungsten alloys are produced commercially: tungsten-titanium, tungsten-tantalum, and tungsten-rhenium (Lassner and Schubert, 1999).

Re is the most important alloying element for tungsten. Re additions increase the ductility at low temperatures and also improve the high temperature strength and plasticity. Moreover, Re additions stabilize the grain structure, increase the recrystallization temperature and improve the weldability. It also improves the corrosion resistance of tungsten (Park, 1993). On the other hand, tantalum-tungsten alloys combine the good corrosion resistance and high elasticity of tantalum with the better high temperature strength of tungsten and tungsten-titanium alloy is used as a sputtering target in the manufacture of microelectronics devices (Lassner and Schubert, 1999).

Another type of tungsten alloys are the tungsten heavy-metal alloys (WHA's). These are a category of tungsten-base materials that typically contain 90 to 98 wt % W in combination with some mix of nickel, iron, copper, and/or cobalt (Ryu and Hong, 2003.). The bulk of WHA production falls into the 90 to 95% W range. As a consequence, WHA's gain their basic properties from those of the tungsten phase, which provides both high density and high elastic stiffness. These are the two properties that give rise to must applications for this family of materials (Lassner and Schubert, 1999).

Currently WHA's are used in various applications. These applications include; damping weights for computer disk drive heads, balancing weights for ailerons in commercial aircraft, helicopter rotors, and for guided missiles, kinetic energy penetrators for defeating heavy armor, fragmentation warheads, radiation shielding, radio isotope containers for cancer therapy devices, weight distribution adjustment in sailboats and race cars (Lassner and Schubert, 1999; Ryu and Hong, 2003).

The first WHA developed was a W-Ni-Cu alloy. Alloys of this ternary system are still occasionally used today, primarily for applications in which ferromagnetic character and electrical properties must be minimized. W-Ni-Cu alloys otherwise offer inferior corrosion resistance and lower mechanical properties than the present industry standard W-Ni-Fe alloys (Lassner and Schubert, 1999).

The majority of current uses for WHA's are best satisfied with the W-Ni-Fe system. Alloys such as 93W-4.9Ni-2.lFe and 95W-4Ni-lFe represent common compositions. The addition of cobalt to a W-Ni-Fe alloy is a common approach for slight enhancement of both strength and ductility. The presence of cobalt within the alloy provides solid-solution strengthening of the binder and slightly enhanced tungsten-matrix interfacial strength. Cobalt additions of 5 to 15% of the nominal binder weight fraction arc most common (Lassner and Schubert, 1999).

For extremely demanding applications, even higher mechanical properties are obtainable from the W-Ni-Co system with nickel-to-cobalt ratios ranging from 2 to 9. Such alloys require resolution/quench, however, due to extensive intermetallic (Co_3W and others) formation on cool down from sintering (anonymous, 2005d; Lassner and Schubert, 1999). A number of special WHA's are known as well. An example is the W-Mo-Ni-Fe quaternary alloy, which utilizes molybdenum to restrict tungsten dissolution and spheroid growth, resulting in higher strengths (but reduced ductility) in the as-sintered product (Lassner and Schubert, 1999).

Beside these alloys, there are tungsten dispersion-strengthened and precipitation hardened composites. First, non-sag tungsten (tungsten doped with potassium) which is used as filaments in lamps is one kind of dispersion-strengthened composites, which have excellent creep resistance. The term non-sag refers to the resistance of the material against deformation (sagging) under its own weight at incandescent temperatures (Lassner and Schubert, 1999).Furthermore, there are oxide-dispersion-strengthened tungsten composites. The addition of small amounts of finely dispersed oxides increases the mechanical properties of tungsten. The most common one is the W-ThO_2 alloy which contains a dispersed second phase of 1 to 2% thorium. The thorium dispersion enhances thermionic electron emission, which in turn improves the starting characteristics of gas tungsten arc welding electrodes. It also increases the efficiency of electron discharge tubes and imparts creep strength to wire at temperatures above one-half the absolute melting point of tungsten (Mabuchi et al, 1997; Lassner and Schubert, 1999; Chen et. al, 2000). However, it is desirable to replace ThO_2 with non-radioactive activators because of the radioactive pollution of thorium during fabrication, service or handling. In the last decade, considerable efforts have been directed to develop new materials, especially to explore new activators. It has been found that tungsten electrodes activated with rare-earth metal

oxides (such as La_2O_3, Y_2O_3, CeO_2, etc.) exhibit superior arc characteristics compared to pure W and W-ThO_2 electrodes (Chen et al, 2000). Particularly, W-La_2O_3 composites exhibit good mechanical properties and have no radioactive potential (Mabuchi et al, 1997). Furthermore, there are studies about strengthening the WHA's by adding Y_2O_3. As a result, the strength of WHA's are improved with decreasing particle size which is proportional to the Y_2O_3 content (Ryu and Hong, 2003.).

Finally, there are carbide-dispersion-strengthened tungsten composites. Hafnium carbide (HfC) is the strongest strengthener for tungsten at elevated temperatures. The outstanding strength of HfC is attributed to its high thermodynamic stability and its comparatively low solubility and diffusivity in tungsten at high temperatures. Furthermore, W-Re alloys strengthened with HfC are the strongest man-made metallic materials at temperatures above 2000 K (Park, 1993; Lassner and Schubert, 1999). There are also other carbides, such as TaC, NbC, ZrC and TiC used as dispersoids (Lassner and Schubert, 1999). Recently, mechanical and thermophysical and ablation properties of TiC/W and ZrC/W at elevated temperatures are studied As a result, it is proved that both of them possess excellent high temperature strength and good thermophysical properties, which make them good candidates for high temperature applications (Song et al, 2002; Song et al, 2003a; Song et al, 2003b).

3.3 Ni-Activated Sintering and W-Ni System

Activated sintering mechanism is explanied in detail in Section 2.2.2.3, stating that addition of small quantities of some transition metals such as Pd, Pt, Ni, Co, and Fe enables major reductions in the sintering temperature of W. One of the activating agents, Ni, dissolves up to 38 wt % W in its solid solution and the solubility of W into Ni is only about 0.1 wt % which is negligible (Massalski, 1990). Moreover, the volume diffusion of W into Ni is rather more rapid than that of Ni into W (Panichkina, 1967). Hayden and Brophy reported a value of 68 kcal/mole for the activation energy for volume self-diffusion of W in the case of activated sintering with Ni, a value much lower than 135 kcal/mole pertaining to pure W (Hayden and Brophy, 1963).

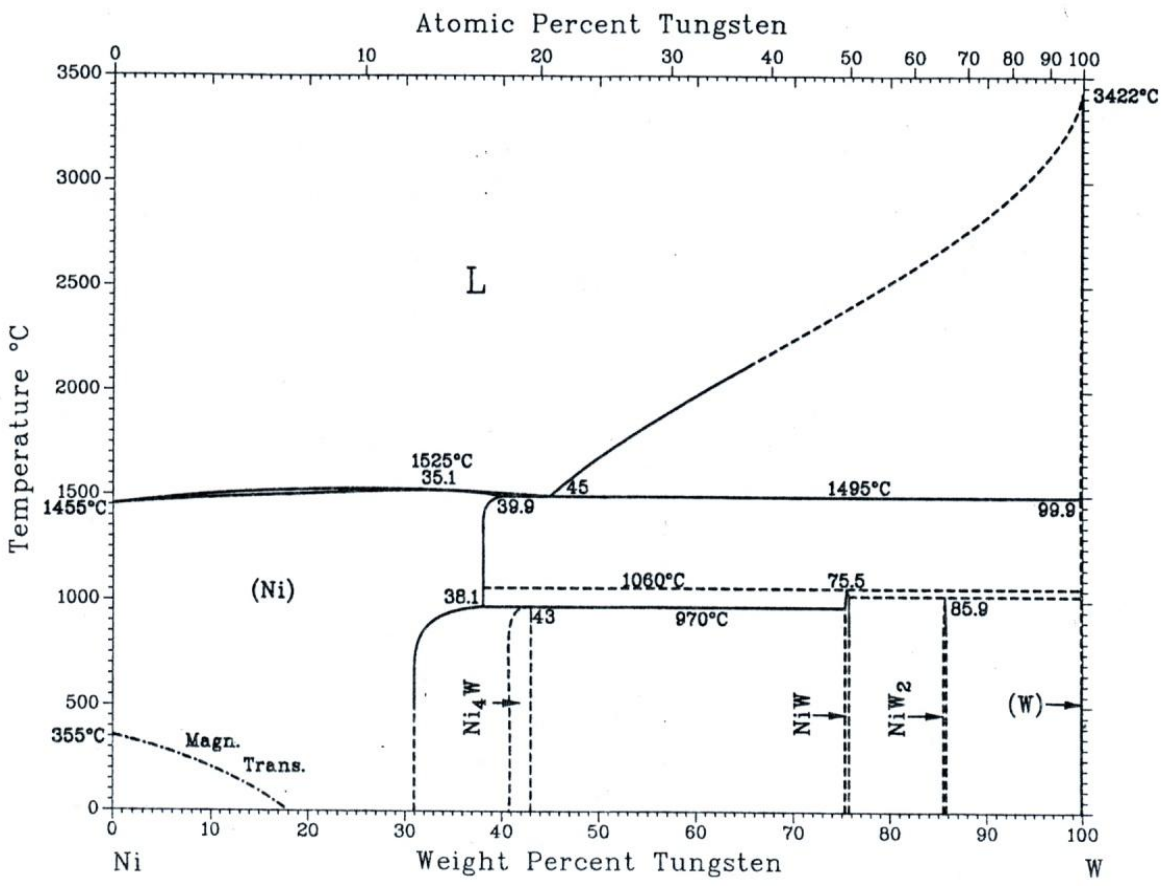

Figure 3.1: Ni-W binary phase diagram (Massalski, 1990).

Activated sintering of W with different transition metal additions have been extensively investigated in the archival literature. German and Munir reported that Pd is the best activator agent for W, and sequentially, Ni, Pt, Co, Fe, Cu addition provides activation (German and Munir, 1976). Even though Pd has been reported as the best activator for W, however its use is limited due to its very high price. Ni is the proper activator agent which can be used instead of Pd, especially at temperature ranges about 1400 ºC(German and Munir, 1976).

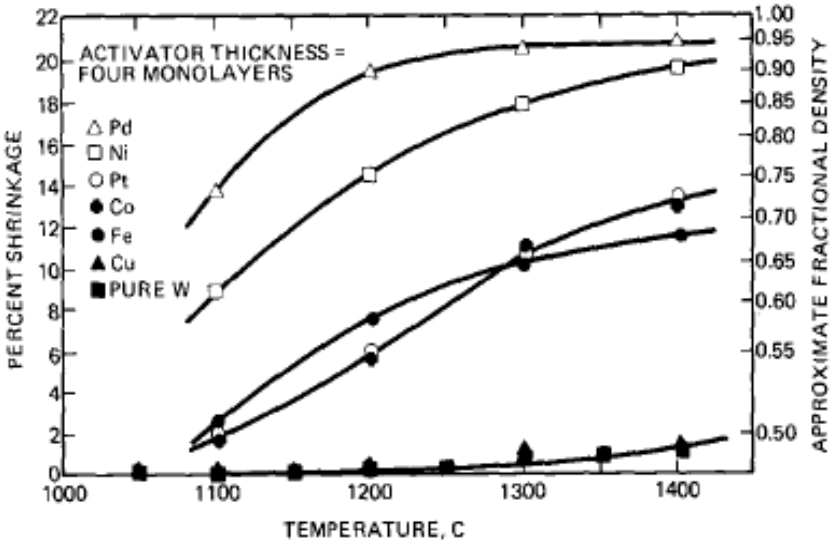

Figure 3.2: Shrinkage dependence on activator type and temperature in activated sintering of W (German and Munir, 1976).

3.4 The Addition of WB and La2O3

In order to improve properties of W, dispersion-strengthened and precipitation hardened composites were developed (Lassner and Schubert, 1999). Investigations regarding the activated sintering of W and W matrix composites reinforced with different refractory carbide, nitride and oxide phases such as TiC, TiN, ZrC, HfC, La_2O_3, Y_2O_3, HfO_2, Sm_2O_3, and ThO_2 have been well documented in the literature (Chen et al., 2009; Genc et al., 2010; Ishijima et al., 2005; Kim et al., 2006; Kurishita et al., 2008; Song et al., 2003b). In addition to these refractory carbide, nitride and oxide materials, transition metal borides are very promising candidates as reinforcements in W due to their high melting point, high hardness, good electrical and thermal conductivities (Munro, 2000). An important advantage of borides over carbides and nitrides is that borides are essentially stoichiometric (Castaing and Costa, 1977). However, there exists no studies in the reported literature on the microstructural and mechanical properties of metal borides reinforced W matrix composites. Among the metal borides, tungsten boride (WB) comes into prominence with its excellent properties such as high melting point, high hardness ($2600Kg/mm^3$), high electrical conductivity and considerable chemical stability.

Tungsten borides have promising characteristics like high melting point, high hardness values (>9 Mohs), high abrasion resistance, chemical inertness, magnetic properties and metal-like electronic conductivity (Lassner and Schubert, 1999). These characteristics have made tungsten borides interesting candidates for industrial applications as abrasive, corrosion-resistant and electrode metarials, which are exposed to exceptional environmental conditions (Coşkun, 2011). Tungsten borides are resistant to thermal shock and good thermal conductor. They are used in temperature applications such as crucibles andingot molds for precision metallurgy (Usta et al., 2005). Moreover tungsten borides are used for developing various composite materials, including metal-boride alloys for filler (borolites) (Gostishchec et al., 2009). W_2B_5 phase has lately been used to improve the thermoelectric properties of B4C ceramics, to improve the electrical conductivity, wear and oxidation resistance, flexural strength anf fracture toughness of carbon composites (Coşkun, 2011). Some physical properties of selected tungsten borides are given in Table 3.2.

Table 3.2: Some physical properites of selected tungsten borides dapted from Lassner and Schubert (1999) and Schackelford and Alexander (2001).

Properties	**W2B**	**WB**	**W_2B_5**
Melting Point (°C)	2780	2920	2980
Enthalpy of Formation- ΔH °298 (kj/mol)	65.3	54.5	192.5
Density (g/cm^3)	17.05	16	13.1
Microhardness (kg/mm^3)	2350	2600	2700
Electrical Resistivity (μ.Ω.cm)	-	25	19
Modulus of Elasticity (GPa)	-	608	755

Above mentioned literature review presented the development of dispersion strenghtened W matrix composites and activated sintering of W. However, there are no detailed studies about the sintering behaviour and microstructural properties of dispersion strengthened W-based composites sintered with the presence a transition

metal borides or both of a transition boride and rare-earth oxide. This study aims to fulfill this gap by focusing on sintering behaviour and mechanical properties of mechanically alloyed and Ni activated sintered WB_2 and La_2O_3 composites. Thus, the objective of the present study is to report on the microstuctural characterization and physical properties of mechanically alloyed and Ni activated W-WB and W-TiB_2-WB composites prepared by mechanical alloying technique.

4. EXPERIMENTAL PROCEDURE

Experimental investigations were carried out in order to develop Ni activated sintered W-WB and W-WB-La_2O_3 composites produced via mechanical alloying and to get better understanding about sintering behavior, microstructural and mechanical properties of developed W-Ni-WB and W-Ni-WB-La_2O_3 composites.

The first group of experiments are the characterization investigations of W-1 weight (wt)% Ni. Effects of different WB additions to the W-1 wt % Ni powders were investigated in the second set of experiments. The third set of experiments investigated the effect of duration of mechanical alloying. Finally, the fourth group of experiments were conducted to reveal the effects of La_2O_3 addition to the W-1 wt.% Ni-2 wt % WB powders. Additionally, all groups of experiments investigate the same sintering regimes on determined composition.

The experimental procedure of the present study is summarized in the flow chart shown in Figure 4.1.

4.1 Preparation of Samples

4.1.1 Mechanical alloying and characterization of powders

In this study elemental tungsten (W) powders (99.9% purity, 4-7 μm average particle size) were used as the matrix of the composite. Tungsten boride (WB) (99.5% purity, 4-6 μm average particle size) and lanthanum oxide (La_2O_3) (%99.99 purity, 25-34 μm average particle size) powders as reinforcement and 1 wt % nickel (Ni) powders (99.9% purity, 3-7 μm average particle size) as activating agent were used to avoid the grain growth and to improve mechanical properties.

Mechanical alloying (MA) experiments were carried out for 3 h, 6 h, 12 h, 18 h and 24 h in a tungsten carbide (WC) vial with WC balls having a diameter of 6.35 mm (¼ inches). The ball-to-powder (BPR) weight ratio was 7:1. W - 1wt % Ni powders were blended and mechenically alloyed (MA'd) for 18 h. W-1 wt % Ni - x wt % WB (x=0.5, 1, 2, 4), and W1Ni - 2 wt % WB - y wt % La_2O_3 (y=0.5, 1) powders (were

mixed and MA'd for 18 h. Moreover, W-1 wt % Ni-2 wt % WB were blended and MA'd for 3 h, 6 h, 12 h, 18 h and 24 h for which both effects of MA and activated sintering were investigated.

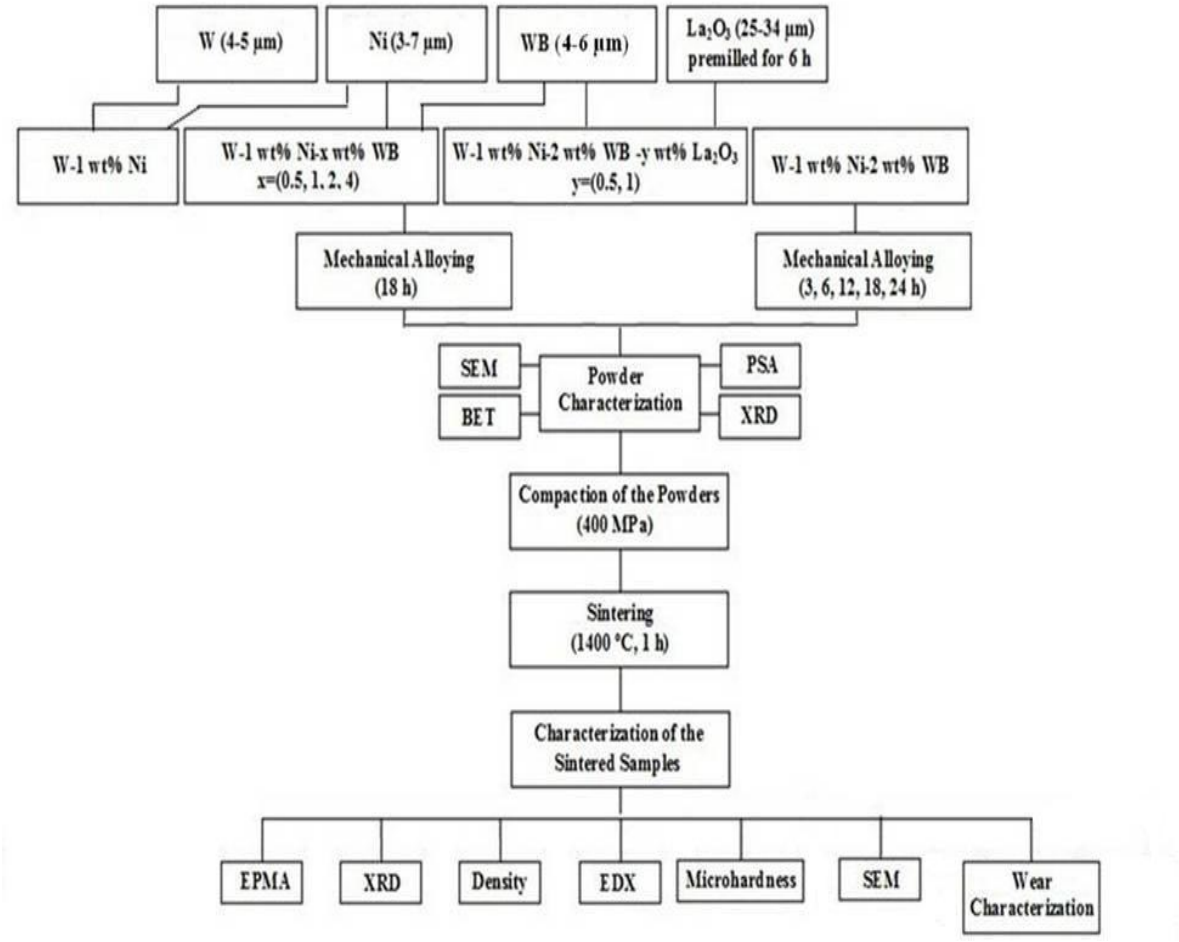

Figure 4.1: The flow chart of the experimental procedure.

Mechanical alloying (MA) experiments were carried out using a Spex™ Duo Mixer/Mill 8000D with a speed of 1200 rpm (Figure 4.2.a). Mechanical alloying (MA) experiments were carried out using a Spex™ Duo Mixer/Mill 8000D with a speed of 1200 rpm High-purity argon was chosen as the milling atmosphere to prevent oxidation and contamination of powder since the presence of air in the vial causes to produce oxides and nitrides in the powder, especially if the powders are reactive in nature. Thus, loading and unloading of the powders into the vial was carried out inside a "Pluslabs™" atmosphere-controlled glove box (Figure 4.2b) in Ar atmosphere.

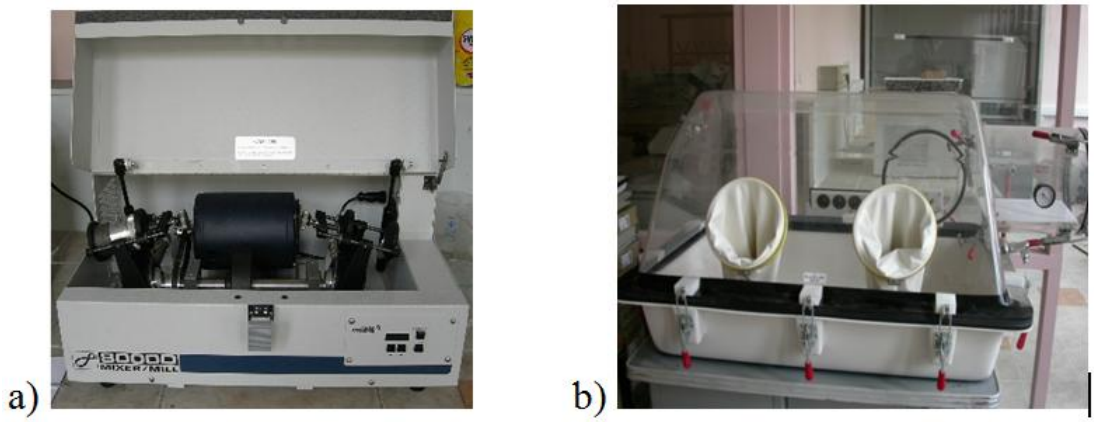

Figure 4.2: a) 8000D™ Spex mill, **b)** Pluslabs™ glove box.

Powder particle size measurements were carried out in a Malvern™ Mastersizer Laser particle size analyzer (Figure 4.3a). Microstructural characterization investigations of MA'd powders were conducted using a Zeiss™ EVO MA scanning electron microscope (SEM) and a PANalytical X'Pert Pro Diffractometer (Figure 4.3b) (XRD) using CuK_{α} radiation at 45 kV and 40 mA. Specific surface area measurements of MA'd powders were made using Quantachrome™ by the Brunauer, Emmett and Teller (BET) method of adsorption of nitrogen gas.

Figure 4.3: a) Malvern™ Mastersizer, **b)** Bruker™ X-Ray Diffractomete (XRD).

4.1.2 Compaction

The mechanically alloyed powders were compacted by cold pressing in a tool-steel die at a pressure of 400 MPa into cylinder shaped green compacts with a diameter of ≈6.36 mm for 1 minute by using a 10 ton capacity "MSE" one-action hydraulic

press. Figure 4.4 shows the picture of the MSE hyraulic pres. Stearic acid was applied onto the walls of the die to take the samples out of the die easily.

Figure 4.4: The Picture of MSE one-action hydraulic press.

4.1.3 Sintering

Sintering was performed at 1400 ^{o}C for 1 hour in a Linn™ 1800 M Vac Graphite furnace. The furnace works under gas sintering conditions using vacuum and H_2, Ar and N_2 gases as sintering media. The sintering regime is shown in Figure 4.5.

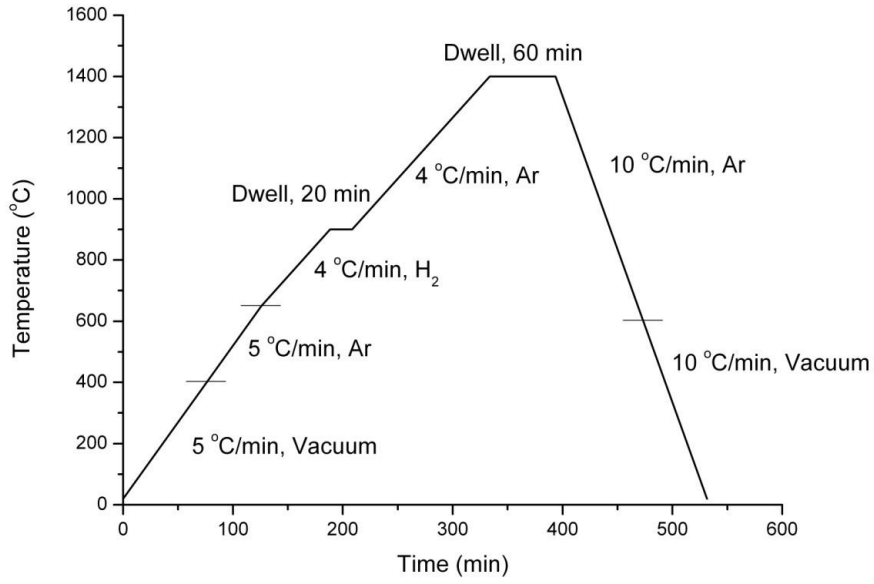

Figure 4.5: The sintering regime in the 1800 M Vac Graphite Linn™ furnace.

4.2 Characterization of Sintered Samples

4.2.1 Microstructural and phase characterization

Microstructural and phase characterization investigations of the sintered samples were carried out using a Hitachi™ 1000 scanning electron microscope (SEM), energy dispersive spectroscopy (EDS) and X-ray diffraction (XRD) techniques. Prior to the characterization investigations, the sintered samples were mounted in bakelite using the Struers™ Labopress-1 machine (Figure 4.6a). After that, samples were polished on the Struers™ Tegrapol-15 automatic polishing machine (Figure 4.6b).

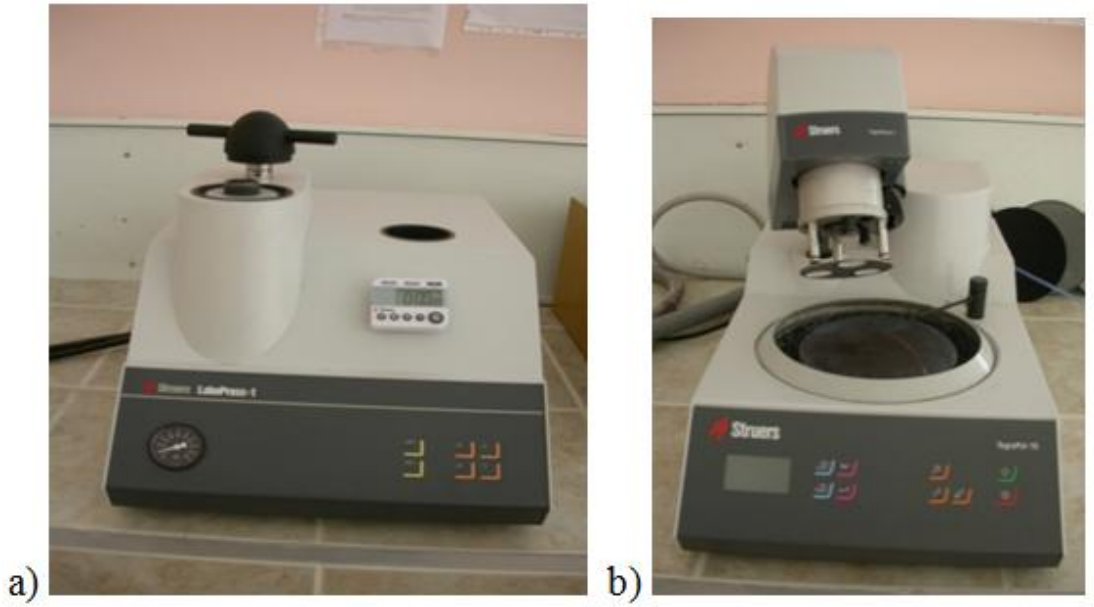

Figure 4.6: a) Struers™ Labopress-1 machine and **b)** Struers™ Tegrapol-15 automatic polishing machine.

For detailed microanalyses quantitative elemental analyses were needed. Therefore, Electron Probe Micro Analyses (EPMA) investigations were performed by Wavelength Dispersive Spectrometer, WDS on the sintered samples of 18h MA'd W1Ni, 18h MA'd W1Ni-2WB and 18h MA'd W1Ni-2WB-1La_2O_3 powders. The system used was CAMECA™-SX100 which was operated at 15 kV.

4.2.2 Density measurements

Sintered densities were measured in a Precisa™ XB220A sensitive balance using the Archimedes method which depends on the relationship between volume and mass (Figure 4.7). Density results are the arithmetic mean of 5 measurements of the same sample.

Figure 4.7: Precisa™ XB220A sensitive balance with the Archimedes kit.

4.2.3 Hardness measurements

Hardness measurements were carried out using a Shimadzu™ micro hardness tester (Figure 4.8) with a Vickers indenter under a load of 100 g for 15 seconds. Results of hardness tests were averaged out of 15 successive indentations.

Figure 4.8: Shimadzu™ micro hardness tester.

4.2.4 Wear characterizations

Sliding wear experiments of the sintered samples of 18h MA'd W1Ni, 18h MA'd W1Ni-2WB and 18h MA'd W1Ni-2WB-1La_2O_3 powders were conducted on a Tribotech™ Oscillating Tribotester to using 6 mm alumina balls under an applied force of 4 N. The tests were done at room temperature in a laboratory atmosphere with a sliding speed of 4 mm/s, a stroke length of 2 mm and a sliding distance of 20 m. Abraded surfaces were characterized using a Veeco™ Dektak 6 M Stylus Profiler and test results are arithmetic means of three different measurements for each sample calculated by integrating the area of the each peak of the surface profile.

5. RESULTS AND DISCUSSIONS

The results of the present research work can be divided into four groups:

1.W - 1 wt % Ni and W-2 wt % WB (18 h MA'd)

2. W - 1 wt % Ni - 2 wt % WB (MA time: 3, 6, 12, 18, 24 h),

3. W - 1 wt % Ni - x wt % WB (x=0.5, 1, 2, 4),

4. W - 1 wt % Ni - 2 wt % WB - y wt % La_2O_3 (y=0.5, 1).

Each experimental group contains studies about the fabrication and characterization of the mechanical alloyed and sintered samples. The First group of experiments examine characterizations of W - 1 wt % Ni and W - 2 wt % WB samples. The second group of experiments investigate the effect in different rates WB addition to the W-1 wt. % Ni powders. The third group experiments investigate the effect of duration of mechanical alloying was determined. Finally, the fourth group of experiments deals with the effects of La_2O_3 dispersoid addition to the W - 1 wt % Ni - 2 wt % WB powders.

XRD patterns and particle size distributions of the powders used in this study are given in Figure 5.1 and Figure 5.2, respectively. Figure 5.1a shows the XRD patterns of the W powders. As seen in this figure, the peaks of W which has a b.c.c. Bravais lattice and $Im\bar{3}m$ space group with the lattice parameter of a = 0.316 nm (ICDD No: 04-0806) can be identified. Figure 5.2 b and c are the XRD patterns of WB (ICDD No: 73 – 1769, a centered tetragonal Bravais lattice and $I4_1$, with the lattice parameters of a = b = 0,311 nm, c = 0,169 nm) and 6 hours pre-milled La_2O_3 (ICDD No: 83 – 1344, a hexagonal Bravais lattice with the lattice parameters of a = b = 0,394 nm, c = 0,614 nm) powders, respectively.

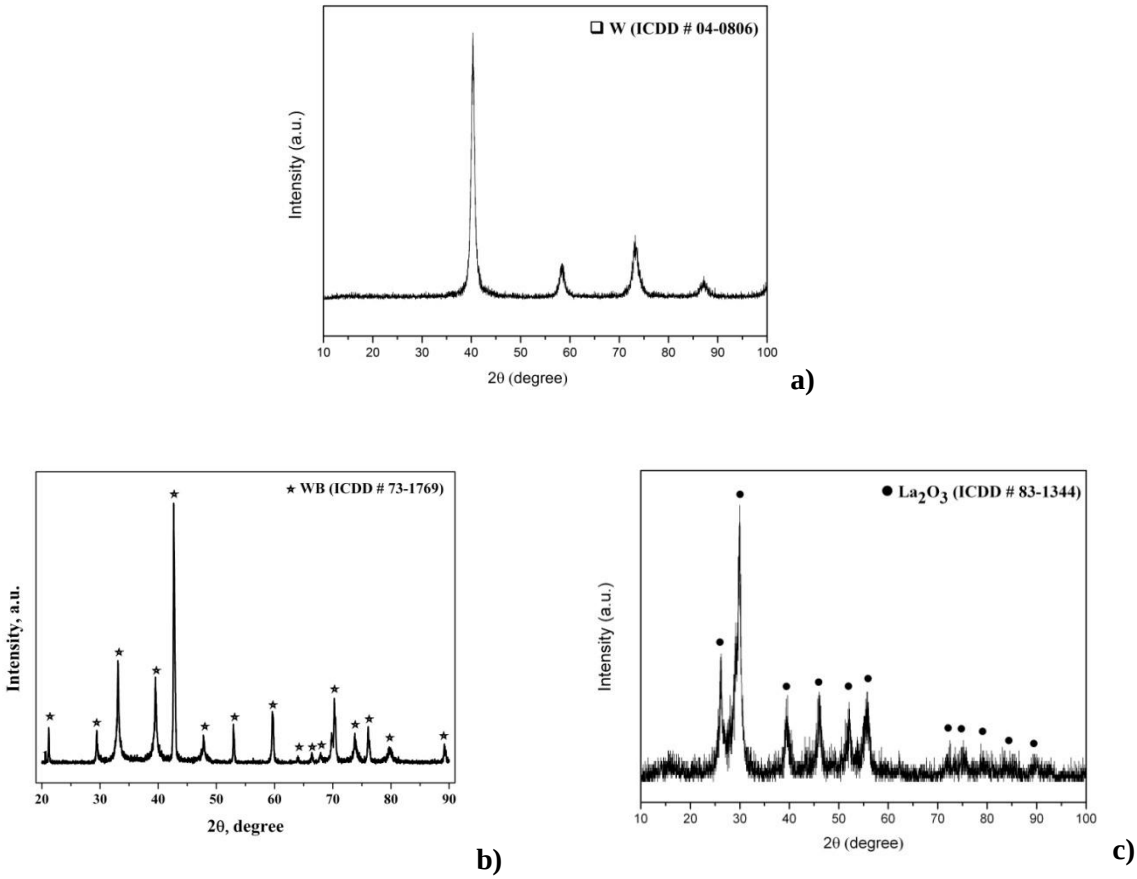

Figure 5.1: XRD patterns of the **a)** W, **b)** WB, **c)** pre-milled La_2O_3 powders.

Figure 5.2a and b show the particle size distributions of WB and pre-milled La_2O_3 powders, respectively. After pre-milling, mean particle size of La_2O_3 has decreased from 34 µm to 1.787 µm (Figure 5.2 b).

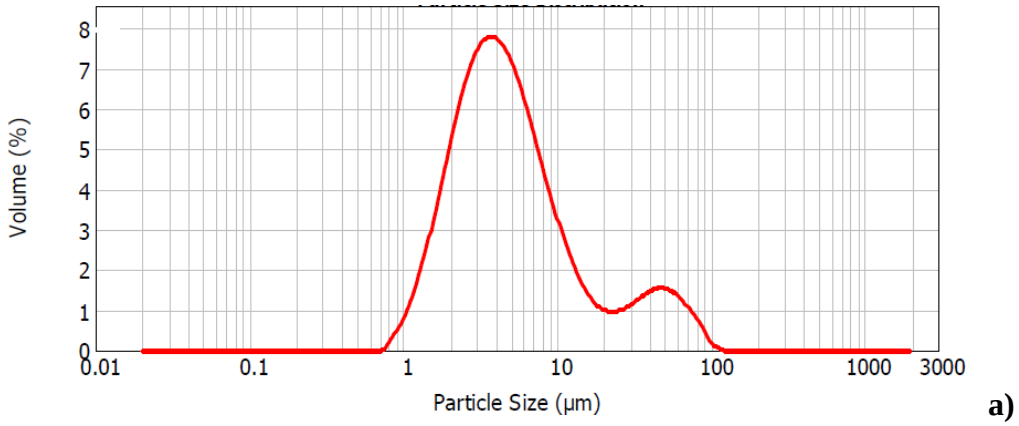

Figure 5.2: Particle size distributions of **a)** WB (D_{mean}=10.039 µm), **b)** pre-milled La_2O_3 (D_{mean}=1.787 µm).

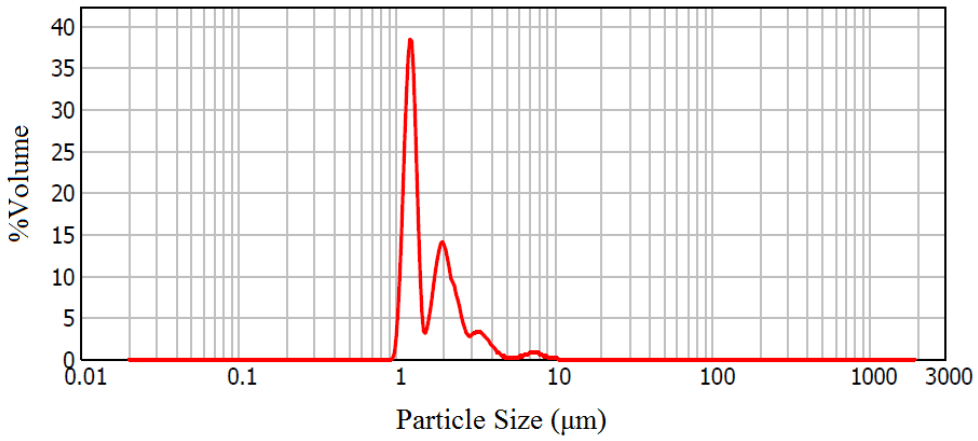

b)

Figure 5.2 (continued): Particle size distributions of a) WB (D_{mean}=10.039 μm), b) pre-milled La_2O_3 (D_{mean}=1.787 μm).

5.1 Characterization Investigation of W-1 wt % Ni and W-2 wt % WB Composites

5.1.1 Characterization of the powders

Figure 5.3 and b show the XRD patterns of the W-1 wt % Ni and W-2 wt % WB powders MA'd for 18 h, respectively. All the peaks seen in the XRD patterns belong to W phase (ICDD # 04-0806) mentioned before. Ni and WB phases are not observed because of their small amounts in overall powder blends.

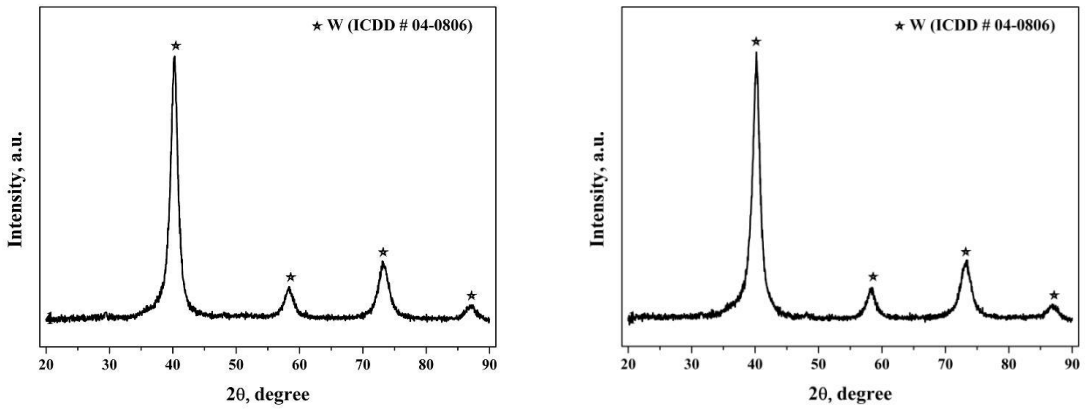

a) b)

Figure 5.3: XRD patterns of W-1 wt % Ni and W-2 wt % WB MA'd for 18h.

Figure 5.4 shows the particle size distributions of the 18 h MA'd W-1 wt % Ni powder. Unimodal particle size distribution of powders indicate a homogeneous distribution. The specific surface area of the W-1 wt % Ni MA'd powder is 1,63 m^2/g.

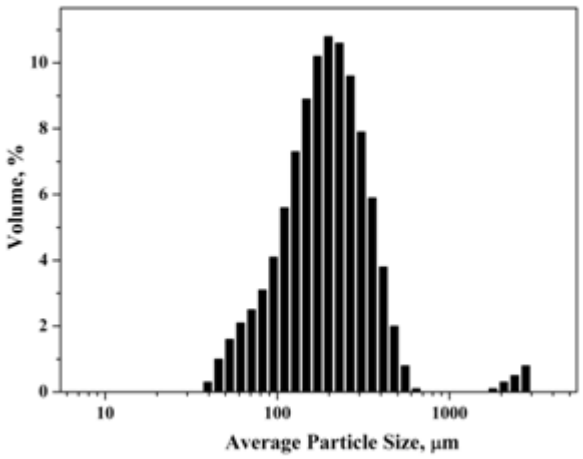

Figure 5.4: Particle size distributions of W-1 wt % Ni MA'd powder (D_{mean}=0.33 μm).

SEM micrographs of the 18 h MA'd W-1 wt % Ni powders is shown in Figure 5.5, revealing that the MA'd powders are mainly consist of submicron particulates, whereas some agglomerates having sizes of about 1 μm are also present in the microstructures. Besides, agglomeration of the powder particles prevents the observation of smaller ones.

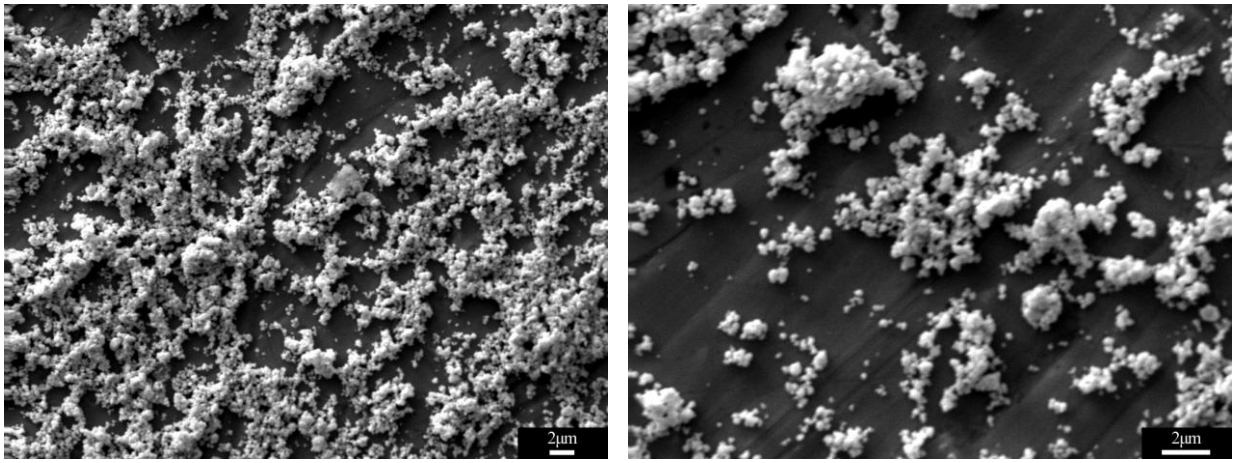

Figure 5.5: SEM micrographs of MA'd W-1 wt % Ni powder. The right micrograph is higher magnification image.

5.1.2 Characterization of the sintered samples

XRD patterns of the sintered W-1 wt % Ni and W- 2 wt % WB powders are given in Figure 5.6. In this figure, only the W phase (ICDD # 04-0806) was identified in MA'd W - 1 wt % Ni and W - 2 wt % WB samples. It is evident from Figure. 5.6 that there is no intermetallic compound formation after sintering of the powder blends.

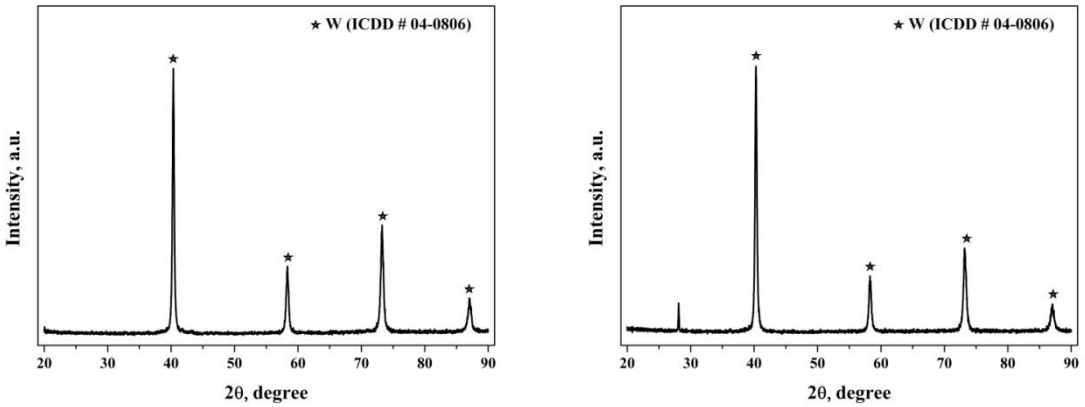

a) **b)**

Figure 5.6: XRD patterns of the MA'd and sintered **a)** W - 1 wt % Ni and **b)**W - 2 wt % WB samples.

Relative density measurement results of the 18 h MA'd W - 1 wt % Ni and W - 2 wt % WB samples are given in Table 5.1. The density value of 18h MA'd and sintered W - 1wt % Ni sample is 95,83 wt %, whereas the density value of 18 h MA'd and sintered W - 2 wt % WB is 90,49 wt %. It is an evident that the presence of Ni as the solid state sintering aid contributes positively to density during sintering. Also seen in Table 5.2, the microhardness value of the samples are compatible with density values.

Table 5.1: Relative density and microhardness values of the sintered samples.

Sample Name	Theoretical Density (g/cm3)	Relative Archimedes' Density (%)	Microhardness (GPa)
W - 1 wt % Ni	19.08	95.83	5.15 ± 0.3
W - 2 wt % WB	19.2	90.49	3.29 ± 0.28

Figure 5.7a and b are the back - scattered electron micrographs of 18 h MA'd and sintered W - 1 wt % Ni. As seen in Figure 5.7a, Ni particles are generally located (dark grey particles) at grain boundaries and generate nickel rich regions. Considering the fractured surface image (Figure 5.7b), nickel rich regions can not be defined by contrast. However, EDS spectra reveal that the tiny grains are nickel rich regions as deduced in Figure 5.21. Figure 5.7 c and d are the SEM micrographs of 18 h MA'd and sintered W - 2 wt % WB. The images which is belongs to 18h MA'd and sintered W - 2 wt % WB demostrate that effectivity of Ni activated sintering, on the sinterability of W.

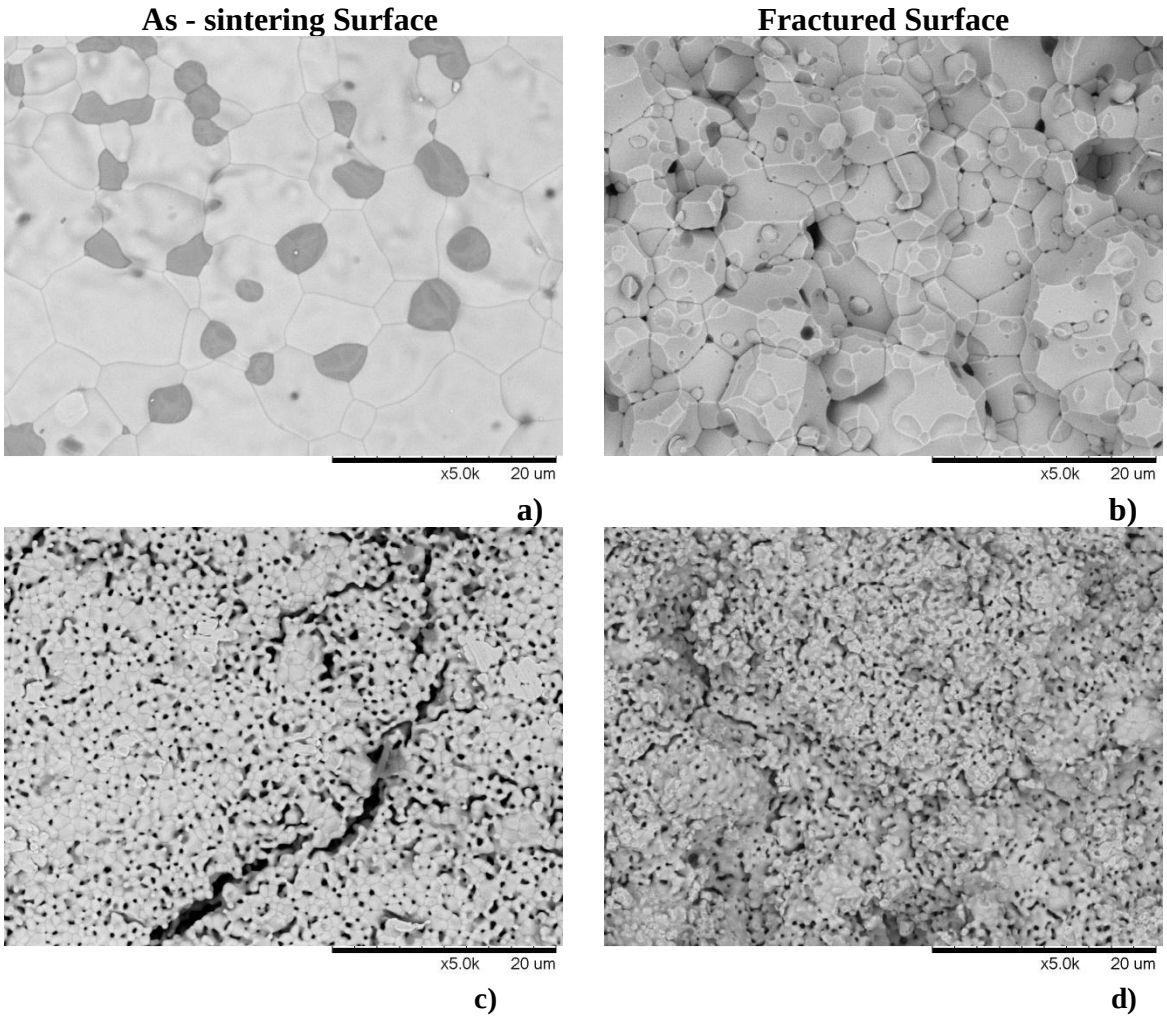

Figure 5.7: Back - scattered SEM micrographs of sintered; **a, b)** W - 1 wt % Ni and **c, d**) W - 2 wt % WB samples.

Electron probe microanalysis (EPMA) back - scatterred image (BSE) and W, Ni, O, C elemental mapping of sintered W - 1 wt % Ni sample MA'd for 18h were given in Figure 5.8. BSE image serve as sample maps for locating spot analysis. Figure 5.8 b and c show W and Ni mapping on BSE image, respectively. Comparing these two

images provide nickel rich regions in Figure 5.8a. Besides these elements, O and C as a result of contamination can be seen in Figure 5.8d and e. Oxygen and carbon existances can be explained by contamination.

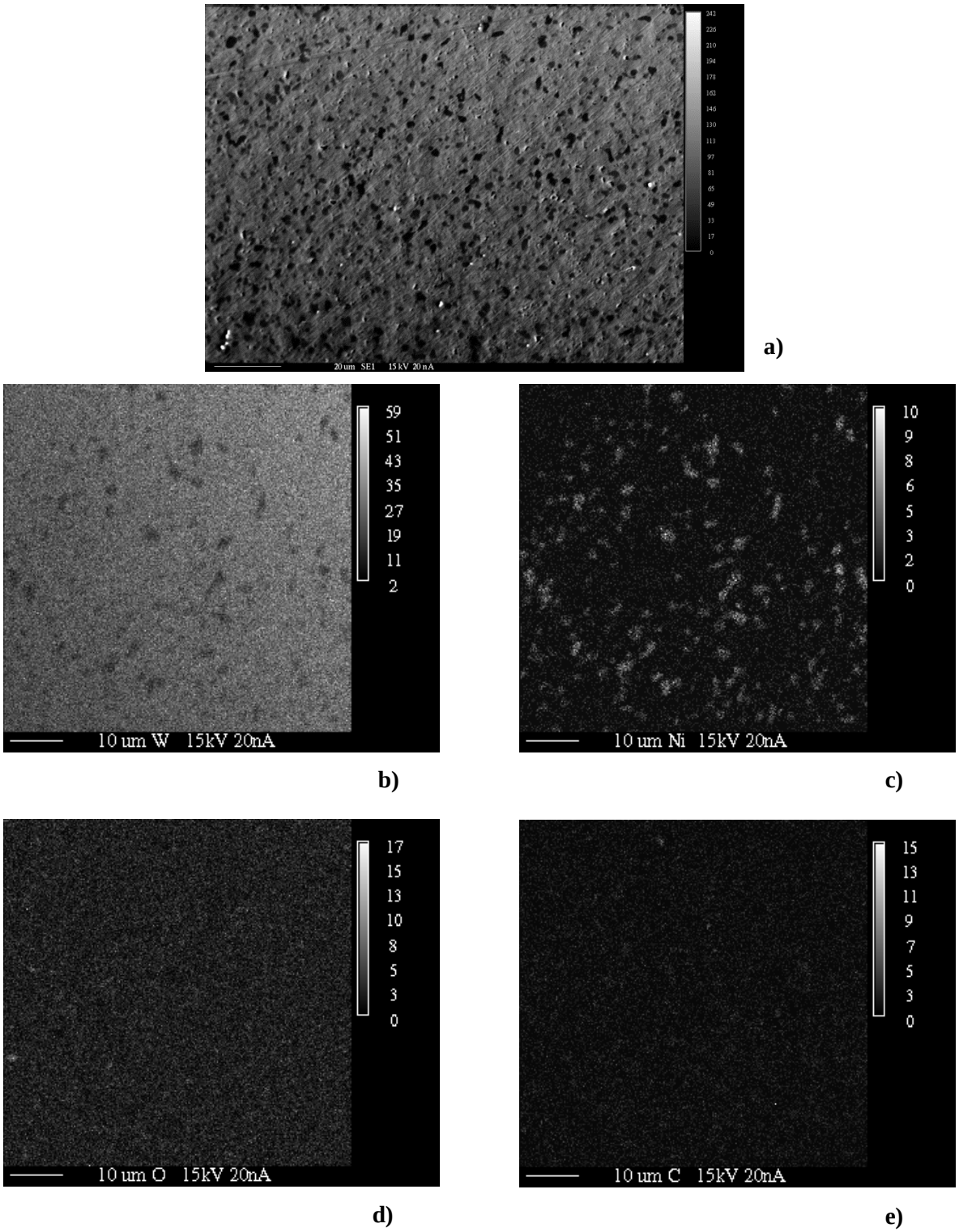

Figure 5.8: a) EPMA micrpgraphs taken from sintered W - 1 wt % Ni sample MA'd for 18h: **a)**BSE image, **b)** W, **c)** Ni, **d)** O**, e)** C elemental mappings.

Figure 5.9 is a back - scattered SEM micrographs taken from the wear tracks of 18 h MA'd and sintered W - 1 wt % Ni sample. The wear amount and average friction coefficient are measured as 4.22 ± 0.021 ($mm^3N^{-1}m^{-1}$) $x10^{-6}$ and 0.42, respectively. As seen in Figure 5.9, the worn surface of the sintered W - 1 wt % Ni sample contains multiple valleys with patches ruptured from the surface and/or the hardfacing alumina balls during sliding wear experiments.

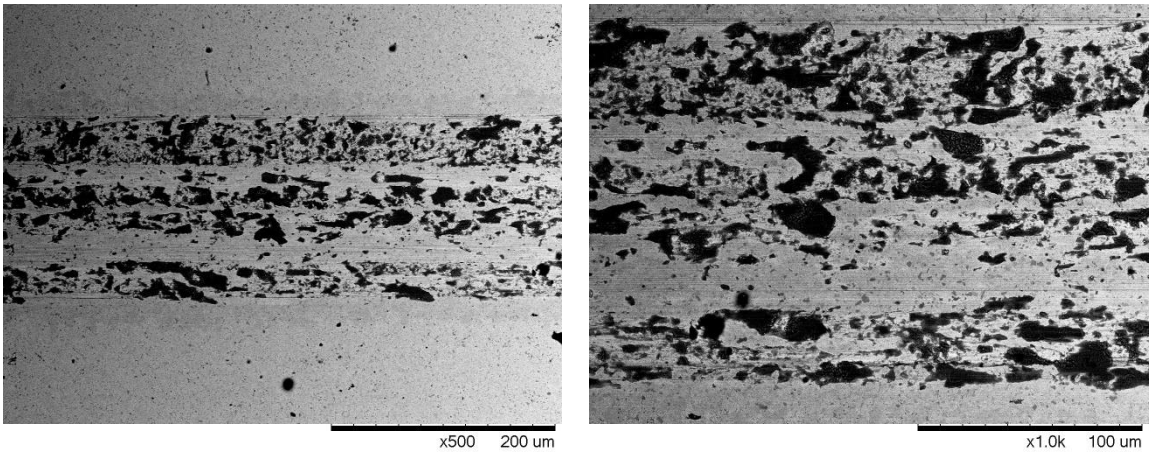

Figure 5.9: Back - scattered SEM micrographs of the wear tracks of the sintered W - 1 wt % Ni sample. Rightmicrograph is higher magnification image of the wear tracks.

5.2 Effect of MA on the W - 1 wt % Ni - 2 wt % WB Composites

5.2.1 Powder characterization during MA

Figure 5.10 is the XRD patterns of W - 1 wt % Ni - 2 wt % WB powders which were MA'd for different durations. The peaks of W can be identified in all samples. However, in these patterns WB peaks are not be observed, probably due to the low content in the blends and peak broadening due to MA. All of the peaks diffracted from these phases belong to the W phase (ICDD No: 04-0806), as mentioned before. It is clear that with increasing MA, peaks are broadened and peak heights are decreased, as a result of grain refinement and due to internal strain accumulation during MA.

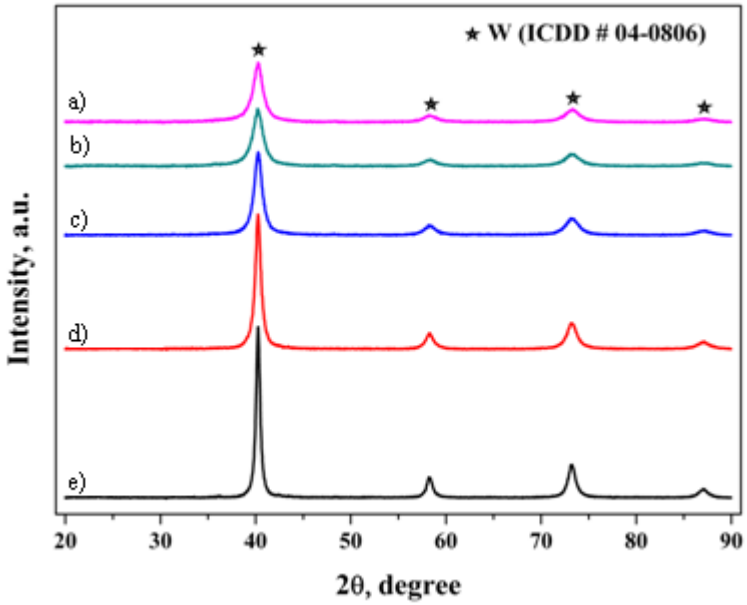

Figure 5.10: XRD patterns of W - 1 wt % Ni - 2 wt % WB **a)** 24 h MA **b)** 18 h MA **c)** 12 h, **d)** 6 h MA, **e)** 3 h MA.

Figure 5.11a–f show the evolution of particle size distributions of W - 1 wt % Ni - 2 wt % WB powders during mechanical alloying. Particle size distribution of the W - 1 wt % Ni - 2 wt % WB MA'd for 3h is bimodal which consist of two peaks (Figure 5.11a). However, an unimodal particle distribution is detected for others MA durations (Figure 5.11b - e). As seen in Figure 5.11, a mean particle size of 0.373 µm (Figure 5.11a) for 3 h MA'd W - 1 wt % Ni - 2 wt % WB powders declines to 0.312 µm (Figure 5.11e) for same powders MA'd for 12 h. Furthermore, according to BET analysis results given in Table 5.2, with increasing MA duration, specific surface area of the powders which is 1,13 m^2/g for the 3h MA'd W - 1 wt % Ni - 2 wt % WB powders increases with MA and has the value of 1,72 m^2/g for the W - 1 wt % Ni - 2 wt % WB powders MA'd for 24 h.

Table 5.2: BET results of W - 1 wt % Ni - 2 wt % W samples MA'd for 3, 6, 12, 18 and 24h.

W - 1 wt % Ni - x 2% WB MA time	3h	6h	12h	18h	24h
BET results (m^2/g)	1.13	1.19	1.27	1.58	1.72

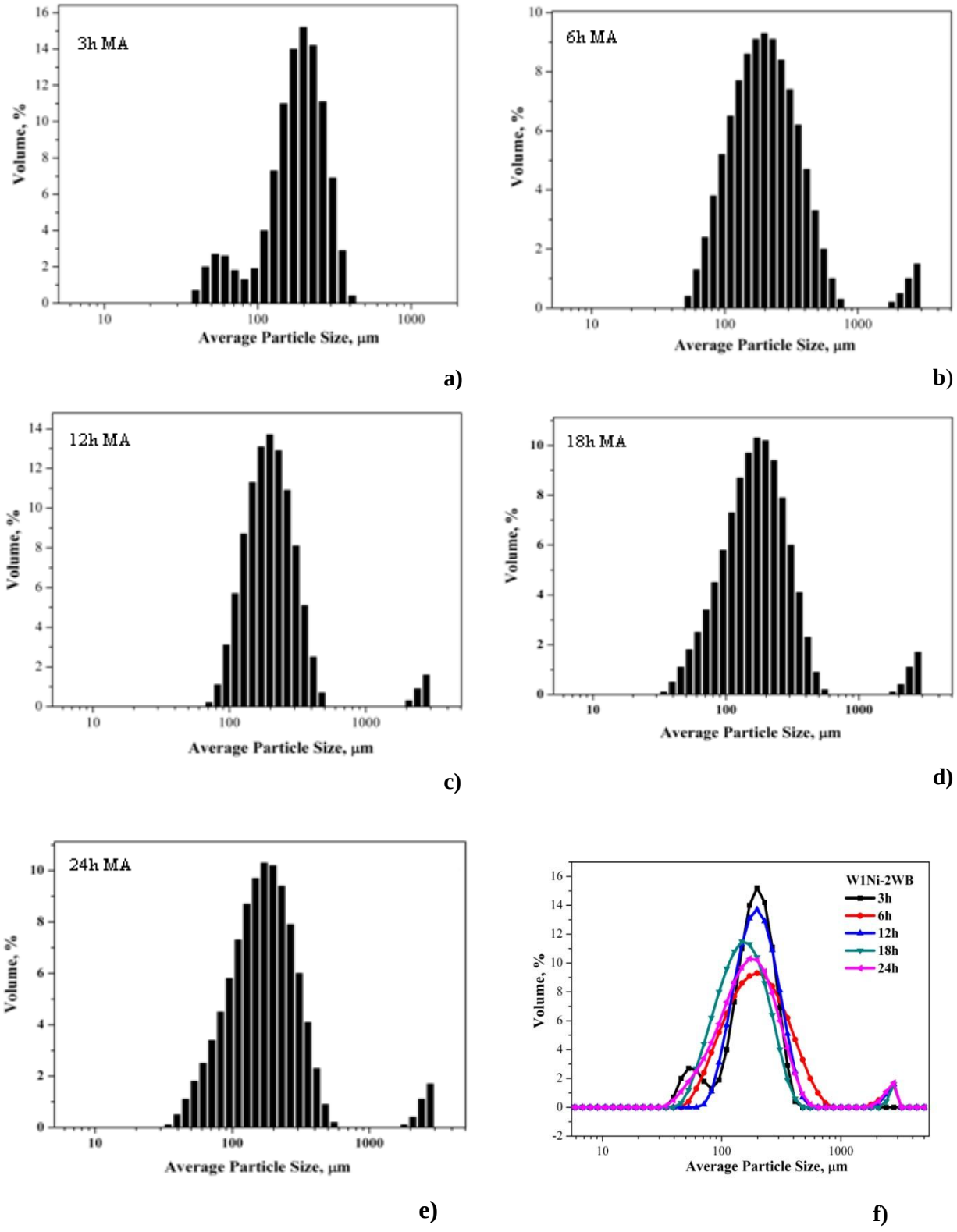

Figure 5.11: Particle size distributions of W - 1 wt % Ni - 2 wt % WB sintered samples **a)** 3 h MA'd (D_{mean}= 0.373 µm), **b)** 6 h MA'd (D_{mean}= 0.365 µm), **c)** 12 h MA'd (D_{mean}= 0.376 µm), **d)** 18 h MA'd (D_{mean}= 0.311 µm), **e)** 24 h MA'd (D_{mean}= 0.312 µm), **f)** comparison for particle size distribution.

Figure 5.12 shows SEM micrographs taken from W - 1 wt % Ni - 2 wt % WB powders for MA'd 3 h, 6 h, 12 h, 18 h and 24 h. These SEM micrographs reveal that spherical - like submicron particles existing throughout the microstructure with some micron sized agglomerates. Particle size with 0.373 μm decrease to size with 0.312 μm, by milling for 3h and 25 h, respectively.

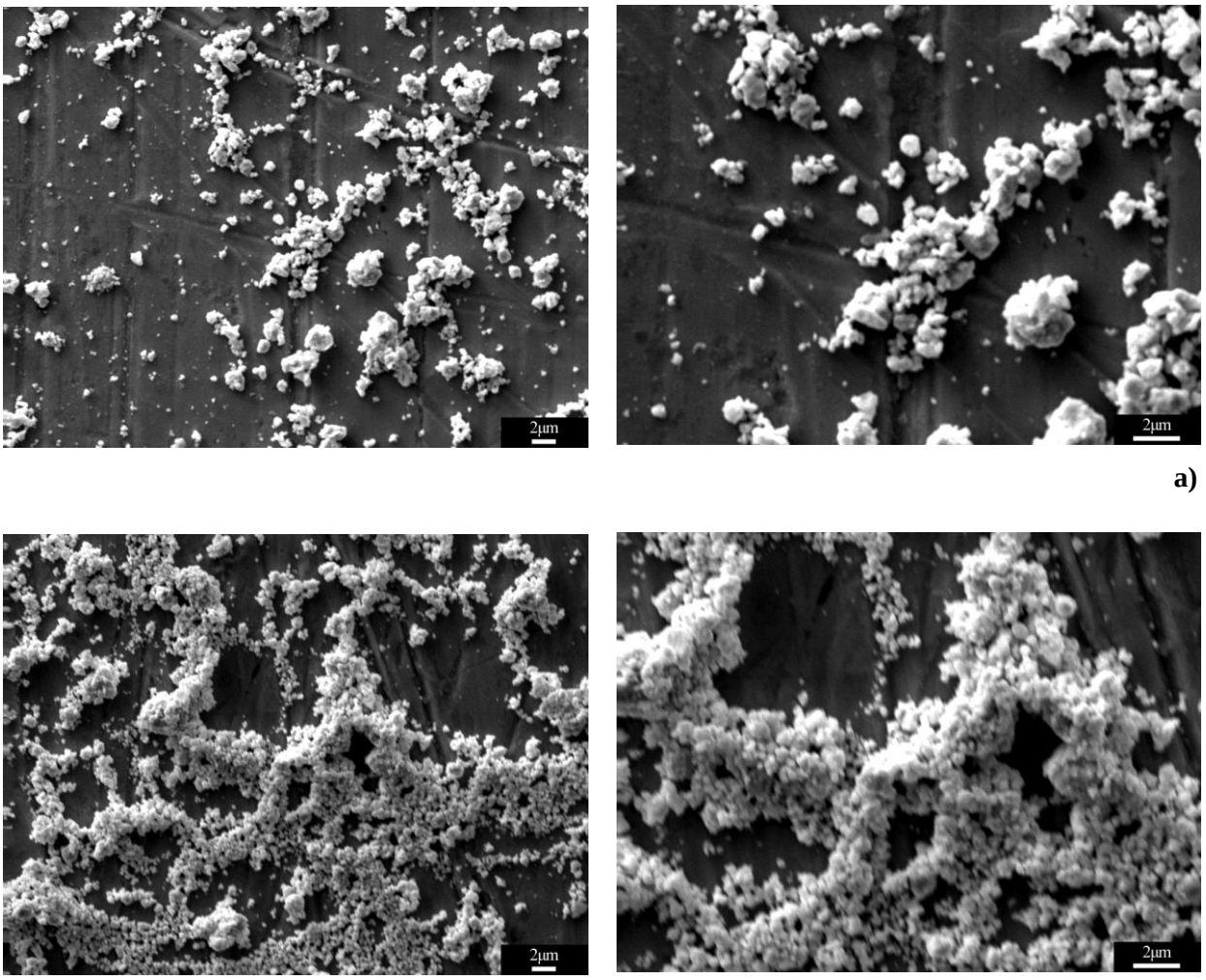

Figure 5.12: SEM micrographs of the W - 1 wt % Ni - 2 wt % WB powders MA'd at different MA durations: **a)** 3 h, **b)** 12 h, **c)** 18 h, **d)** 24 h. Right micrographs are higher magnification images.

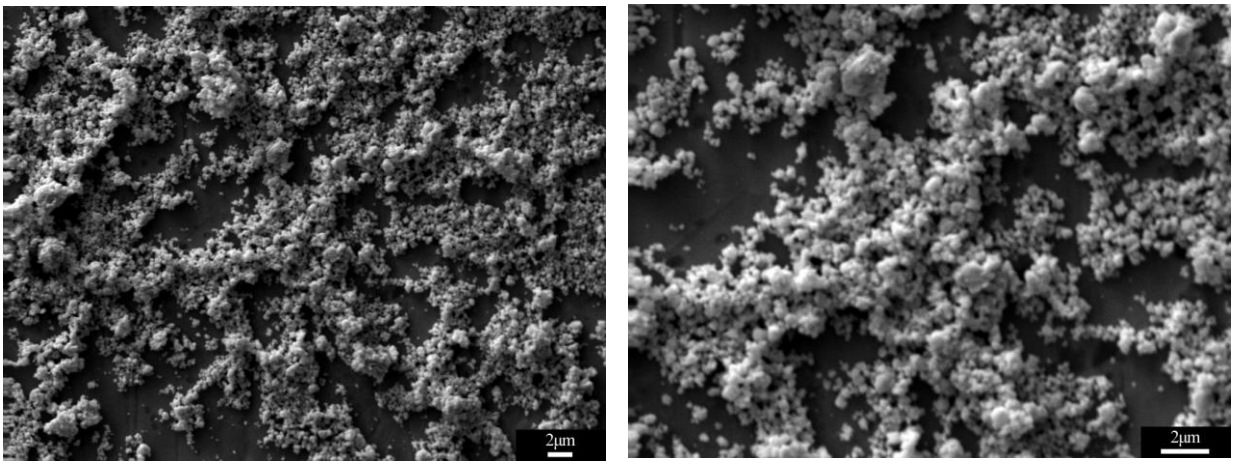

c)

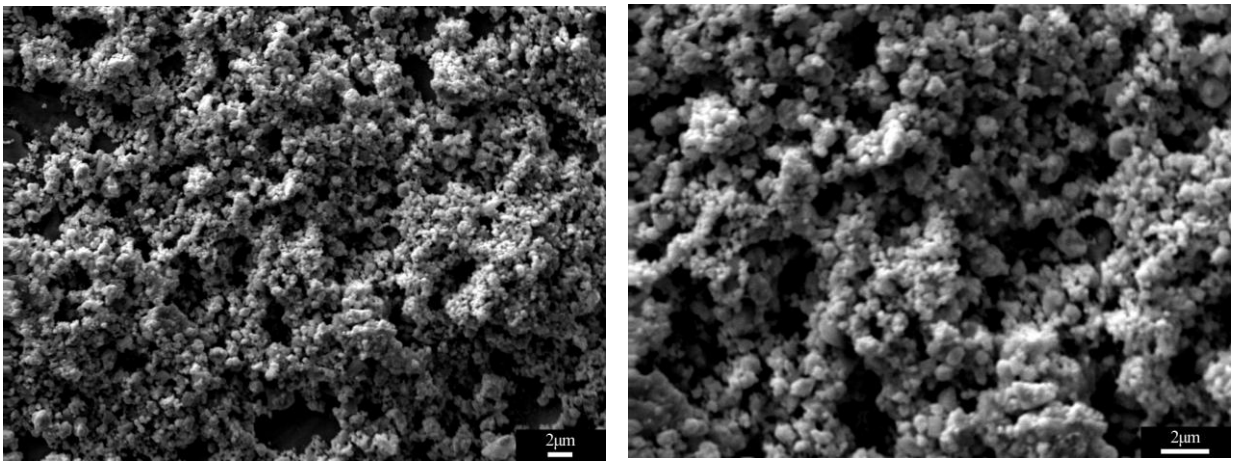

d)

Figure 5.12 (continued): SEM micrographs of the W - 1 wt % Ni - 2 wt % WB powders MA'd at different MA durations: **a)** 3 h, **b)** 12 h, **c)** 18 h, **d)** 24 h. Right micrographs are higher magnification images.

5.2.2 Characterization of the sintered samples

Figure 5.13 shows the XRD patterns of the sintered W - 1 wt % Ni - 2 wt % WB powders MA'd for 3, 6, 12, 18, 24h. Only W peaks are observed. In the XRD patterns, revealing no intermetallic compound formation after sintering of the MA'd powder composites.

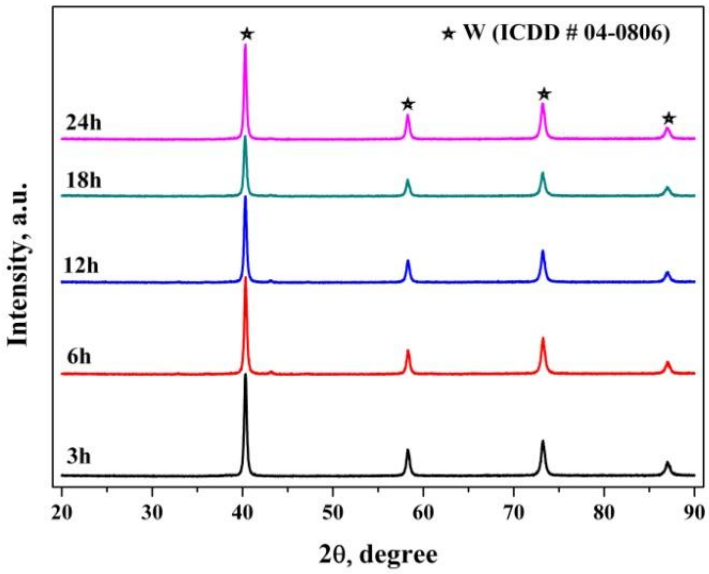

Figure 5.13: XRD patterns of the MA'd and sintered W - 1 wt % Ni - 2 wt % WB samples.

The relative density measurements and theoretical density values of the samples of the W - 1 wt % Ni - 2 wt % WB MA'd at different durations are given in Table 5.3. The relative density values of the W - 1 wt % Ni - 2 wt % WB samples MA'd at different durations are higher than >95%, except for the 3 h MA'd sample. The highest density is 97,89% belonging to the 18 h MA'd sample. Generally, it is expected that relative density values increase with increasing mechanical alloying durations. However, it should be mentioned here that there are small density fluctuations. It is believed that increasing milling durations causes the contamination of powders by milling media, WC, which has a density of 15.8 g/cm^3. As a result of WC contamination, theoretical densities decrease, so the relative density remains almost the same with increasing mechanical alloying durations. As seen in the Table 5.3, the microhardness values increase slightly with increasing MA durations as a result of grain refinement during MA. Moreover, the W - 1 wt % Ni - 2 wt % WB sample MA'd for 18 h has the highest microhardness value, 6,45±0,24 GPa. Taking everything into consideration, 18h seems to be best milling time for the W - 1 wt % Ni - 2 wt % WB

Table 5.3: Relative density and microhardness values of the sintered samples.

Sample Name	Theoretical Density (g/cm3)	Relative Archimedes' Density (%)	Microhardness (GPa)
W - 1Ni - 2WB 3h MA'd	18,98	92,92	4,90±0,31
W - 1Ni - 2WB 6h MA'd		96,64	5,41±0,37
W - 1Ni - 2WB 12h MA'd		95,64	5,72±0,25
W - 1Ni - 2WB 18h MA'd		97,89	6,45±0,24
W - 1Ni - 2WB 24h MA'd		94,93	6,42±0,25

Figure 5.14 consists of SEM micrographs from both of fractured and as sintered surfaces of the W - 1 wt % Ni - 2 wt % WB sintered samples MA'd for different milling durations. The surface images taken as sintering surface reveal similar features in all sintered microstructures and almost no porosity. Moreover, Ni particles are generally located (dark grey particles) at grain boundaries and generate nickel pools. Micron and submicron WB particles have a homogenous distribution throughout the microstructure that are located both at grain boundaries and at grain interiors in W1Ni matrix for all the sintered samples. The addition of WB particles in W1Ni matrix has positive effects on the microstructure of the composites because the grain size of W1Ni matrix decreases resulting from the pinning effect of WB particles on the growth of tungsten grains. Furthermore, WB particles located at grain interiors contribute to the mechanical properties of the composites, as seen from microhardness results in Table 5.2. In Figure 5.14g, the nickel rich regions can't be observed for 18 h MA'd W - 1 wt % Ni - 2 wt % WB. However, EPMA analysis of W - 1 wt % Ni - 2 wt % WB (Figure 5.19) reveal the presence of nickel rich regions. The morphologies reveal that there are no remarkable difference on grain sizes.

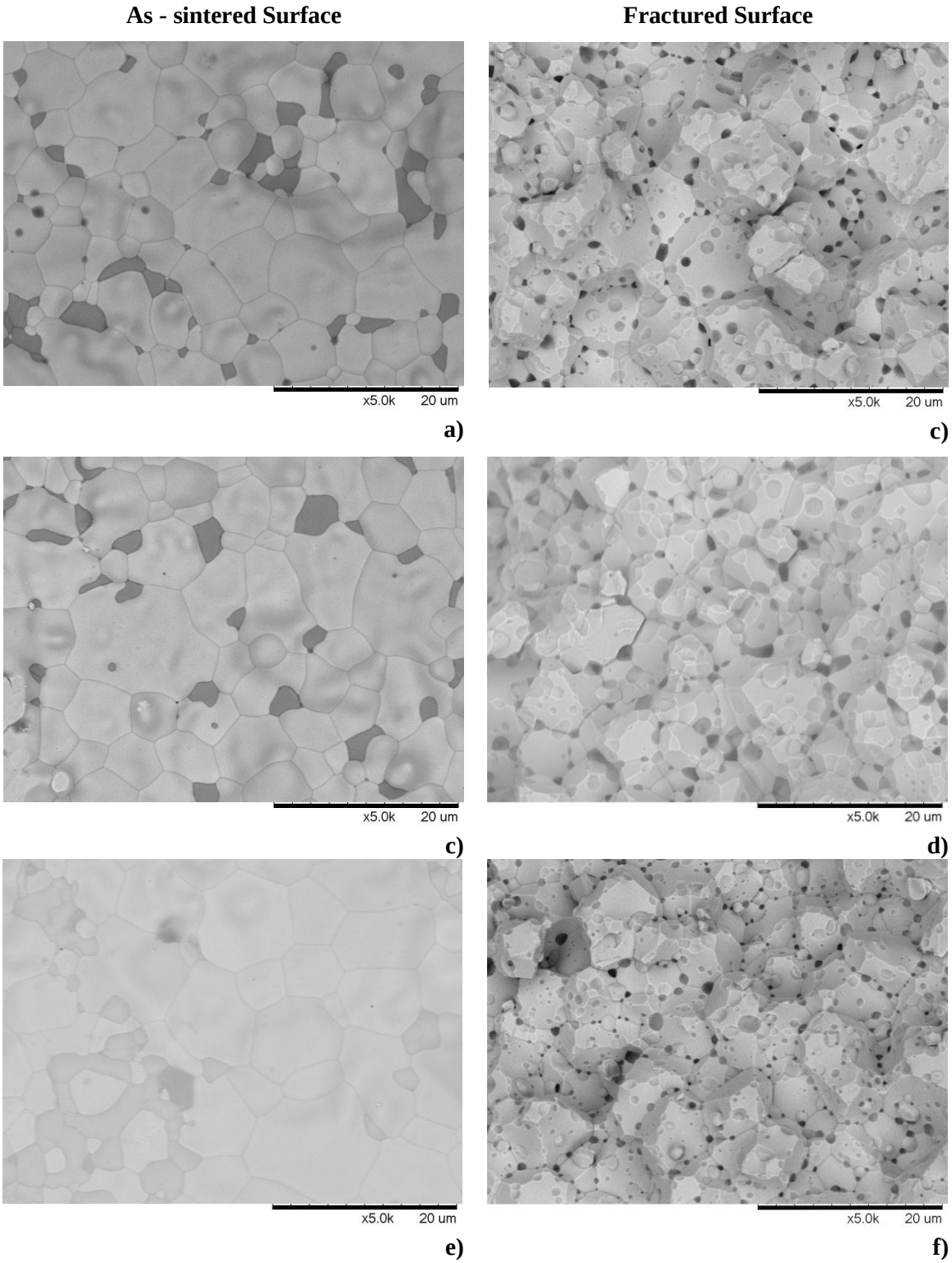

Figure 5.14: Back - scattered SEM micrographs taken from sintered W - 1 wt % Ni - 2 wt % WB samples.MA'd for: **a, b)** 6 h, **c, d)** 12 h, **e, f)** 18 h, **g, h)** 24 h.

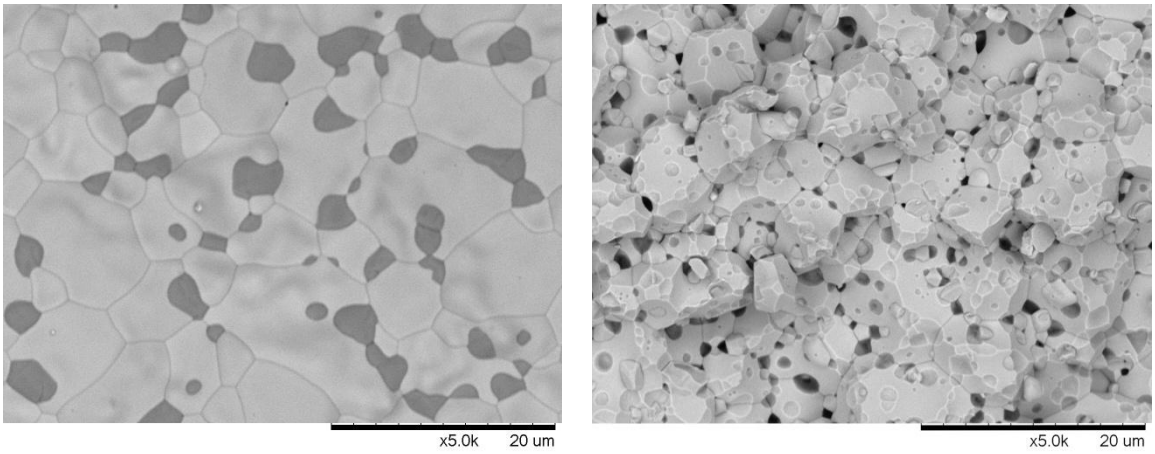

g) **h)**

Figure 5.14(continued): Back - scattered SEM micrographs taken from sintered W - 1 wt % Ni - 2 wt % WB samples.MA'd for: **a, b)** 6 h, **c, d)** 12 h, **e, f)** 18 h, **g, h)** 24 h.

5.3 The Effects of WB Content on W - 1 wt % Ni Composites

5.3.1 Characterization of the powders

XRD patterns of W - 1 wt % Ni - 0.5 wt % WB, W - 1 wt % Ni - 1 wt % WB powders, W - 1 wt % Ni - 2 wt % WB, W - 1 wt % Ni - 4 wt % WB MA'd for 18 h are shown in Figure 5.15. All of the peaks belong to W phase (ICDD No: 04-0806). Peaks for WB are not seen, probably due to its small amount (0.5, 1, 2 ,4 wt %) in the powder blend.

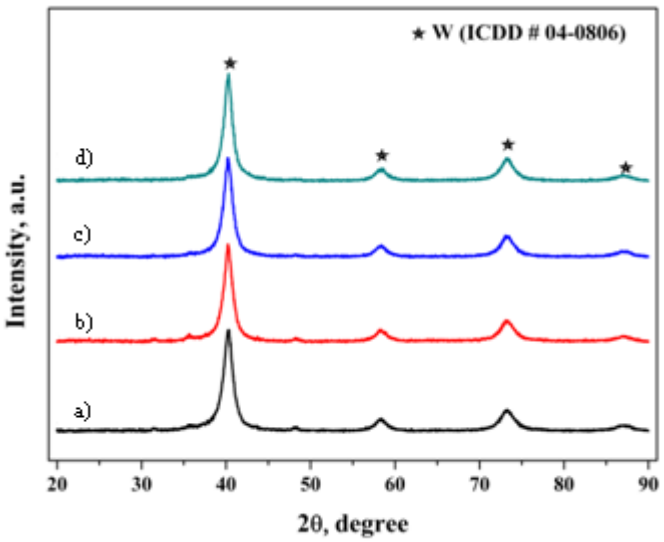

Figure 5.15: XRD patterns of 18 h MA'd: **a)** W - 1 wt % Ni - 0.5 wt % WB, **b)** W - 1 wt % Ni - 1 wt % WB powders, c) W - 1 wt % Ni - 2 wt % WB, d) W - 1 wt % Ni - 4 wt % WB.

Figure 5.16 a-d show the particle size distributions of the W - 1 wt % Ni - 0.5 wt % WB, W - 1 wt % Ni - 1 wt % WB, W - 1 wt % Ni - 2 wt % WB, W - 1 wt % Ni - 4 wt % WB powders MA'd for 18 h in order to investigate the effect of WB addition on particle size distribution. As seen in these figures, all powders have almost the same mean particle sizes of about 0.35 μm indicating that the addition of WB powders has no significant effect on particle size distributions. Considering the BET results is given in Table 5.3, with increasing WB (0.5, 1, 2, 4) content, specific surface areas of the powders show an increasing trend for first three powders.

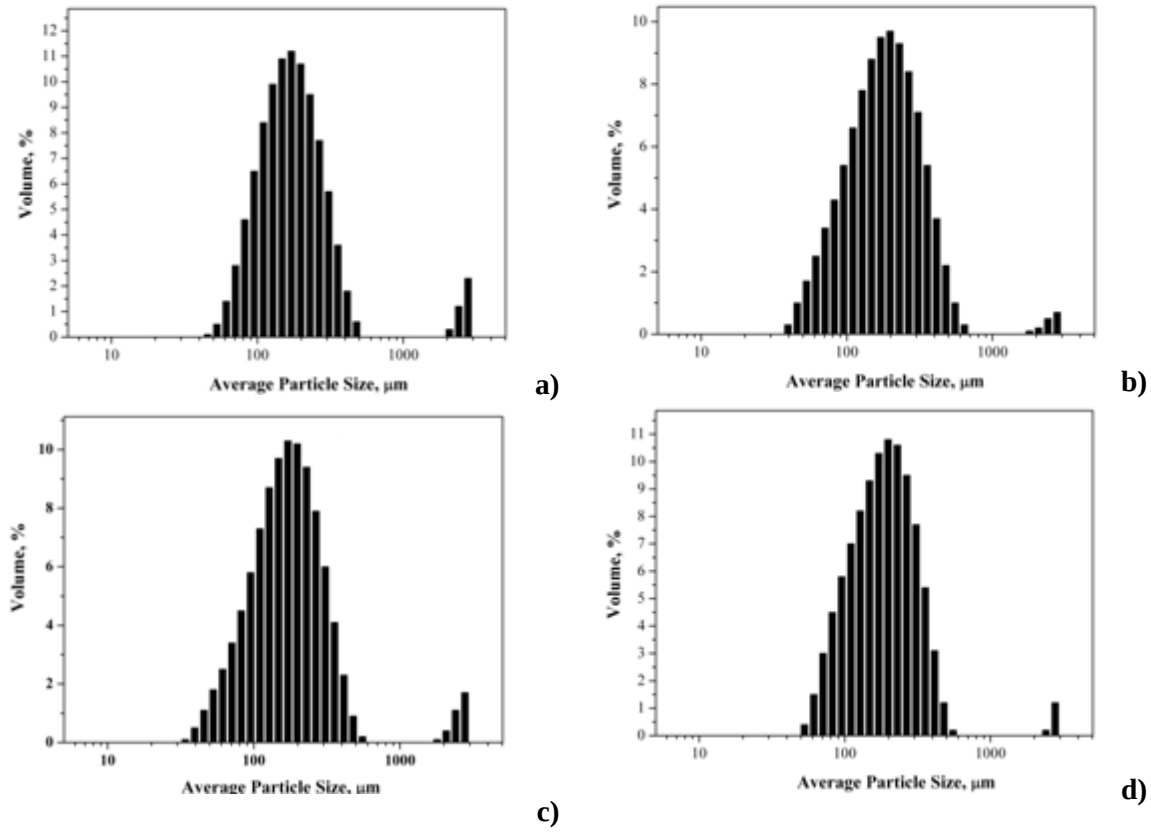

Figure 5.16: Particle size distributions of **a)** W - 1 wt % Ni - 0.5 wt % WB (D_{mean}= 0.347 μm), **b)** W - 1 wt % Ni - 1 wt % WB powders (D_{mean}= 0,346 μm), **c)** W - 1 wt % Ni - 2 wt % WB (D_{mean}= 0.323 μm), **d)** W - 1 wt % Ni - 4 wt % WB (D_{mean}= 0.361 μm) , all MA'd for 18 h.

Table 5.4: BET results of W - 1 wt % Ni - 0.5 wt % WB, W - 1 wt % Ni - 1 wt % WB powders, W - 1wt %Ni - 2wt %WB, W - 1wt %Ni - 4wt %WB MA'd for 18 h.

Sample Name **W - 1 wt % Ni - x wt % Ni**	x=0.5 wt % WB	x=1 wt % WB	x=2 wt % WB	x=4 wt % WB
BET results (m^2/g)	1.40	1.50	1.58	1.44

5.3.2 Characterization of the sintered samples

Figure 5.17 shows the XRD patterns of the sintered W - 1 wt % Ni - 0.5 wt % WB, W - 1 wt % Ni - 1 wt % WB, W - 1 wt % Ni - 2 wt % WB, W - 1 wt % Ni - 4 wt % WB powders MA'd for 18h. All peaks seen in the figure belong to the b.c.c. W (ICDD # 04 - 0806) phases. Any diffraction peaks pertaining to WB phase or other phases are not present, as expected.

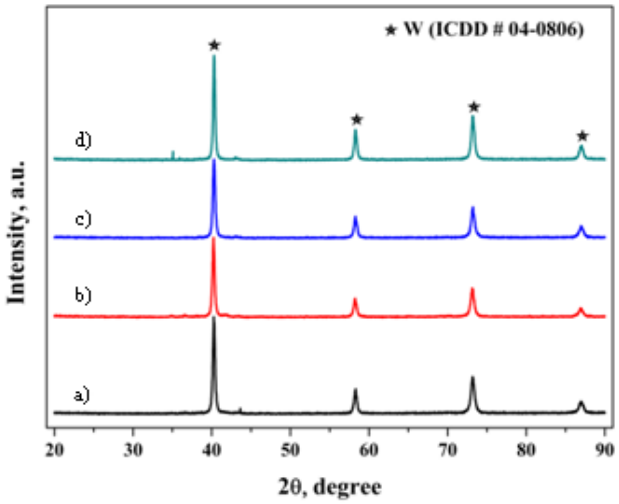

Figure 5.17: XRD patterns of 18 h MA'd sintered **a)** W - 1 wt % Ni - 0.5 wt % WB, **b)** W - 1 wt % Ni - 1 wt % WB, **c)** W - 1 wt % Ni - 2 wt % WB, **d)** W - 1 wt % Ni - 4 wt % WB.

Relative density values and microhardness values of the sintered W - 1 wt % Ni - x wt % WB (x=0.5, 1, 2, 4) samples are given in Table 5.5. The relative density values of the W - 1 wt % Ni - x wt % WB (x=0.5, 1, 2, 4) sintered samples vary about between 91,5 and 97,9 %. There is a increasing tendency in the relative density values of the sintered samples MA'd at the same durations, with increasing WB contents. That result indicates that the WB content has some effect with Ni on the resultant sinter densities. In general, relative density values and microhardness values increase with increasing WB content.

Table 5.5: Relative density and microhardness values of the sintered W - 1 wt % Ni - x wt % WB (x=0.5, 1, 2, 4) samples MA'd for 18 h.

Sample Name	Theoretical Density (g/cm3)	Relative Archimedes' Density (%)	Microhardness (GPa)
W - 1 wt % Ni - 0,5 wt % WB	19.05	91.6	6.07±0.38
W - 1 wt % Ni - 1 wt % WB	19.02	91.7	6.05±0.27
W - 1 wt % Ni - 2 wt % WB	18.98	97.9	6.45±0.35
W - 1 wt % Ni - 4 wt % WB	18.88	96.7	6.58±0.36

Figure 5.18a - f are the SEM micrographs showing the effect of increasing WB contents on the microstructural morphologies of the sintered W - 1 wt % Ni - x wt % WB (x=0.5, 1, 2, 4) samples MA'd for 18h. Figure5.18a and b belong to W - 1 wt % Ni - 0,5 wt % WB sintered sample revealing some porosities are compatible with the relative density values (91.6 %). In addition to Ni has a dominant role in densification MA'd composites, WB contents also effect densification.

As Sintered Surface **Fractured Surface**

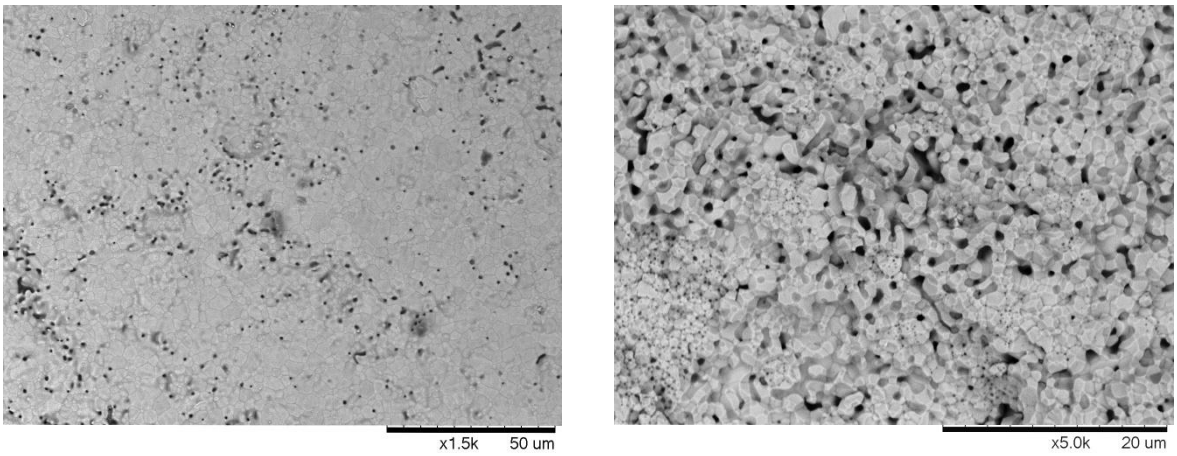

a) **b)**

Figure 5.18: Back - scattered SEM micrographs of 18 h MA'd and sintered **a,b)** W - 1 wt % Ni - 0.5 wt % WB, **c,d)** W - 1 wt % Ni - 2 wt % WB, **e,f)** W - 1 wt % Ni - 4 wt % WB samples.

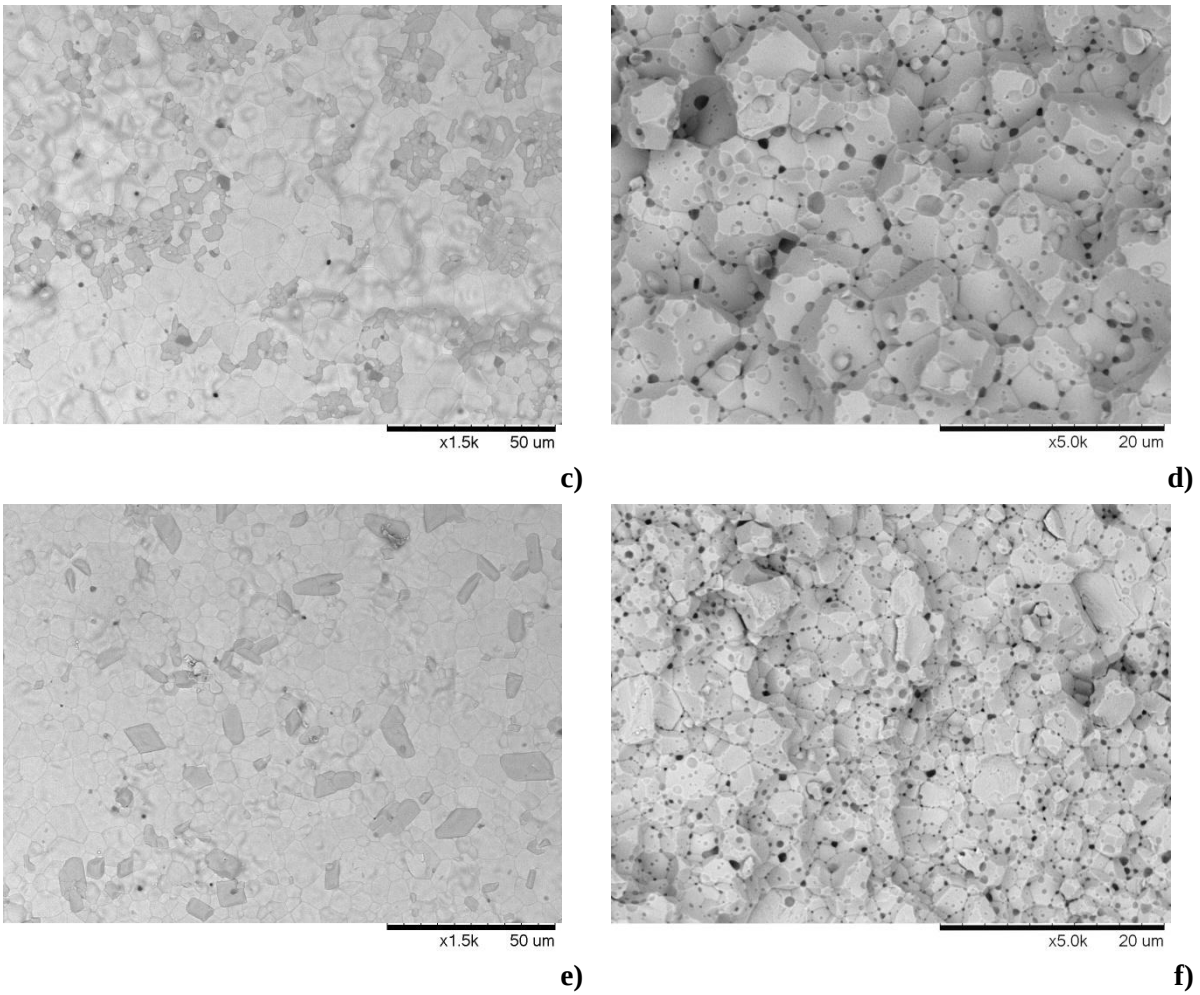

Figure 5.18 (continued): Back-scattered SEM micrographs of 18 h MA'd and sintered **a,b)** W - 1 wt % Ni - 0.5 wt % WB, **c,d)** W - 1 wt % Ni - 2 wt % WB, **e,f)** W - 1 wt % Ni - 4 wt % WB samples.

EPMA BSE image and W, Ni, O, C elemental mapping of the sintered W - 1 wt % Ni - 2 wt % WB sample MA'd for 18h are shown in Figure5.19a-5.19f. Figure 5.19c belong to Ni mapping on BSE image reveals the exsistance of nickel rich regines. In addition, O and C mapping are also shown in Figure 5.19d and 5.19e. The precence of oxygen and carbon is due to contamination.

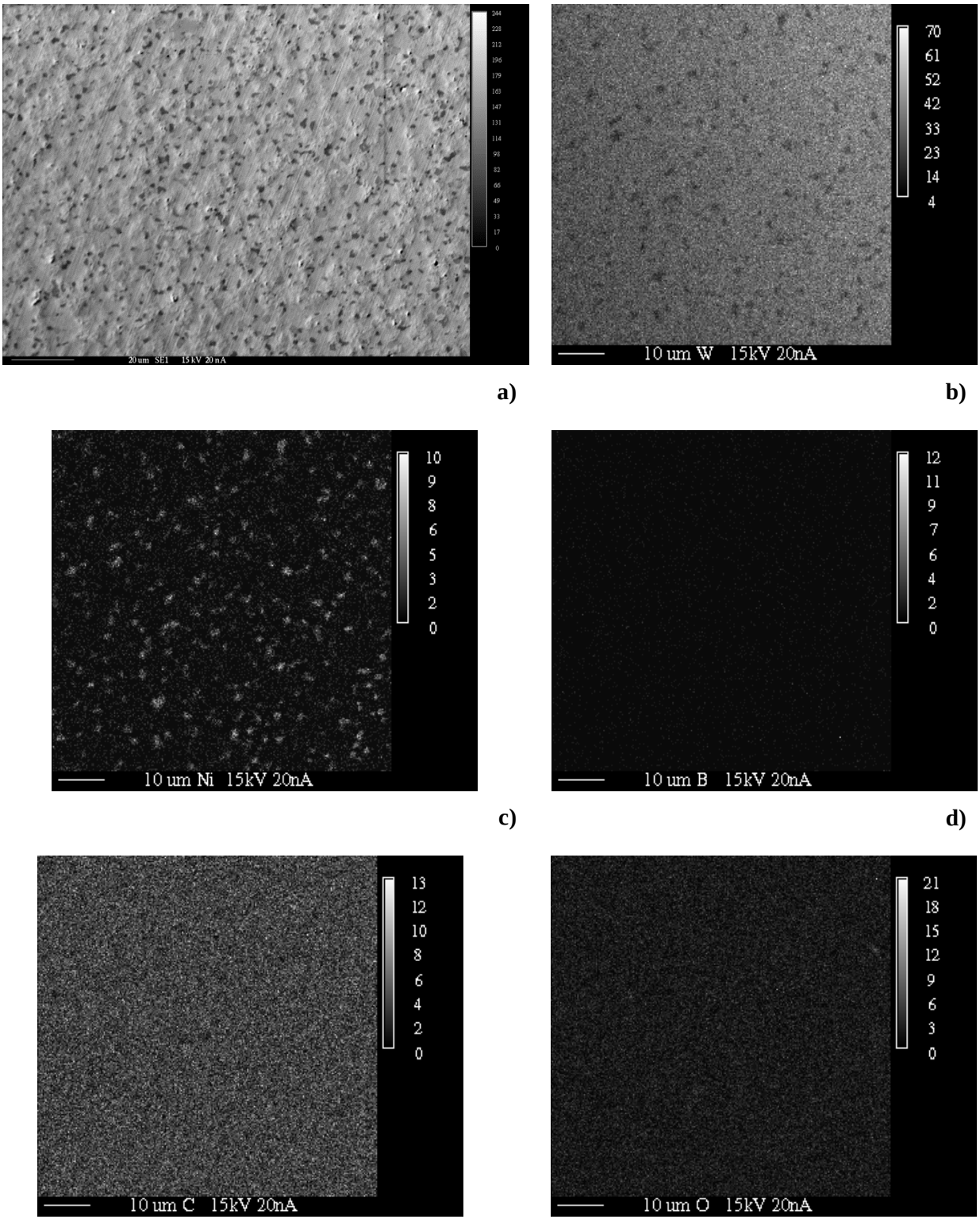

Figure 5.19: EPMA micrographs taken from the sintered W - 1 wt % Ni - 2 wt % WB sample MA'd for 18h: **a)** BSE image, **b)** W, **c)** Ni, **d)** B, **e)** C, **f)** O elemental mappings.

High magnification SEM micrographs and EDS spectra of the sintered W - 1 wt % Ni - 2 wt % WB sample MA'd 18h are given in Figures 5.20 and 5.21. Tungsten, nickel and oxygen elements are detected in both images. On the basis of EDS spectral evidence, it indicates that the light gray tiny grains are nickel rich regions.

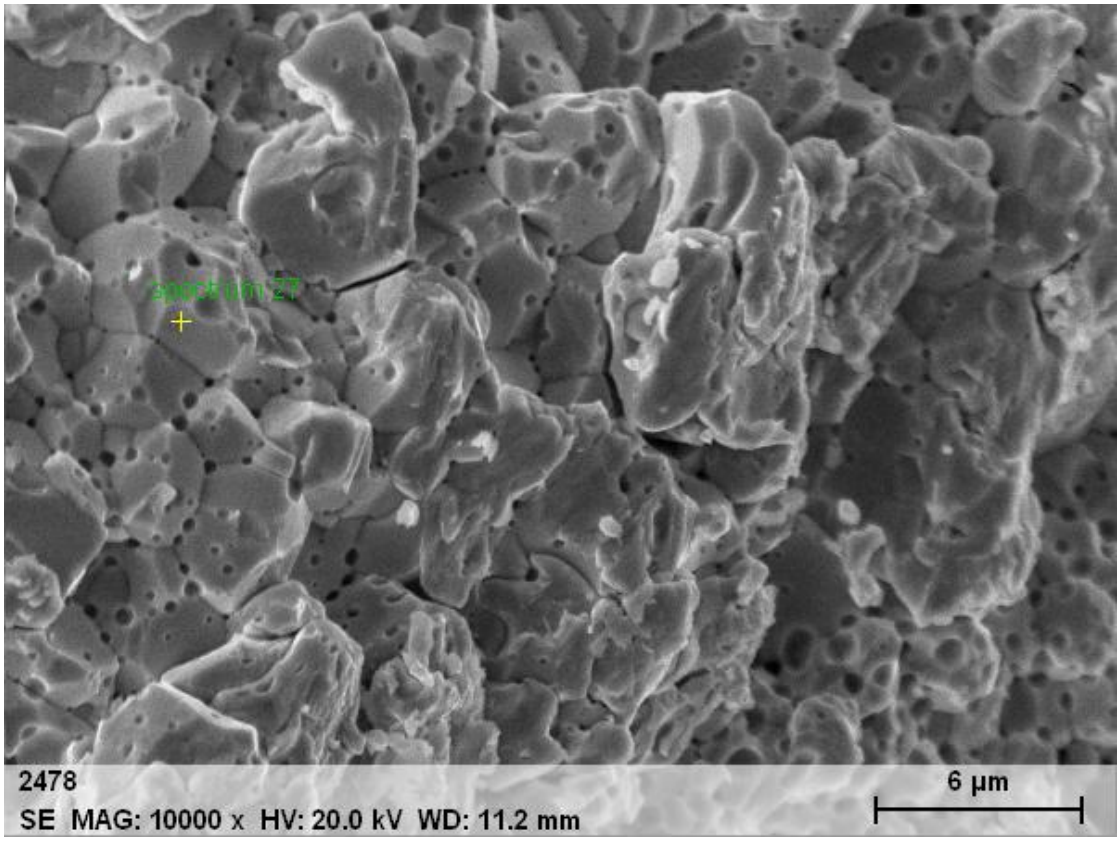

Spectrum 27

Element	Weight %	Atomic %	Error %
Oxygen	0,24	2,64	0,1
Tungsten	98,88	94,73	3,7
Nickel	0,88	2,64	0,1

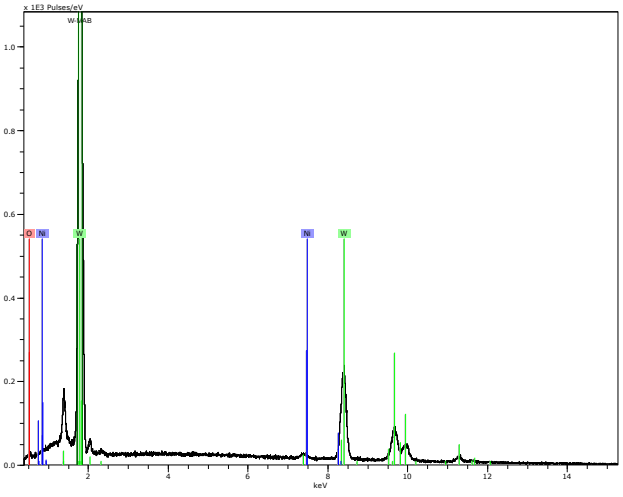

Figure 5.20: High magnification SEM micrograph and respective EDS spectrum of the sintered W - 1 wt % Ni - 2 wt % WB sample MA'd or 18h**.**

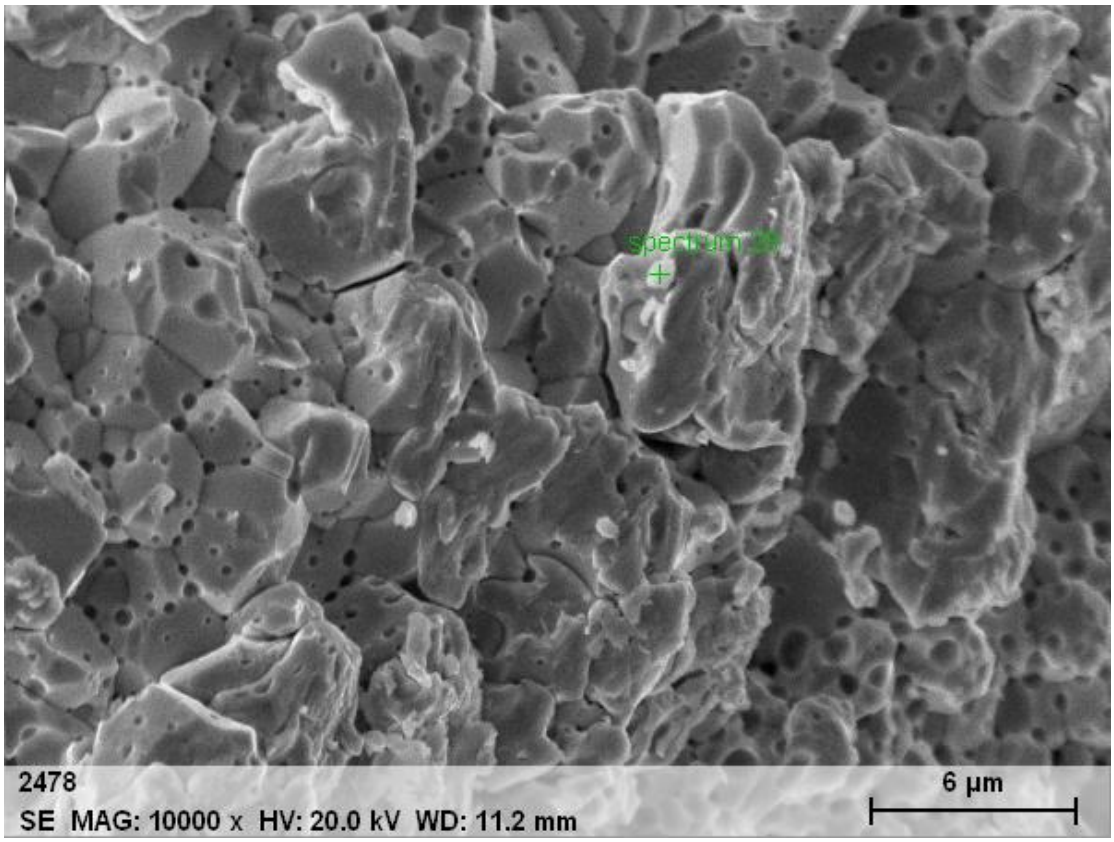

Spectrum 28

Element	Weight %	Atomic %	Error %
Oxygen	3,06	22,55	0,6
Tungsten	85,69	54,89	3,2
Nickel	11,24	22,55	0,4

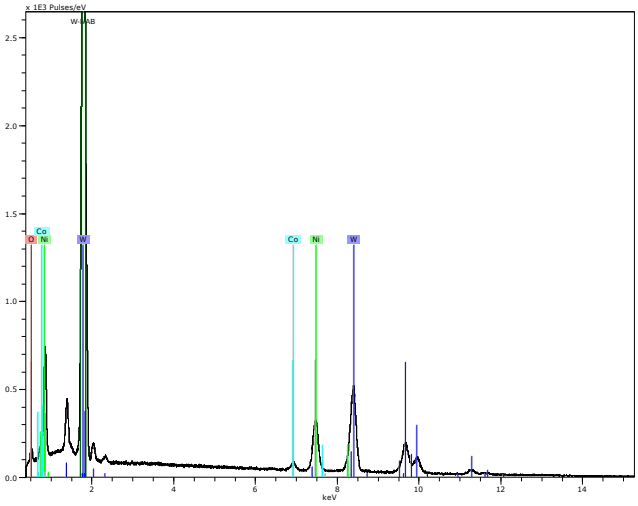

Figure 5.21: High magnification SEM micrograph and respective EDS spectrum of the sintered W - 1 wt % Ni - 2 wt % WB sample MA'd for 18h.

Figure 5.22 shows the back-scattered SEM micrograph of worn surfaces of the sintered W - 1 wt % Ni - 2 wt % WB sample MA'd for 18h. The wear amount and average friction coefficient are measured as 1,84 ± 0.025 ($mm^3N^{-1}m^{-1}$) $x10^{-6}$ and 0.46, respectively. As seen in Figure 5.22, the worn surface of the sintered W - 1 wt % Ni - 2 wt % WB sample contains multiple valleys with patches ruptured from the surface and/or the hardfacing alumina balls during sliding wear experiments.

Comparing Fig. 5.9 and 5.22, one can see the significant effect of the WB addition on the wear resistance of the composite: The wear amount of the sintered W1Ni sample decreases with the addition of WB particles from about 4.22±0,021 to 1.84±0,005 ($mm^3N^{-1}m^{-1}$) $x10^{-6}$.

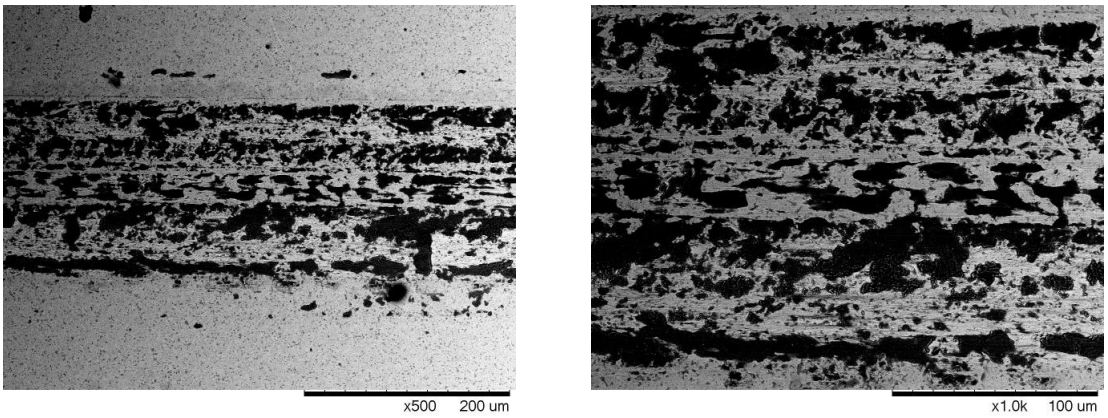

Figure 5.22: Back-scattered SEM micrographs of the wear tracks of the sintered W - 1 wt % Ni - 2 wt % WB sample. Right micrograph is higher magnification image of the wear tracks.

5.4 The Effect of La_2O_3 on the W - 1 wt % Ni - 2 wt % WB Composite

5.4.1 Characterization of the powders

XRD patterns of 18 h MA'd W - 1 wt % Ni - 2 wt % WB - 0.5 wt % La_2O_3, W - 1 wt % Ni - 2 wt % WB - 1 wt % La_2O_3 powders are shown in Figure 5.23a–b. As clearly seen in these figures, b.c.c. W phase is identified in all powder samples. WB or La_2O_3 phases are not observed due to small additions.

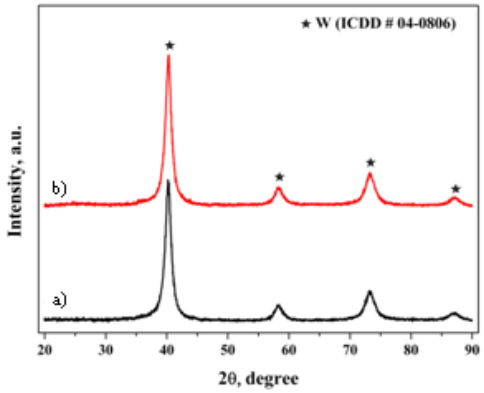

Figure 5.23: XRD patterns of **a)** W - 1 wt % Ni - 2 wt % WB - 0.5 wt % La_2O_3 **b)** W - 1 wt % Ni - 2 wt % WB - 1 wt % La_2O_3 powders MA'd for 18h.

The effect of La_2O_3 and TiB_2 addition on the particle size can be seen in Figure 5.24a and 5.24b. W - 1 wt % Ni - 2 wt % WB - 0.5 wt % La_2O_3 18h MA'd powders have mean particle size of 0.399 μm whereas the W - 1 wt % Ni - 2 wt % WB - 1 wt % La_2O_3 18h MA'd powders have mean particle size of 0.294 μm. According to these results, mean particle size is decreased by increasing La_2O_3 addition.

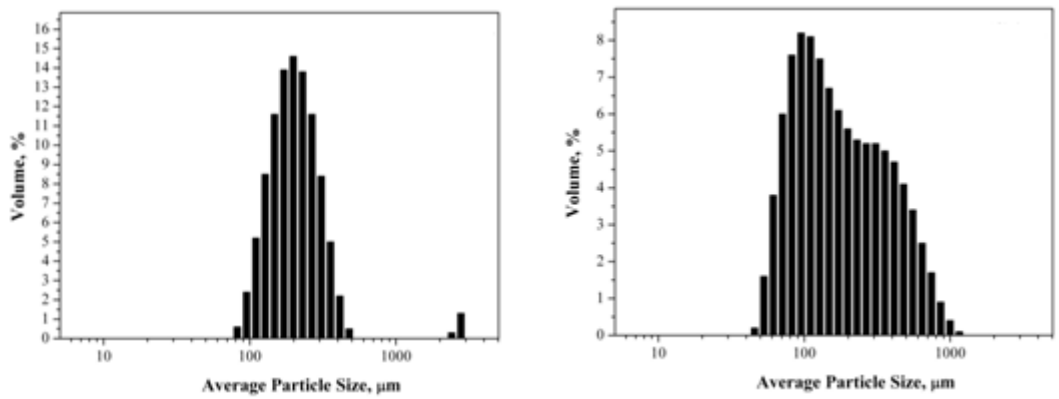

a) **b)**

Figure 5.24: Particle size distributions of a) W - 1 wt % Ni - 2 wt % WB - 0.5 wt % La_2O_3 (D_{mean}=0.399 μm), b) W - 1 wt % Ni - 2 wt % WB - 1 wt % La_2O_3 powders 18h MA'd (D_{mean}=0.294 μm).

Figure 5.25 shows the representative SEM micrographs taken from the W - 1 wt % Ni - 2 wt % WB - 1 wt % La_2O_3 powders MA'd for 18 h. The SEM micrographes reveal that the microstructure consists of spherical like submicron particles with some micron sized agglomerates.

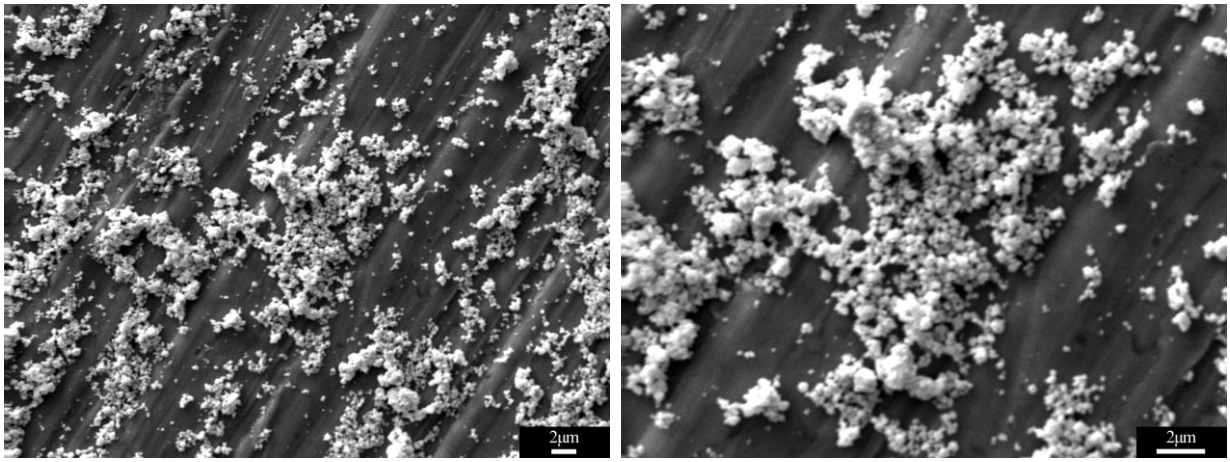

Figure 5.25: SEM micrograph of the W - 1 wt % Ni - 2 wt % WB - 1 wt % La_2O_3 powder MA'd for 18h. The right migrograph has a higher magnification.

5.4.2 Characterization of the sintered samples

Figure 5.26 shows the XRD patterns of the sintered W - 1 wt % Ni - 2 wt % WB - 0.5 wt % La_2O_3, W - 1 wt % Ni - 2 wt % WB - 1 wt % La_2O_3 samples MA'd for 18 h. Only the W (ICDD # 04 - 0806) is identified. Alhough these samples contain the phases, no peaks are diffracted from WB or La_2O_3 phases due to their small amounts.

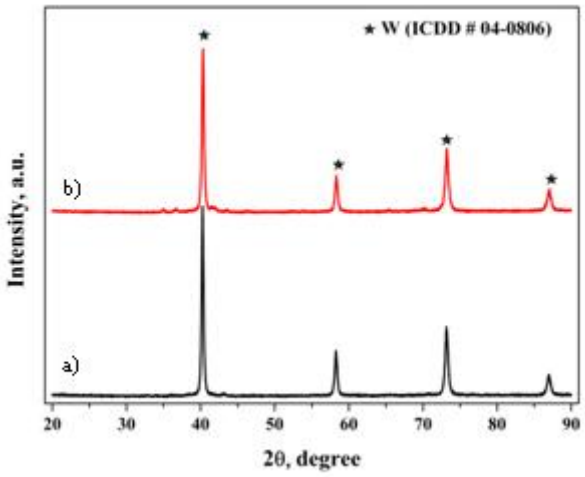

Figure 5.26: XRD patterns of the 18 h MA'd and sintered **a)** W - 1 wt % Ni - 2 wt % WB - 0,5 wt % La_2O_3, **b)** W - 1 wt % Ni - 2 wt % WB - 1 wt % La_2O_3 samples.

The relative density measurements and corresponding theoretical density values of the 18 h MA'd and sintered samples of the W - 1 wt % Ni - 2 wt % WB - y wt % La_2O_3 (y=0.5,1) system are given in Table 5.4. Although an increasing tendency in the relative density values are observed in Table 5.4 with increasing WB contents, relative density values do not drastically increase with La_2O_3 addition. However, microhardness values increase with increasing La_2O_3 contents.

Table 5.6: Relative density and microhardness values of the sintered samples

Sample Name	Theoretical Density (gr/cm3)	Relative Archimedes' Density (%)	Microhardness (GPa)
W - 1 wt % Ni - 2 wt % WB - 0,5 wt % La_2O_3	18.79	96.47	5.35
W - 1 wt % Ni - 2 wt % WB - 1 wt % La_2O_3	18.62	96.97	6.02

SEM micrographs taken from both as-sintered and fractured surfaces of the MA'd for 18 h and sintered W - 1 wt % Ni - 2 wt % WB - 0.5 wt % La_2O_3 are given in Figure 5.27a and b and W - 1 wt % Ni - 2 wt % WB - 1 wt % La_2O_3 are given in Figure 5.27 c and d. The micrographs show homogeneously distributed micron scale black particles consisting of both WB and La_2O_3 phases. The black particles are located both at grain boundaries and grains interiors.

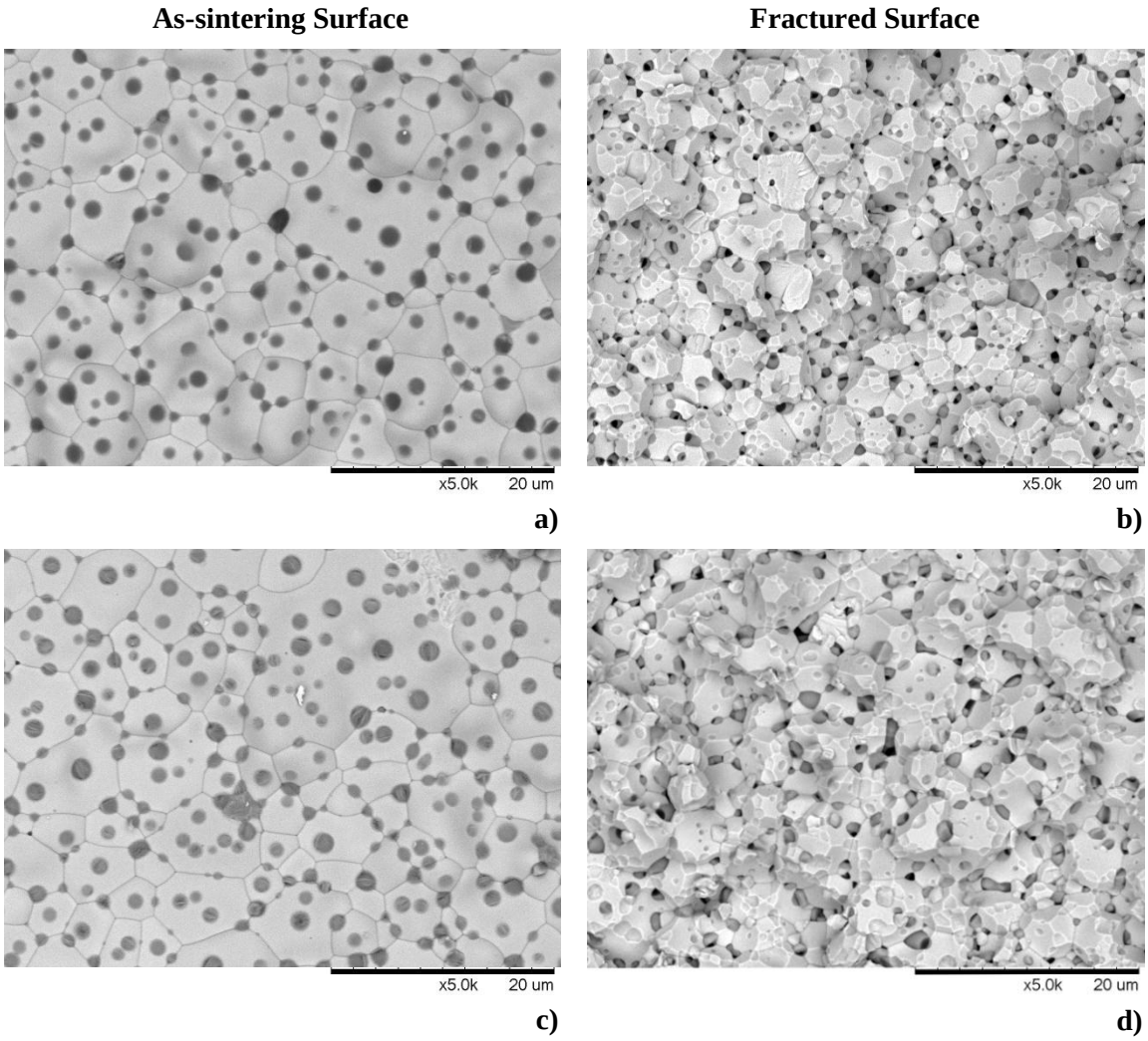

Figure 5.27: Back-scattered SEM micrographs of 18 h MA'd and sintered **a, b)** W - 1 wt % Ni - 2 wt % WB - 0.5 wt % La_2O_3, **c, d)** W - 1 wt % Ni - 2 wt % WB - 1 wt % La_2O_3 samples.

EPMA BSE image and W, Ni, O, C elemental mappings of 18h MA'd and sintered W - 1 wt % Ni - 2 wt % WB - 1 wt % La_2O_3 sample are given in Figures 5.28a-f. Figure 5.28b showing Ni mapping on the BSE image is indicating nickel rich regions. Besides these elements, La, B and O have homogenous distributions can be seen in Figure 5.28d, e and f.

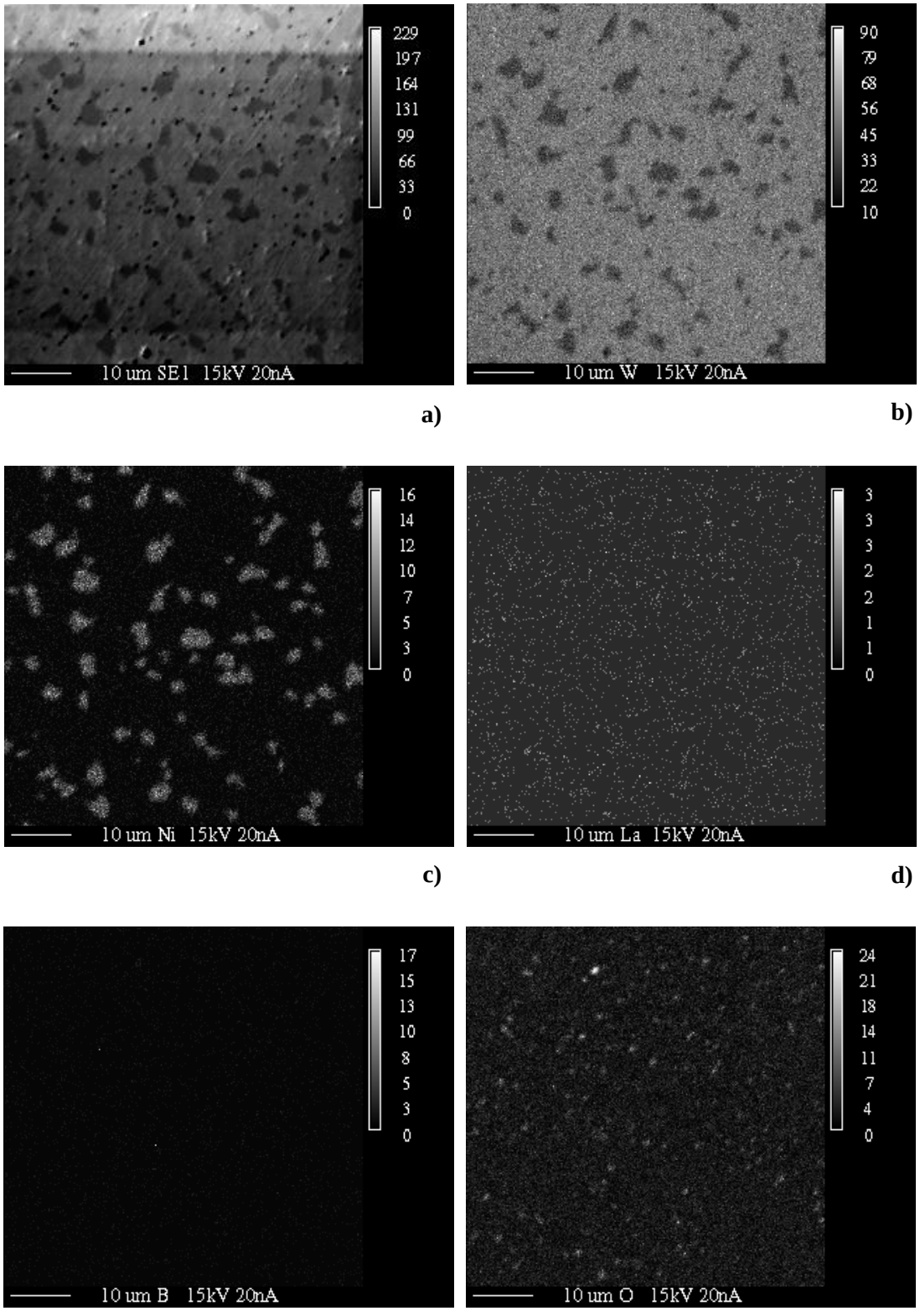

Figure 5.28: EPMA micrographs taken from the sintered W - 1 wt % Ni - 2 wt % WB - 1 wt % La_2O_3 sample MA'd for 18h: **a)** BSE image, **b)** W, **c)** Ni, **d)** La, **e)** B, **f)** O elemental mappings.

High magnification SEM pictures and EDS analysis of 18h MA'd and sintered W - 1 wt % Ni - 2 wt % WB - 1 wt % La_2O_3 are given in Figure 5.29 and 5.30. Tungsten, nickel, lanthanum and oxygen elements detected in both images. Comparising EDS analyses reveals all element have homogenous distribution but tiny grains are lanthanum and nickel rich regines.

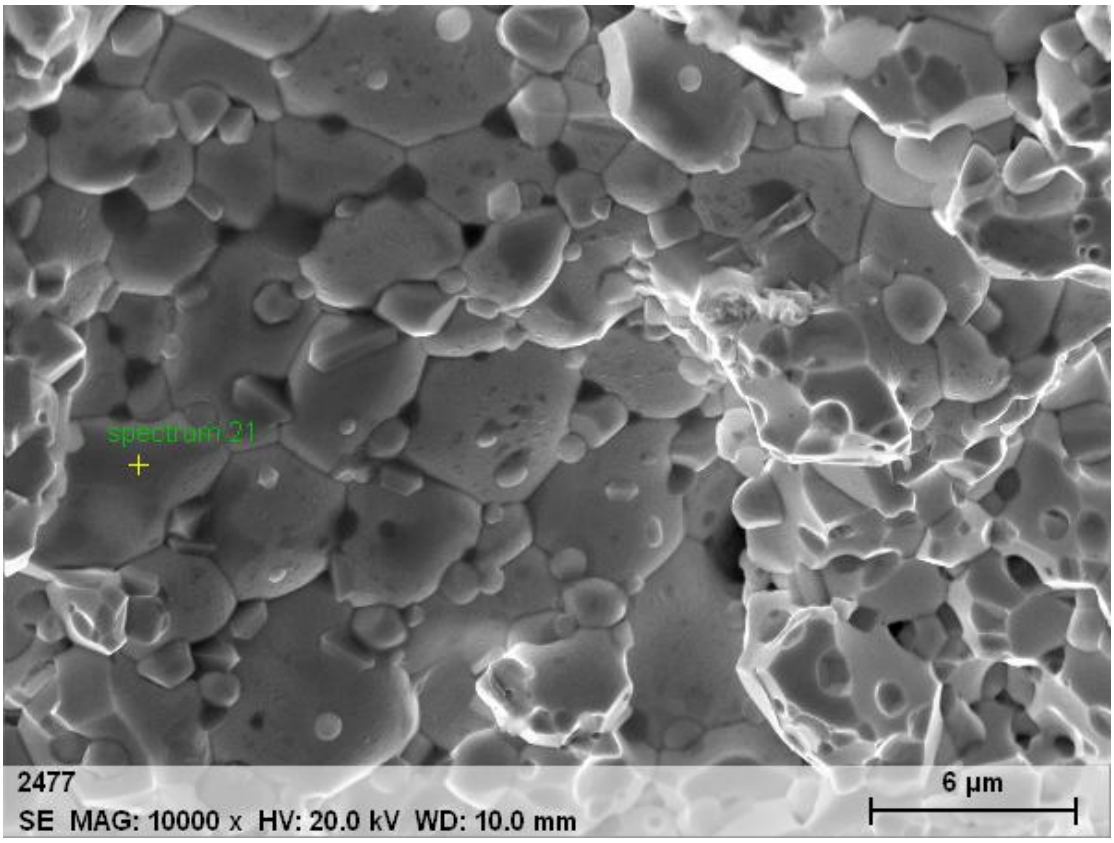

Spectrum 21

Element	Weight %	Atomic %	Error %
Oxygen	0,17	1,84	0,1
Lanthanum	0,86	1,10	0,1
Tungsten	98,37	95,21	6,2
Nickel	0,61	1,84	0,1

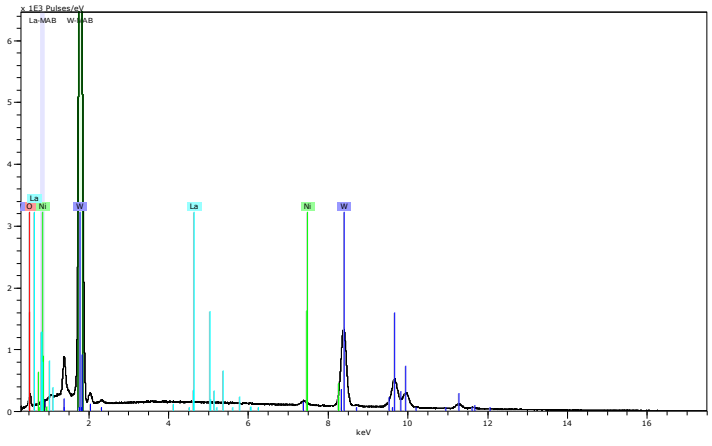

Figure 5.29: High Magnification SEM picture and EDS analyses of W - 1 wt % Ni - 2 wt % WB - 1 wt % La_2O_3 sample.

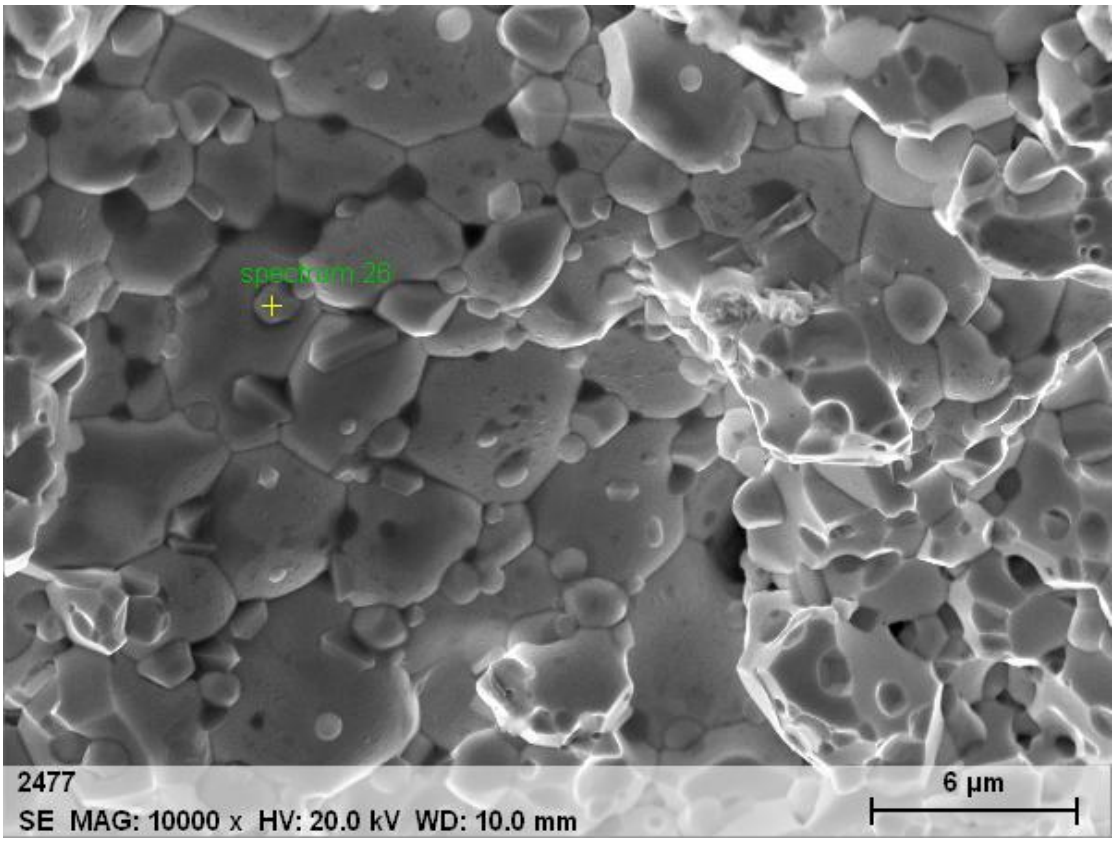

Spectrum 26

Element	Weight %	Atomic %	Error %
Oxygen	0,86	9,00	0,2
Lanthanum	1,19	1,44	0,1
Tungsten	97,95	89,56	3,4

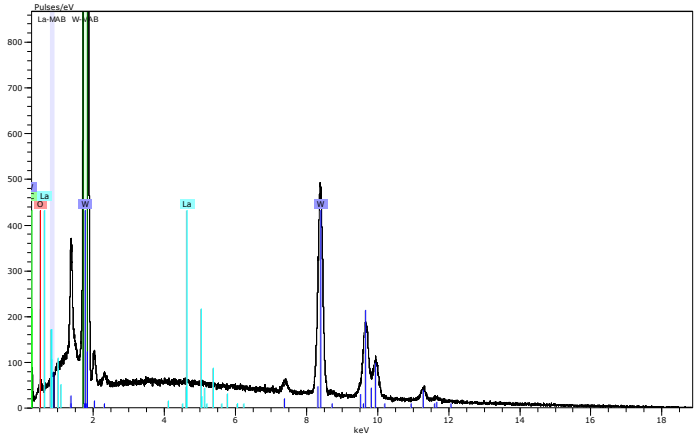

Figure 5.30: High magnification SEM picture and EDS analyses of W-1 wt % Ni - 2 wt % WB - 1 wt % La_2O_3 sample**.**

Figure 5.31 shows the back - scattered SEM micrograph of worn surfaces of 18 h MA'd and sintered W - 1 wt % Ni - 2 wt % WB - 1 wt % La_2O_3 sample. The wear amount and average friction coefficient are measured as 4,64 ±0,021 ($mm^3N^{-1}m^{-1}$) $x10^{-6}$ and 0.45, respectively.

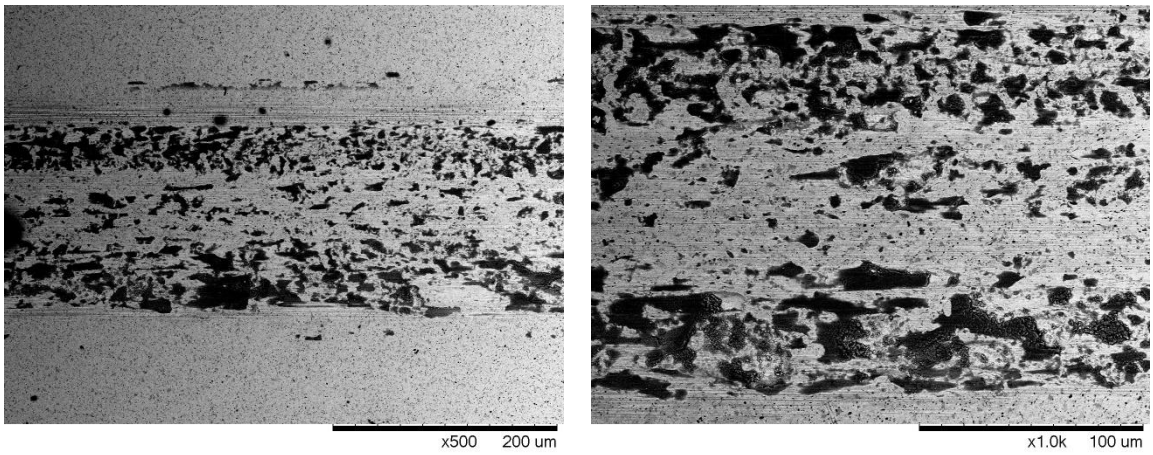

Figure 5.31: Back-scattered SEM micrographs of the wear tracks of 18h MA'd and sintered W - 1 wt % Ni - 2 wt % WB - 1 wt % La_2O_3 sample. The right hand side is higher magnification image of the wear tracks.

Wear characterizations results of 18 h MA'd and sintered W - 1 wt %Ni,W - 1 wt %Ni - 2 wt %WB and W - 1 wt % Ni - 2 wt % WB - 1 wt % La_2O_3 samples are given in Table 5.5. According to the results, W - 1 wt % Ni - 2 wt % WB - 1 wt % La_2O_3 sample has the highest wear amount. Addition of WB causes drastically increasing of wear resistance for W - 1 wt % Ni sample. On the other hand, WB and La_2O_3 additives cause decrease of wear resistance.

Table 5.7: Effects of WB and/or La_2O_3 additions of W - 1 wt % Ni composites on wear characterizations.

Sample Name	**Relative wear loss**	**Wear amount ($mm^3N^{-1}m^{-1}$) $x10^{-6}$**	**Max. friction coefficient**	**Average friction coefficient**
W - 1 wt % Ni	0,91	4,22±0,019	0,56	0,42
W - 1 wt %Ni - 2 wt % WB	0,39	1,84±0,005	0,56	0,46
W - 1 wt % Ni - 2 wt % WB - 1 wt % La_2O_3	1	4,64±0,021	0,57	0,45

6. CONCLUSIONS

In this study, W – 1 wt % Ni, WB, La_2O_3 powders are selected as starting powders. W – 1 wt % Ni, W – 1 wt % Ni - x wt % WB (x=0.5, 1, 2, 4), W – 1 wt % Ni - 2 wt % WB - y wt % La_2O_3 (y=0.5, 1) powders are MA'd for 18 h and W – 1 wt % Ni - 2 wt % WB powders are MA'd for different durations and sintered at 1400 ^oC for 1h where the W – 1 wt % Ni samples are chosen as a control group. XRD, particle size distrubition, SEM and BET experiments are done to characterize the powders. XRD, Archimedes' density, Vickers microhardness, SEM, sliding wear experiments are conducted to investigate the characteristics of the sintered samples. According to the results;

1. Particle size distributions of the powders slightly decrease with MA and submicron particles are generally obtained for all samples.
2. Peak intensities decrease and peaks are broadened with increasing MA durations in XRD analyses.
3. All the peaks belong to W phase (ICDD # 04-0806) in XRD analyses of the MA'd powders.
4. MA duration or WB and La_2O_3 additives have no significant effects on morphology of powders.
5. WB, Ni and La_2O_3 phases are not observed in XRD analyses of the powders due to the small amounts or peak broadening.
6. Generally, submicron particles with micron sized agglomerates are seen in SEM investigations of the powders. WB or/and La_2O_3 additions to the W - 1 wt % Ni matrix have no significant effect on decreasing particle size.
7. Specific surface area of powders increase with MA time, are consistent with mean particle size.
8. Relative Archimedes's density values generally increase with incresing MA durations.
9. Relative Archimedes' density values increase with increasing WB content.

10. In addition to Ni has a dominant role in densification MA'd composites, WB contents also effect densification.
11. The sintered samples of W - 1 wt % Ni - 2 wt % WB - 18 h MA'd and W - 1 wt % Ni - 2 wt % WB - 0.5 wt % La_2O_3 - 18h MA'd powders have higher relative Archimedes' density values than the sintered samples of W - 1 wt % Ni - 18 h MA'd powders.
12. The sintered samples of W - 1 wt % Ni - 2 wt % WB - 1 wt % La_2O_3 - 18h MA'd powders have the highest relative Archimedes' density values of 97.89%.
13. Vickers microhardness values increase with increased mechanical alloying durations of the powders.
14. Microhardness values slightly increase with increased amount of WB.
15. WB addition provide increasing Vickers microhardness values of the sintered W - 1 wt % Ni sample.
16. The sintered W - 1 wt % Ni - 2 wt % WB - 18 h MA'd samples have the highest Vickers microhardness value of 6,45 GPa where the value is 5,15 GPa for the sintered samples of W - 1 wt % Ni - 18 h MA powders.
17. While 2 wt % WB addition decreases wear resistance of W - 1 wt % Ni, 1 wt % La_2O_3 addition increase wear resistance of W - 1 wt % Ni - 2 wt % WB.

REFERENCES

Akovali, G. and Uyanik, N. (2001). Introduction in Handbook of Composite Manifacturing, Ed. G. Akovali, Rapra Technology Ltd.

Askeland, D.R. (1984). The Science and Engineering of Materials, Brooks/Cole Engineering Division, CA.

Asthana, R., Kumar, A., Dahotre, N.B. (2006). Composite Materials in Materials Processing and Manufacturing Science: 397-484.

Asthana, R., Kumar, A., Dahotre, N.B. (2006). Powder Metallurgy and Ceramic Forming in Materials Processing and Manufacturing Science: 167-245.

Åström, B. Thomas. (2001), ASM International Handbook, Processing of Metal Matrix Composites: 1359-1381.

Baci, F.M. (1997). Heat Transfer During Consolidation of Metal Matrix Composites by The HIP Process,M.Sc Thesis, Ohio University.

Benjamin, J. S. (1970), Metallurgical Transactions, 1: 2943

Benjamin, J.S. (1992). Fundamentals of mechanical alloying. Materials Science Forum, 88-90: 1-18.

Boch, P. and Leriche, A. (2001). Sintering and Microstructure of Ceramics in Ceramic Materials Edited by Philippe Boch and Jean- Claude Niepce, HERMES Science Europe Ltd.

Brophy, J.H., Hayden, H.W., Prill, A.L. and Wulff, J. (1963). The Investigation of the Activated Sintering of Tungsten Powder. Final Report, Prepared under U.S. Navy, Bureau of Naval Weapons Contract NO w 61-0326-d, Massachusetts Institute of Technology, Cambridge, Massachusetts.

Cahn, R.W. (2001). The Coming of Materials Science, Pergamon, Amsterdam.

Campbell, F.C. (2006). Metal Matrix Composites in Manufacturing Technology for Aerospace Structural Materials: 419-457

Castaing, J., Costa, P. (1977). Boron and refractory borride, Springer-Verlag, N.Y., 390.

Chawla, N. and Chawla, K.K. (2006). Metal Matrix Composites, Springer, N.Y.

Chawla, N. and Shen, Y.L. (2001). Mechanical behavior of particle reinforced metal matrix composites, Advanced Engineering Materials, 3: 357-370.

Chen, Z. Zhou, M. and Zuo, T., (2000). Morphological evolution of second-phase particles during thermomechanical processing of W-La_2O_3 alloy, Scripta mater., 43: 291–297.

Clyne, T.W.. (2000). An Introductory Overview of MMC Systems, Types, and Developments in Vol.3 Metal Matrix Composites of Comprehensive Composite Materials, Elsevier.

Clyne, T.W. (2001). Metal matrix composites: matrices and processing, in Encyclopaedia of Materials: Science and Technology, Ed. Mortensen, A., Elsevier.

Clyne, T.W. and Withers, P.J. (1993). Introduction to Metal Matrix Composites, Cambridge University Press, Cambridge.

Coskun, S. (2006). Development and Characterization Investigations of Mechanically Alloyed W-SiC and W-SiC-Y_2O_3 Composites. *M.Sc. Thesis*, I.T.U., Istanbul.

Coskun, S. (2011). Synthesis, development and characterization of W-based compounds, composites and hybrid materials. *Ph.D. Thesis*, I.T.U., Istanbul.

Das, K. Bandyopadhyay, T.K., Das, S., (2002). A Review on the various synthesis routes of TiC reinforced ferrous based composites. *Journal of Materials Science*, 37: 3881-3892.

Davis, J. (1993), ASM Speciality Handbook: Aluminum and Aluminum Alloys,HPB-Ohio, Columbus.

Delogu, F. Orrù, R. and Cao, G**.,** (2003). A novel macrokinetic approach for mechanochemical reactions, *Chemical Engineering Science*, 58: 815-821.

El-Eskandarany. (2001). Mechanical Alloying for Fabrication of Advanced Engineering Materials, Noyes Publications, New York.

El-Eskandarany, M.S., **Mahday, A.A., Ahmed,H.A and Amer, A.H.** (2000). Synthesis and characterizations of ball-milled nanocrystalline WC and nanocomposite WC–Co powders and subsequent consolidations, *Journal of Alloys and Compounds*, 312: 315–325.

Fecht, H.J. (2002). Nanostructured materials and composites prepared by solid state processing, in Nanostructured Materials: Processing, Properties and Potential Applications, Ed. Koch, C.C., Noyes Publications, New York.

Genc, A., Coşkun, S., Öveçoğlu, M.L. (2010). Fabrication and properties of mechanically alloyed and Ni activated sintered W matrix composites reinforced with Y_2O_3 and TiB_2 particles, Materials Characterization., 61: 740-748.

German, R.M. (1985), Liquid Phase Sintering, Plenum Press, New York.

German, R.M. (1996.) Sintering Theory and Practice, John Wiley & Sons, Inc.

German, R.M and Munir, Z.A. (1976). Enhanced Low-Temperature Sintering of Tungsten. Metallurgical Transactions A, 7A: 1873-1877.

German, R.M and Munir, Z.A. (1982). Activated Sintering of Refractory Metals by Transition Metal Additions. Rev. *Powder Metall. Phys. Ceram.*,2: 9.

Goff, A. (2003). Modeling and synthesis of a piezoelectric ceramic-reinforced metal matrix composites. MS Thesis, Virginia Polytechnic Institute and State University, Blacksburg, VA.

Gostishchev, V.V., Boiko V.F. and Pinegina, N.D. (2009). Magnesiothermal synthesis of W-WB powders in ionic melts, *Theorical Foundations of Chemical Engineering*, 43: 468-472.

Han, B.Q., Lavernia, E.J. and Mohamed, F.A. (2005). Mechanical properties of nanostructured materials, *Rev.Adv.Mater.Sci*., 9: 1-16.

Hayden, H.W. and Brophy, J.H. (1963). The Activated Sintering of Tungsten with Group VIII Elements, *Journal of Electrochemical Society*, 110: 805-810.

Hansen, N. (1971). Dispersion Strengthened Aluminum Products--Manufacture, Structure and Mechanical Properties, Riso National Laboratory, Denmark.

Huda, M.D., Hashmi, M.S.J. and El-Baradie, M.A. (1995). MMCs: materials, manufacturing and mechanical properties. *Key Engineering Materials*, 104-107: 37-64.

Ibrahim, I.A., Mohamed, F.A. and Lavernia, E.J. (1991). Particulate reinforced metal matrix composites–a review. Journal of Materials Science, 26: 1137-1156.

Tang, F., X. Wu, S. Ge, J. Ye, H. Zhu, M. Hagiwara, J.M. Schoenung. (2008). Dry sliding friction and wear properties of B4C particulate-reinforced Al-5083 matrix composites, Wear 264, 555–561.

Tang, H.G., Ma, X.F., Zhao, W., Yan, X.W., Yan, J.M. and Zhu, C.J. (2004). Crystallization of mechanically alloyed amorphous W–Mg alloy under high pressure, *Solid State Communications*, 129: 147–150.

Tjong, S.C. and Ma, Z.Y. (2000). Microstructural and mechanical characteristics of in situ metal matrix composites, Materials Science and Engineering, 29: 49-113.

Kainer, K.U. ed. (2006). Metal Matrix Composites, Weinheim,Wiley-VCH

Kang, S-J.L. (2005). Sintering Densification, Grain Growth and Microstructure. Elsevier.

Kim, Y., Hong, M.H., Lee, S.H., Kim, E.P., Lee, S., Noh, J.W. (2006). The effect of yttrium oxide on the sintering behaviour and hardness of tungsten, *Metals and Materials International*, 12: 245-248

Kim, Y., Lee, H.K., Kim, E., Cheong, D., Hong, S.H. (2009) Fabrication of hihg temperature oxides strengthened tungsten composites by spark plasma sintering process, *International Journal of Refractory Metals & Hard Metals.*, 27**:** 842-846.,

Kurishita, H., Matsuso, S., Arakawa, H., Hirai, T., Linke, J., Kawai, M. (2009). Development of nanostructured W and Mo materials, Advanced Materials Research, 59: 18-30.

Krajnikov, A.V., Demidik, A.N., Ortner, H.M. (1997). Mechanical properties and interface boundary composition of ferritic steel strengthened by yttrium and titanium disperse oxides, *Materials Science and Engineering A*, 234-236**:** 357-360.

Khomskaya, V.I. (2010). Structure formed in two-phase (α + γ) field and mechanical properties of a cryogenic alloy 10N7, *The Physics of Metal and Metallography*, 110, 2: 188-198.

La Caer, G., **Delcroix, P., Begin-Colin, S. and Ziller, T.** (2002). High-energy ball-milling of alloys and compounds, *Hyperfine Interactions,* 141-142: 63-72.

Lassner, E. (1999). Tungsten: Properties, Chemistry, Technology of the Element, Alloys, and Chemical Compounds, Kluwer Academic,Plenum Publishers,NY.

Lassner, E. and Schubert, **W.D**. (1999). Tungsten: Properties, Chemistry, Technology of the Element, Alloys and Chemical Compounds, Kluwer Academic, New York.

Lee, K.H., Yoon, J.K., Lee, J.K., Doh, J.M., Hong, K.T. and Yoon, W.Y. (2004). Growth Kinetics of W_5Si_3 Layer in WSi_2/W System, *Surface & Coatings Technology*, 187: 146-153.

Lloyd, D.J. (1994). Particle reinforced aluminium and magnesium matrix composites, *International Materials Reviews*, 39: 1-23.

Li, C. and German, R.M. (1983). The Properties of Tungsten Processed by Chemically Activated Sintering, *Metallurgical Transactions A*, 14A: 2031-2041.

Lindroos, V.K., Hellman, J.T., Lou, D., Nowak, R., Pagounis, E., Liu, X.W. and Penttiren, I.M. (2004). Designing with metal matrix composites, in Handbook of Mechanical Alloy Desi*gn*, Eds. Totten, G.E., Xie, L. and Funatani, K, M. Dekker, New York.

Lindroos, V.K., Hellman, J.T., Lou, D., Nowak, R., Pagounis, E., Liu, X.W. and Penttiren, I.M. (2004). Designing with metal matrix composites, *Handbook of Mechanical Alloy Design*, Eds. Totten, G.E., Xie, L. and Funatani, K, M. Dekker, New York.

Liu, Y.B., Lim, S.C., Lu, L. and Lai, M.O. (1994). Recent development in the fabrication of metal matrix particulate composites using powder metallurgy techniques. *Journal of Materials Science*, 29: 1999-2007.

Orowan, E. (1948), Internal Stresses in Metals and Allovs, Inst. of Metals, London, pp. 451-65.

Ohring, M. (1995). Engineering Materials Science, Stevens Institute of Technology, New Jersey, USA: 463-486.

Mabuchi, M. Okamoto, K., Satio, N., et al., (1996). Tensile properties at elevated temperatures of W-1%La_2O_3, *Materials Science & Engineering A*, 214: 174-176.

Mabuchi, M. Okamoto, K., Saito, N., Asahina, T. and Igarashi, T., (1997). Deformation behavior and strengthening mechanisms at intermediate temperatures in W-La_2O_3, *Materials Science & Engineering A*, 237: 241-249.

Massalski, T.B. (1990). Binary alloy phase diagrams, 2nd ed., ASM, Metals Park, OH, USA.

Mazumdar, S.K. (2002). Composite Manifacturing, Materials, Product and Process Engineering, CRC Press LLC, Florida.

Miracle, D.B. (2005). Metal matrix composites-from science to technological significance, *Composite Science and Technology*, 65: 2526-2560.

Munro, R.G. (2008.) Material properties of titanium diborride, *Journal of Research of the National Institute of Standarts and Technology*, 105: 709-720.

Monov, V., Sokolov, B., Stoenchev, S. (2012). Grinding in ball mills: grinding and process control, *Cybernetics and Information Technologies*, 12: 2.

Mott N.F. **and F.R.N. Nabarro**, (1948), Strength of Solids, Physical Society, London: 1-19.

Newkirk, J.W. and Kohser, R.A. (2004). Designing with powder metallurgy alloys, Handbook of Mechanical Alloy Design, Eds. Totten, G.E., Xie, L. And Funatani, K, M. Dekker, New York.

Ovecoglu, M.L., (1987). Development of a dispersion-strengthened Al-Fe-Ce alloy by mechanical alloying and related theoretical modeling of dislocations in composite materials. PhD Thesis, Stanford University, Los Angeles, CA .

Park, S.J., Seo, M. K. (2011). Interface sciene and composites, Elsevier, Oxford.

Panichkina, V.V. (1967). Activated sintering of tungsten with small additions of nickel, *Poroshkovaya Metallurgiya* (In Russian), 2: 1-5.

Rahaman, M.N. (2005), Ceraöic Processing and Sintering, Taylor and Francis e-library.

Redsten, A.M., Klier, E.M., Brown, A.M., Dunand, D.C. (1995). Mechanical properties and microstructure of cast oxide-dispersion-strengthened aluminum, *Materials Science and Engineering A*, 201: 88-102.

Ring, T.A. (1996). Sintering in Fundamentals of Ceramic Powder Proscessing and Synthesis: 781-874.

Ryu, H.J., Hong, S.H. and Baek, W.H., (2000). Microstructure and mechanical properties of mechanically alloyed and solid-state sintered tungsten heavy alloys, *Materials Science and Engineering A*, 291: 91–96.

Ryu, H.J., Hong, S.H. (2003). Fabrication and properties of mechanically alloyed oxide-dispersed tungsten heavy alloys, *Materials Science & Engineering A*, 363**:** 179-184.

Sakasegawa, H., Tamura, M., Ohtsuka, S., Ukai, S., Tanigawa, H.,Kohyama, A., Fujiwara, M. (2008). Precipitation behaviour of oxide particles in mechanically powder of oxide-dispersion-strengthened steel, *Journal of Alloys and Compounds*: 452: 2-6.

Schwartz, M.M. (1984). Composite Materials Handbook, McGraw-Hill, New York.

Schwartz, M.M. (1997). Composite Materials-Vol.2., Prentice Hall, Portland, OR.

Song, G.M., Wang, Y.J. and Zhou, Y. (2002). The mechanical and thermophysical properties of ZrC/W composites at elevated temperature, *Materials Science and Engineering A*, 334: 223–232.

Song, G.M., **Zhou, Y. and Wang, Y.J.** (2003)a. Effect of carbide articles on the ablation properties of tungsten composites, *Materials Characterization*, 50: 293– 303.

Song, G.M., Wang, Y.J. and Zhou, Y. (2003b). Thermomechanical properties of TiC particle-reinforced tungsten composites for high temperature applications, International Journal of *Refractory Metals & Hard Materials*, 21: 1–12.

Soni, P.R. (2001), Mechanical Alloying: Fundamental and Applications, Cambridge International Science Publishing, Cambridge.

Stjernstoft, T. (2004). Machining of some difficult-to-cut materials with rotary cutting tools, PhD Thesis, K.T.H., Stockholm.

Sun, L.Z., Liu, H.T. and Ju, J.W. (2003). Effect of particle cracking on elastoplastic behaviour of metal matrix composites, *Int. J. Numer. Meth. Eng*, 56: 2183–2198.

Suryanarayana, C. (2001). Mechanical alloying and milling, Progress in Materials and Science, 46: 1-184.

Suryanarayana, C., Ivanov, E. and Boldyrev, V.V. (2001). The science and technology of mechanical alloying, *Materials Science and Engineering A*, 304–306: 151–158.

Tang, H**.G., Ma, X.F., Zhao, W., Yan, X.W., Yan, J.M. and Zhu, C.J.** (2004). Crystallization of mechanically alloyed amorphous W–Mg alloy under high pressure, *Solid State Communications*, 129: 147–150.

Tjong, S.C. and Ma, Z.Y. (2000). Microstructural and mechanical characteristics of in situ metal matrix composites, *Materials Science and Engineering*, 29: 49-113.

Toth, I.J. and Lockington, N.A. (1967). The Kinetics of Metallic Activation Sintering of Tungsten. *J. Less-Common Met.*, 12: 353-365.

Upadhyaya, G.S. (2000). Sintered Metallic and Ceramic Materials: Preparation, Properties, and Applications**,** Wiley, New York.

Upadhyaya, G.S. (2001). Some issues in sintering science and technology. *Materials Chemistry and Physics*, 67: 1-5.

Usta, M., **Ozbek, I., Ipek, M., Bindal, C. And UCİSİK, A.H.** (2005). The characterization of boried pure tungsten, *Surface & Coatings Technology*, 194, 330-334.

Vacek, J. (1959). On Influencing the Sintering Behavior of Tungsten. *Planseeberiche fur Pulvermetallurgie*, 7: 6-17.

Yang J., Chung D.D.L. (1989). Casting particulate and fibrous metal-matrix composites by vacuum infiltration of a liquid metal under an inert gas pressure, *Journal of Materials Science*, 24, 3605-3612.

Zhang, F.L., Wang, C.Y. and Zhu, M. (2003). Nanostructured WC/Co composite powder prepared by high energy ball milling, *Scripta Materialia*, 49: 1123–1128.

Zweck, A., Luther, W. (2003). Applications of Nanotechnology in Space Developments and Systems. Technological Analysis, VDI Technology Center Future Technologies Division, Duesseldorf, Germany.

CURRICULUM

Full Name: Didem OVALI

Place and Date of Birth: Beyoğlu / 27.08.1987

Permanent Address: Merkez Mh. Kemaliye Sk. No: 26/3

Güngören/İST.

College: Ataköy High School (2001-2005)

University: Gebze Institute of Technology

Deptartment of Materials Science and Engineering (2005-2010)

Conference Proceedings

- **KONYAR M.**, OVALI, D., YATMAZ H.C., DURAN C, ÖZTÜRK K. (2010). "Photocatalytic Efficiency of ZnO/TiO_2 Composite Plates in Degradation of RR180 Dye Solutions",*Advances in Science and Technology Vol. 65,pages 244-250.*